NAVAL POSTGRADUATE SCHOOL

MONTEREY, CALIFORNIA

THESIS

PERFORMANCE COMPARISON BETWEEN ROUGH AND SMOOTH-CAST BLADES IN A LOW-SPEED MULTISTAGE COMPRESSOR

by

Rebecca A. Manry

June, 2006

Thesis Advisor:	Garth V. Hobson
Second Reader:	Raymond P. Shreeve

THIS PAGE INTENTIONALLY LEFT BLANK

REPORT DOCUMENTATION PAGE			Form Approved OMB No. 0704-0188
Public reporting burden for this collection of information is estimated to average 1 hour per response, including the time for reviewing instruction, searching existing data sources, gathering and maintaining the data needed, and completing and reviewing the collection of information. Send comments regarding this burden estimate or any other aspect of this collection of information, including suggestions for reducing this burden, to Washington headquarters Services, Directorate for Information Operations and Reports, 1215 Jefferson Davis Highway, Suite 1204, Arlington, VA 22202-4302, and to the Office of Management and Budget, Paperwork Reduction Project (0704-0188) Washington DC 20503.			
1. AGENCY USE ONLY ***(Leave blank)***	**2. REPORT DATE** June 2006	**3. REPORT TYPE AND DATES COVERED** Master's Thesis	
4. TITLE AND SUBTITLE Performance Comparison between Rough and Smooth-Cast Blades in a Low-Speed Multistage Compressor		**5. FUNDING NUMBERS**	
6. AUTHOR(S) Manry, Rebecca A.			
7. PERFORMING ORGANIZATION NAME(S) AND ADDRESS(ES) Naval Postgraduate School Monterey, CA 93943-5000		**8. PERFORMING ORGANIZATION REPORT NUMBER**	
9. SPONSORING /MONITORING AGENCY NAME(S) AND ADDRESS(ES) N/A		**10. SPONSORING/MONITORING AGENCY REPORT NUMBER**	
11. SUPPLEMENTARY NOTES The views expressed in this thesis are those of the author and do not reflect the official policy or position of the Department of Defense or the U.S. Government.			
12a. DISTRIBUTION / AVAILABILITY STATEMENT Approved for public release; distribution is unlimited		**12b. DISTRIBUTION CODE** A	

13. ABSTRACT (maximum 200 words)

A performance comparison between smooth-cast and rough-cast blades was conducted in a low-speed multistage compressor. The purpose was to show that rough-cast blades can be used for initial performance tests of low-speed compressors. A baseline performance was established with smooth-cast epoxy blades and then compared to rough-cast aluminum blades. The pressure-rise coefficient versus flow coefficient and velocity triangles were used as the measure for comparison between the different blade types. The velocity triangles were constructed and compared across the span (hub-to-tip) of the second-stage. This was done by using two probes that could traverse radially along the blade and sense the flow velocity and angle relative to the compressor axis. Measurements were taken at six different locations from the hub-to-tip of the blade. The performance tests were conducted at four different throttle settings: near stall, open throttle, nominal operating point (NOP), and near the NOP. Results showed that although there were some differences between the smooth-cast and rough-cast blades, the overall performance was very similar. As a result, rough-cast blades could be used for initial performance tests or as the initial stages of a compressor in order to set up the flow for the evaluation of a new stage of smooth blades. The use of rough-cast blades in early stages would save the time and money needed to produce large numbers of high precision smooth-cast blades.

14. SUBJECT TERMS Low-Speed Multistage Compressor, Blade Roughness, Performance Measurements			**15. NUMBER OF PAGES** 123
			16. PRICE CODE
17. SECURITY CLASSIFICATION OF REPORT Unclassified	**18. SECURITY CLASSIFICATION OF THIS PAGE** Unclassified	**19. SECURITY CLASSIFICATION OF ABSTRACT** Unclassified	**20. LIMITATION OF ABSTRACT** UL

NSN 7540-01-280-5500

Standard Form 298 (Rev. 2-89)
Prescribed by ANSI Std. 239-18

THIS PAGE INTENTIONALLY LEFT BLANK

Approved for public release; distribution is unlimited.

PERFORMANCE COMPARISON BETWEEN ROUGH AND SMOOTH-CAST BLADES IN A LOW-SPEED MULTISTAGE COMPRESSOR

Rebecca A. Manry
Lieutenant, United States Navy
B.S., United States Naval Academy, 2001

Submitted in partial fulfillment of the
requirements for the degree of

MASTER OF SCIENCE IN MECHANICAL ENGINEERING

from the

NAVAL POSTGRADUATE SCHOOL
June 2006

Author: Rebecca A. Manry

Approved by: Garth V. Hobson
Thesis Advisor

Raymond P. Shreeve
Second Reader

Anthony J. Healey
Chairman, Department of Mechanical Engineering and
Astronautical Engineering

THIS PAGE INTENTIONALLY LEFT BLANK

ABSTRACT

A performance comparison between smooth-cast and rough-cast blades was conducted in a low-speed multistage compressor. The purpose was to show that rough-cast blades can be used for initial performance tests of low-speed compressors. A baseline performance was established with smooth-cast epoxy blades and then compared to rough-cast aluminum blades. The pressure-rise coefficient versus flow coefficient and velocity triangles were used as the measure for comparison between the different blade types. The velocity triangles were constructed and compared across the span (hub-to-tip) of the second-stage. This was done by using two probes that could traverse radially along the blade and sense the flow velocity and angle relative to the compressor axis. Measurements were taken at six different locations from the hub-to-tip of the blade. The performance tests were conducted at four different throttle settings: near stall, open throttle, nominal operating point (NOP), and near the NOP. Results showed that although there were some differences between the smooth-cast and rough-cast blades, the overall performance was very similar. As a result, rough-cast blades could be used for initial performance tests or as the initial stages of a compressor in order to set up the flow for the evaluation of a new stage of smooth blades. The use of rough-cast blades in early stages would save the time and money needed to produce large numbers of high precision smooth-cast blades.

THIS PAGE INTENTIONALLY LEFT BLANK

TABLE OF CONTENTS

LIST OF FIGURES

THIS PAGE INTENTIONALLY LEFT BLANK

LIST OF TABLES

THIS PAGE INTENTIONALLY LEFT BLANK

ACKNOWLEDGMENTS

I would like to thank Professor Garth Hobson for this wonderful opportunity. I appreciated your patience and understanding, as well as your ability to adapt and overcome any challenge with great calm and ease. Your active involvement with your thesis students shows a true desire for everyone to have a great learning experience and successful thesis projects.

I would like to thank Rick Still and John Gibson for their many hours of hard work and support. Without you, this project would have been impossible for me. I appreciated your dedication to all of the thesis students in helping us to succeed. Most especially, I appreciated your smiles, the jokes, and the laughter.

I would like to thank Professor Raymond Shreeve and Doug Seivwright for their support and encouragement. Your willingness to help out or answer questions whenever needed was greatly appreciated.

The dynamics of everyone at the Turbopropulsion Lab make for an incredible working environment and learning experience. Your eagerness to try new things, your active involvement and concern for the students, and your ingenuity at correcting problems with ease are very admirable and greatly appreciated. It was an honor and pleasure to work with all of you. Thank you!

THIS PAGE INTENTIONALLY LEFT BLANK

I. INTRODUCTION

The ability to use rough-cast blades for initial performance tests of compressors would be very cost beneficial. The intent here is to show that the overall performance of a two-stage low-speed axial-compressor is not significantly dependant upon having smooth-cast blades, which are more expensive to produce than rough-cast blades. Even if the rough-cast blades have a loss in performance compared to the smooth-cast blades, it might prove to be small enough that it can be accounted for when designing axial-compressors. Companies spend millions of dollars producing smooth-cast blades for their initial tests on newly designed compressors. Instead, they might use much cheaper rough-cast blades and get a good idea of the overall performance of the new design. Also in multistage compressor testing, of new stage designs, the initial few stages might be made of rough-cast blades to set up the flow to a smooth set of test blades installed as an embedded stage.

Many comparisons of blade geometries have been done in the past, but there is much less research comparing smooth-cast blades to rough-cast blades, especially in low-speed axial-compressors. Gbadebo, Hynes, and Cumpsty [Ref. 1] reported a study on how blade roughness affects three-dimensional separation. The experiment was done on a single-stage low-speed axial-compressor. Their study looked at the effect of roughness on stator blades from long term engine operation. The results showed that there was a significant performance loss in the compressor due to the three-dimensional separation caused by the roughness.

Suder, Chima, Strazisar and Roberts [Ref. 2] reported a study on how adding roughness and thickness affects a high-speed axial-compressor rotor. Their results showed that a smooth coating produced about half of the performance loss of a rough coating, for the same thickness. Both cases showed significant performance loss compared to the smooth bare metal blade.

Bammert and Woelk [Ref. 3] reported a study on a three-stage axial-compressor comparing smooth and emery-grain roughness blades. In reference 1 it is reported that they observed that the overall efficiency reduced between 6 and 13% over the range of different roughness grades considered, and there was a maximum reduction of 30% in the overall pressure ratio. [Ref. 1]

In the present experiment, smooth-cast blades made of cast epoxy were used for the baseline performance measurements. Sand-cast aluminum blades were then used for the rough-cast blade comparison. The second-stage of the axial-compressor was used for inter blade probe measurements.

A secondary purpose of the present study was to replace the old epoxy blades in the low-speed multistage compressor, which had reached the end of their useful life, with more robust cast-aluminum blades. These blades will be used in the future for inlet distortion studies on a multistage compressor.

II. EXPERIMENTAL APPARATUS

A. LOW-SPEED MULTISTAGE COMPRESSOR BUILD #1

1. Overall Layout

The Low-Speed Multistage Compressor (LSMSC) at NPS, shown in Figure 1, is a horizontally mounted open loop 914mm (36in) diameter machine. Ambient air is drawn from outside the building in through an inlet bellmouth nozzle and through the 36in diameter ducting, and outflows into the building through an annular diffuser.

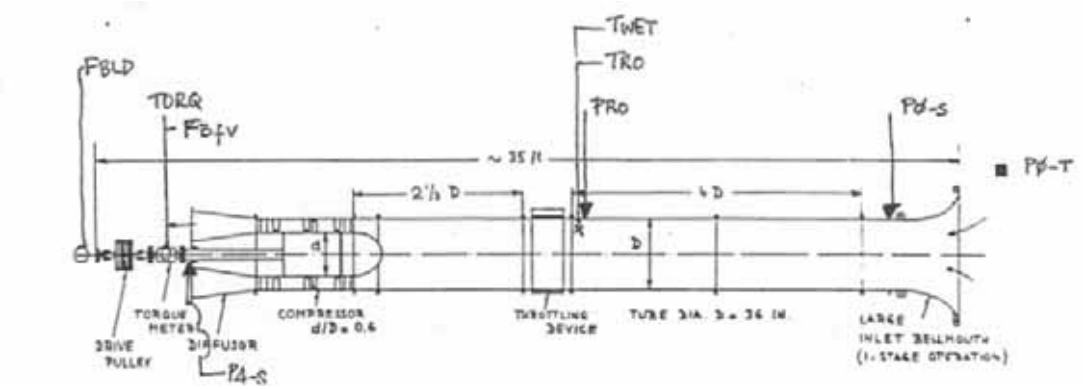

Figure 1. Low-speed compressor test facility detail

The inlet flow can be throttled by placing various sets of screens in the path of the air flow. Each screen has a different flow resistance; therefore, various throttle settings can be achieved by changing the combination and number of screens. The housing for the screens is located four diameters behind the inlet bellmouth nozzle as shown in Figure 1.

The drive shaft of the compressor connects to a belt drive aft of the diffuser. The compressor is powered by a 112kW (150HP) synchronous motor. The belt drive has a fixed rotational speed of 1610 RPM, which produces a blade tip speed of 77.08 m/s (252.9 ft/s). The rotor hub and shaft were supported by a radial bearing in the front and a thrust bearing in the rear.

2. Test Section and Blading

The test section is located two diameters beyond the screen housing area. The shell casing for the test section is 76.2 mm (3in) thick and manufactured from heavy cast iron material. The test section was designed to accommodate a total of three stages of rotor and stator blades. The setup for build #1 was one row of 32 blades of inlet guide vanes (IGVs), one row of 32 blades of exit guide vanes (EGVs), and two stages of 30 rotor blades and 32 stator blades located in the aft stages of the machine (the first stage being removed).

The blades were smooth-cast and made of epoxy. The blade height (b) was 183mm (7.20in). The hub-to-tip ratio was 0.60. The design blade tip clearance (e) was 0.02in and the tip gap-to-blade height ratio (e/b) was .003. Figure 2 [Ref. 4] shows the design velocity diagram for one stage of symmetric blading.

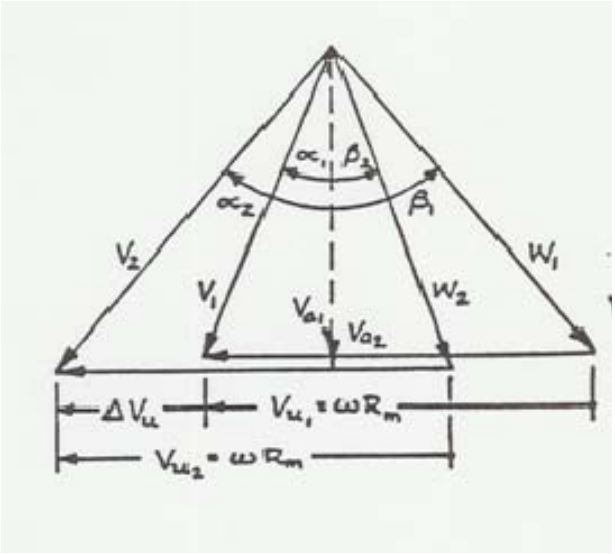

Figure 2. Design velocity diagram for the symmetric blading.

The rotor and stator blade profiles were developed from a circular arc camber line and a C-4 thickness distribution, though slightly flattened at the leading edge. The blading was a repeating stage design and imposed a forced-vortex flow field in the radial direction. Tables 1-3, from Moyle [Ref. 4] show

design data for the blading geometry. The inlet guide vanes and exit guide vanes were also developed using the circular arc camber lines and thickness distributions from Moyle.

Table 1. Spanwise distribution of symmetric blading design flow data

	Rotor						Stator				
r/r_t	φ	W_1	β_1	$\Delta\beta$	D_R	σ_R	V_2	α_2	$\Delta\alpha$	D_S	σ_S
0.60	0.70	0.86	35.08	27.83	.250	1.06	0.96	31.04	22.57	.424	1.22
0.70	0.68	0.86	37.47	24.54	.305	0.98	0.92	35.09	20.12	.415	1.01
0.80	0.65	0.85	40.00	20.32	.356	0.92	0.87	39.88	18.60	.407	0.85
0.90	0.61	0.84	43.78	15.76	.402	0.92	0.87	39.88	18.60	.400	0.72
1.00	0.54	0.82	48.59	09.63	.427	0.85	0.78	52.45	17.36	.376	0.62

Table 2. Thickness distribution for modified C-4 circular arc profiles used for symmetric blading

x/c%	1.25	2.50	5.00	7.50	10.0	15.0	20.0	30.0	50.0	70.0	90.0
y/t%	16.8	19.1	26.8	32.4	37.0	43.5	47.3	50.0	45.7	40.5	16.0
r/t%	12.0										6.00

Table 3. Spanwise distribution of symmetric blading geometric design data

	b = 183 mm (7.20 in)							
	Rotor				Stator			
r/r_t	γ	ξ	c/b	t/c	γ	ξ	c/b	t/c
0.60	15.71	40.48	.333	.125	16.07	29.26	.361	.065
0.70	20.30	37.42	.361	.098	21.10	29.28	.347	.076
0.80	25.56	32.54	.389	.076	26.21	31.44	.333	.087
0.90	32.19	26.34	.417	.068	31.20	36.91	.319	.100
1.00	40.96	16.00	.444	.062	34.71	47.58	.306	.114

B. LOW-SPEED MULTISTAGE COMPRESSOR BUILD #2

Once the baseline measurements had been obtained, the compressor was disassembled and rebladed with new cast-aluminum blades. The disassembly and reblading procedure is shown pictorially in Appendix I.

1. Overall Layout

The overall layout did not change for build #2. The only change was a new bearing arrangement. Originally, a thrust bearing was installed on the aft end of the rotor shaft. The original rear thrust bearing was replaced with a high-temperature, deep-groove ball bearing.

2. Test Section and Blading

The test section was the same setup as build #1. In build #2 the blades were rough-cast aluminum blades. They were the same shape as build #1. The blade height (b) was 180mm (7.10in). The hub-to-tip ratio was 0.60. However, the blade tip clearance (e) was 0.12in and the tip gap-to-blade height ratio (e/b) was 0.017. Also, the epoxy inlet guide vanes were replaced with old precision cast- aluminum blades that produced a forced-vortex inlet flow field to the first rotor.

C. INSTRUMENTATION AND DATA ACQUISITION

1. Probe Types and Sensors Used

Spanwise inlet flow surveys were obtained using a fixed radial rake with twelve Kiel tips. This probe was used to determine the average inlet total pressure and was located ahead of the inlet guide vanes.

Inlet and outlet radial surveys of the flow to the second-stage were performed using a three-hole pneumatic probe (designated as the S Cobra) downstream of the second-stage rotor and a five-hole United Sensor pneumatic probe (designated Y) downstream of the second-stage stator blade. These two probes were traversed radially from hub-to-tip. The probes measured flow velocity and angle relative to the compressor axis, based on prior calibrations performed in a free-jet.

All other total and static pressures were measured with fixed pneumatic probes or static ports. Thermocouples were used to measure all temperatures. [Ref. 4]

2. Data Acquisition/Processing using HP VEE Software

The data acquisition system used Scanivalves to access all the pressures from the probes and throughout the test section [Ref. 4]. Compressor speed was measured with a once-per-revolution sensor and the value was manually recorded. The Scanivalves fed the information into the HP75000 series B VXI-Bus mainframe. This system was controlled and accessed by HP VEE software. All raw data from the test runs were accessed through the HP VEE program. The HP VEE program was used to process the data and calculate the required performance parameters.

THIS PAGE INTENTIONALLY LEFT BLANK

III. EXPERIMENTAL PROCEDURES

A. LSMC SETUP

The LSMC setup was a modified version of the two setups for Moyle's Lab #1 and Lab #2 [Ref. 4]. The probe surveys downstream of the second-stage rotor and stator were a modified version of Lab #2, where the probe surveys were taken downstream of the first-stage stator and second-stage rotor (see Figure 3. The rest of the measurements were from Lab #1 as shown in Figure 4 . The modifications to Moyle's lab programs can be found in Appendix B.

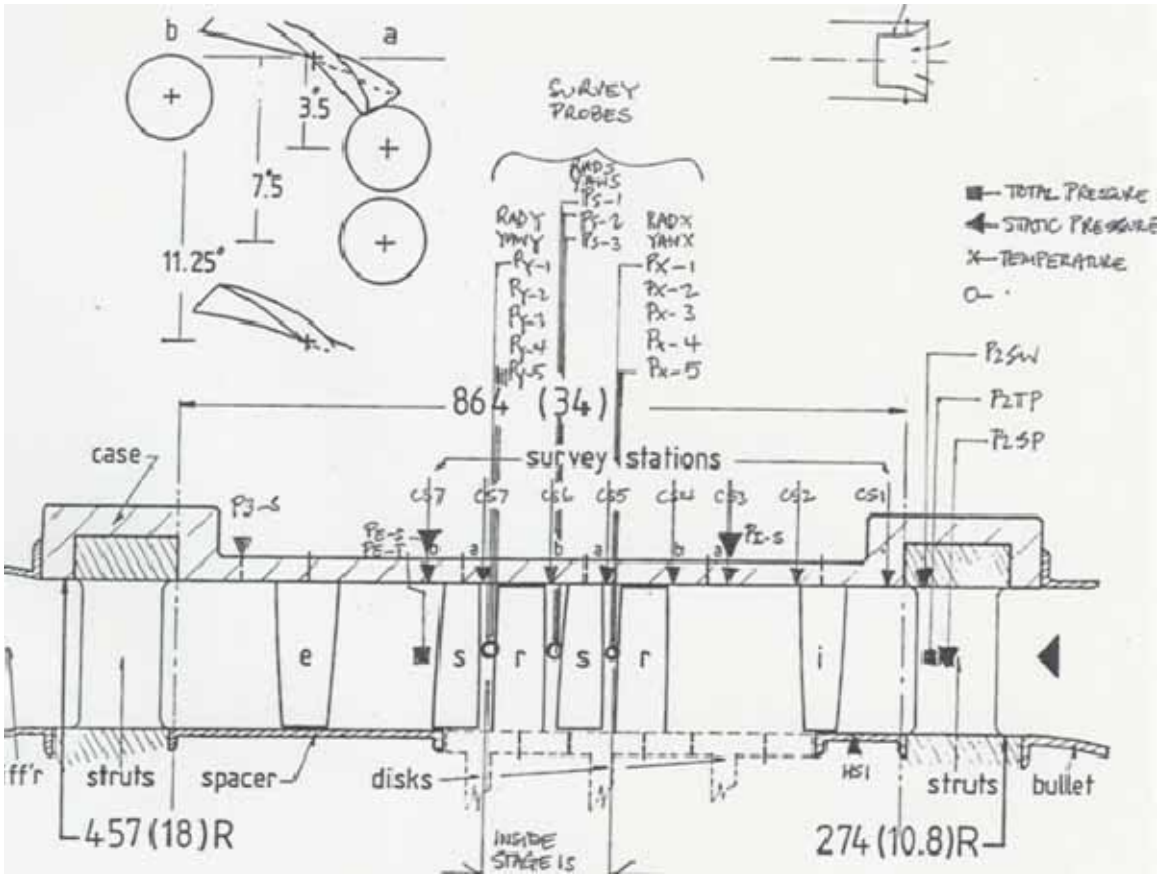

Figure 3. Low-speed compressor test section detail for lab #2.

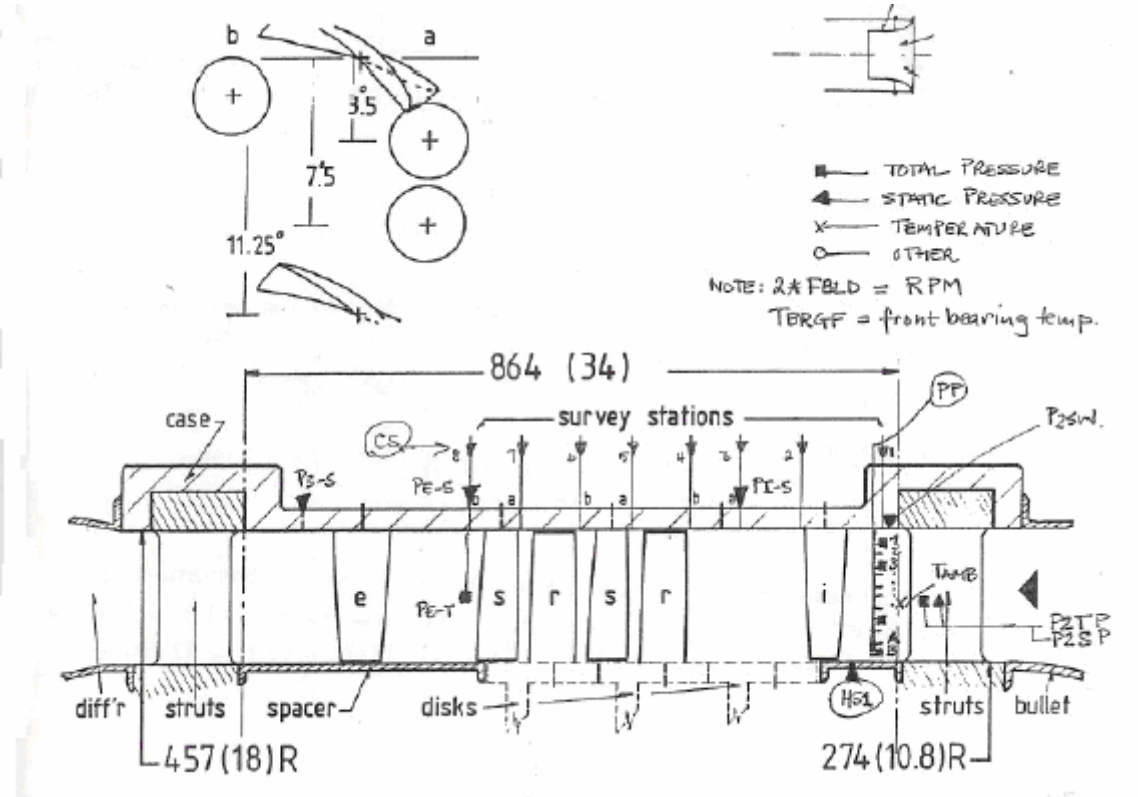

Figure 4. Low-speed compressor test section detail for lab #1.

B. PROBE SURVEYS

1. Probe Surveys Downstream of the Rotor

Probe surveys downstream of the second-stage rotor were conducted using the three-hole (Cobra) pneumatic probe (labeled S). This probe was traversed radially from hub-to-tip to six different locations along the span of the blade. The probe was balanced and aligned in the flow using a U-tube water manometer. The following depths (in inches) were measured on the S-probe: 2.92, 3.82, 4.72, 5.62, 6.52, and 7.42.

2. Probe Surveys Downstream of the Stator

Probe surveys downstream of the second-stage stator were conducted using the five-hole pneumatic probe (labeled Y). As with the S-probe, this probe was traversed radially from hub–to-tip to six different locations along the span of the blade. The Y-probe was yaw-balanced, the same as the S-probe. The following scale settings (in inches) were set on the Y-probe: .9, 1.8, 2.7, 3.6, 4.5,

and 5.4. There was a difference in the settings between the Y-probe and the S-probe in order to obtain the same immersion depths. The S-probe's scale was offset compared to the Y-probe, with a starting value at the case wall of 2.02in instead of 0.

C. DATA PROCESSING

HP VEE software was used to process the data. The program was a modified version of two existing programs used to run Moyle's Lab #1 and Lab #2 [Ref. 4]. The original program for Lab #2 was modified to access probes from both Lab #1 and Lab #2 as well as process the data for both labs. All data were saved from the HP VEE program and transferred into an Excel spreadsheet. The raw data and processed data can be found in Appendix C. The data were processed using the HP VEE program and Microsoft Excel. The calculations were checked independently of the program using the equations given in Appendix D.

THIS PAGE INTENTIONALLY LEFT BLANK

IV. RESULTS

A. PERFORMANCE RESULTS BUILD #1

Performance measurements were taken at four different throttle settings. Near stall was represented by throttle setting 5+4+3+2+1 (each number indicates a particular screen that was inserted into the throttle housing). Open throttle was throttle setting 5. Nominal Operating Point (NOP) was designated as throttle setting 5+4+3.

1. Pressure-rise Coefficient versus Flow Coefficient

The pressure-rise coefficient versus flow coefficient is the conventional performance map for a compressor. Figure 5 plots twice times the pressure-rise coefficient (defined in Appendix D) versus flow coefficient, which is the pumping characteristic of the compressor.

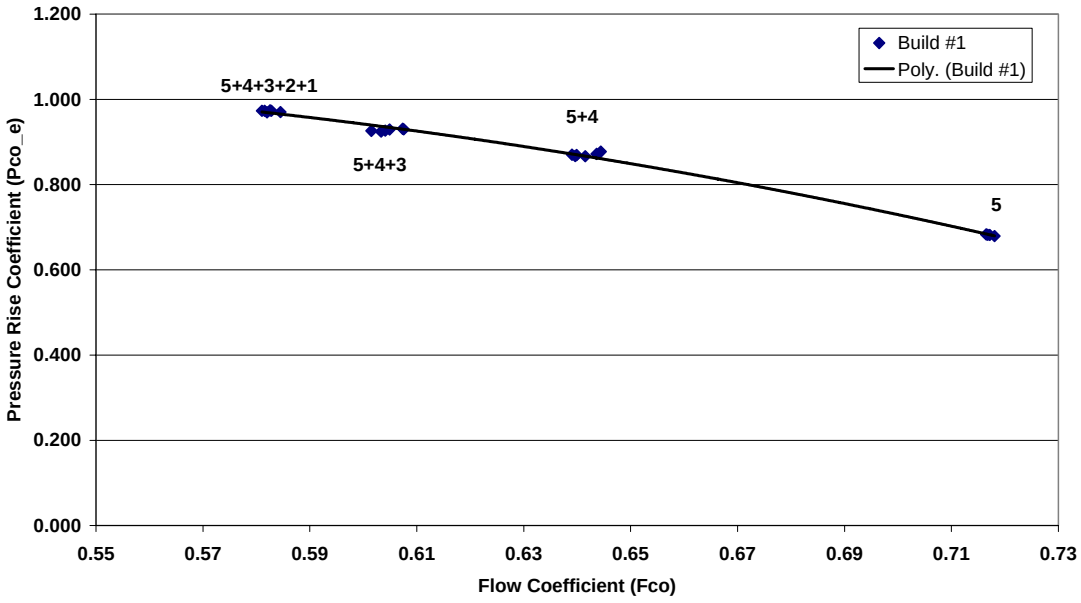

Figure 5. Pressure-rise coefficient versus flow coefficient for build #1

The design pressure-rise coefficient versus flow coefficient for the two-stage compressor [Ref. 4] is reproduced as Figure 6.

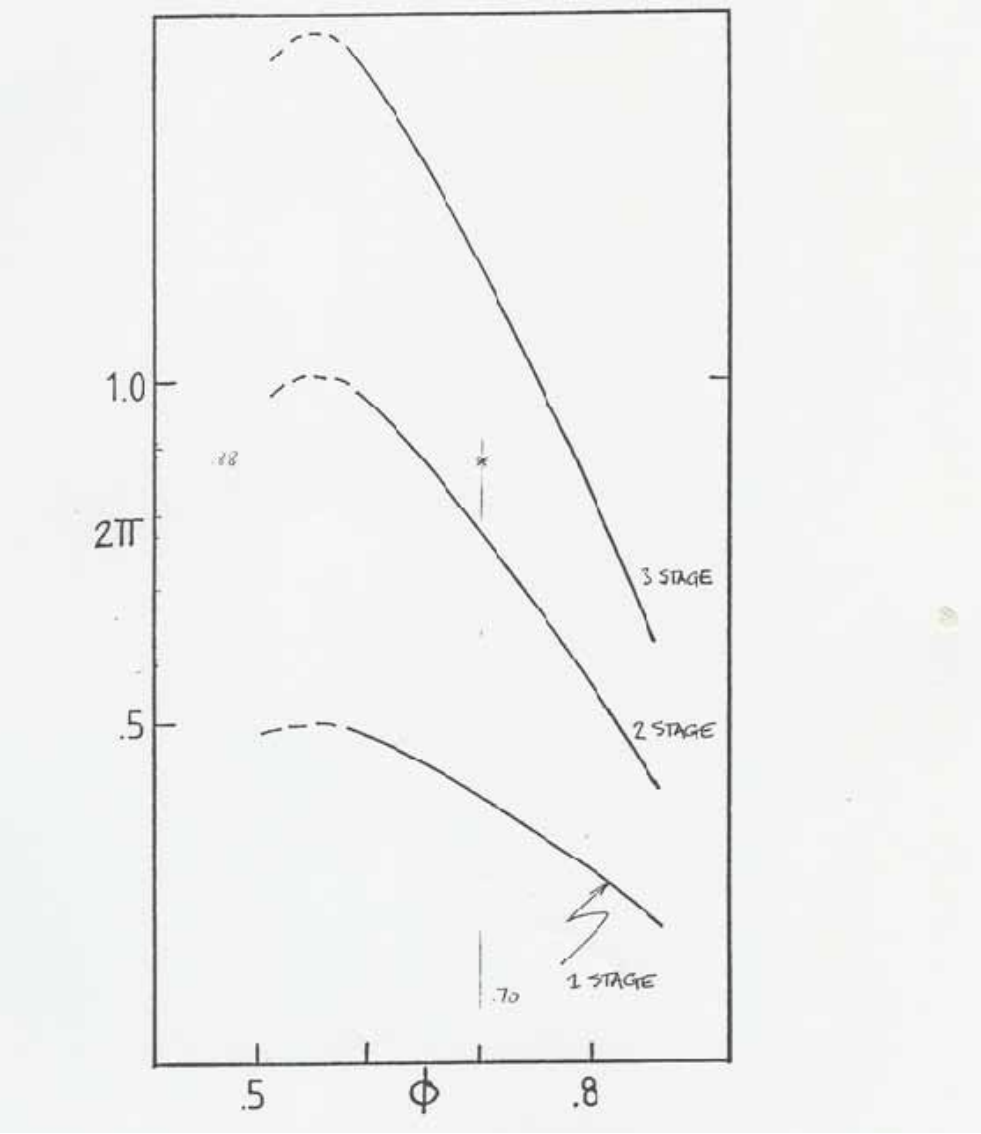

Figure 6. Stage design pressure-rise, flow rate characteristic based on the off-design velocity and loss correlation.

2. Efficiency versus Flow Coefficient

The efficiency is a measure of the losses within the compressor. Figure 7 shows a plot of the efficiency versus the flow coefficient. A peak efficiency of 74% was found near stall and an efficiency of 73.5% was found at the nominal operating point.

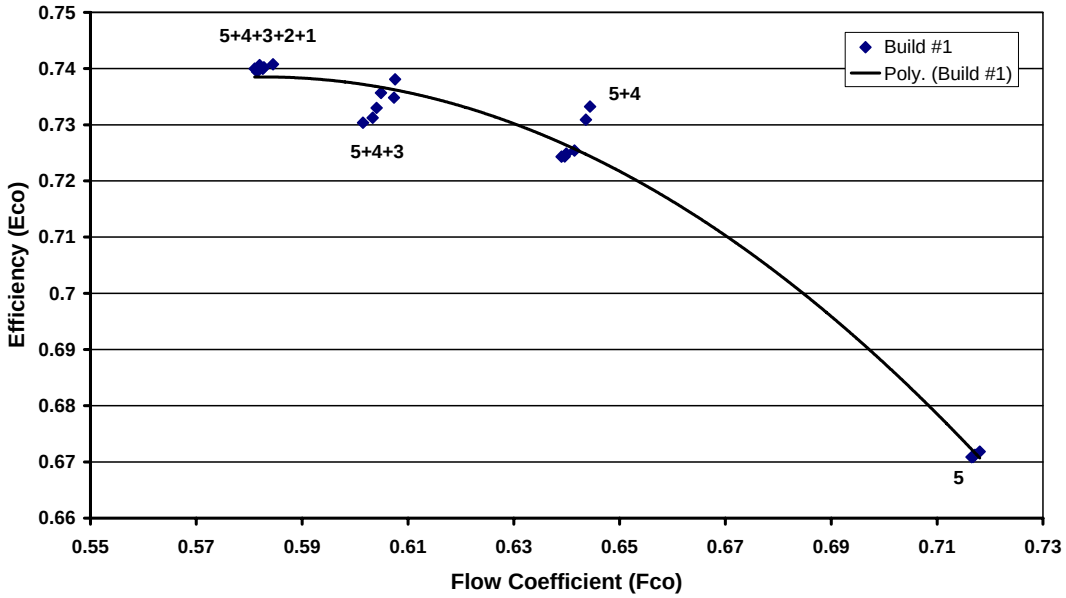

Figure 7. Efficiency versus flow coefficient for build #1

B. PROBE SURVEYS BUILD #1

1. Total Pressure versus Radial Distance

Figures 8-11 show the total pressure measured by the three-hole and five-hole probes (S and Y respectively) versus the radial distance along the blade. The data set for open throttle (throttle setting 5) is incomplete. Data were only taken from locations 2 through 5 before the compressor had to be shut down due to problems with the forward bearing.

The off-design settings near stall and open throttle had non-uniform total - pressure profiles, showing how the tip became more highly loaded near stall compared to open throttle where the tip had very little load. Both throttle settings 5+4 and 5+4+3+2+1 showed a more uniform shape since they are closer to the nominal operating conditions. The uniform shape showed that there was nearly equal loading at the tip and hub at the NOP.

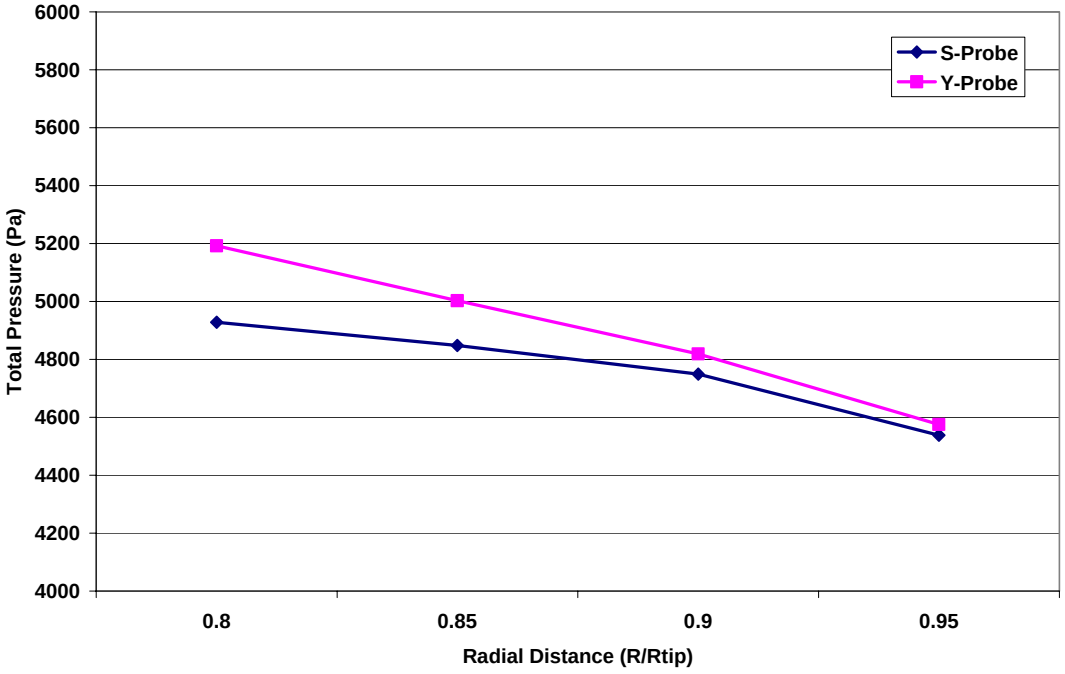

Figure 8. Total pressure versus radial distance for open throttle (5)

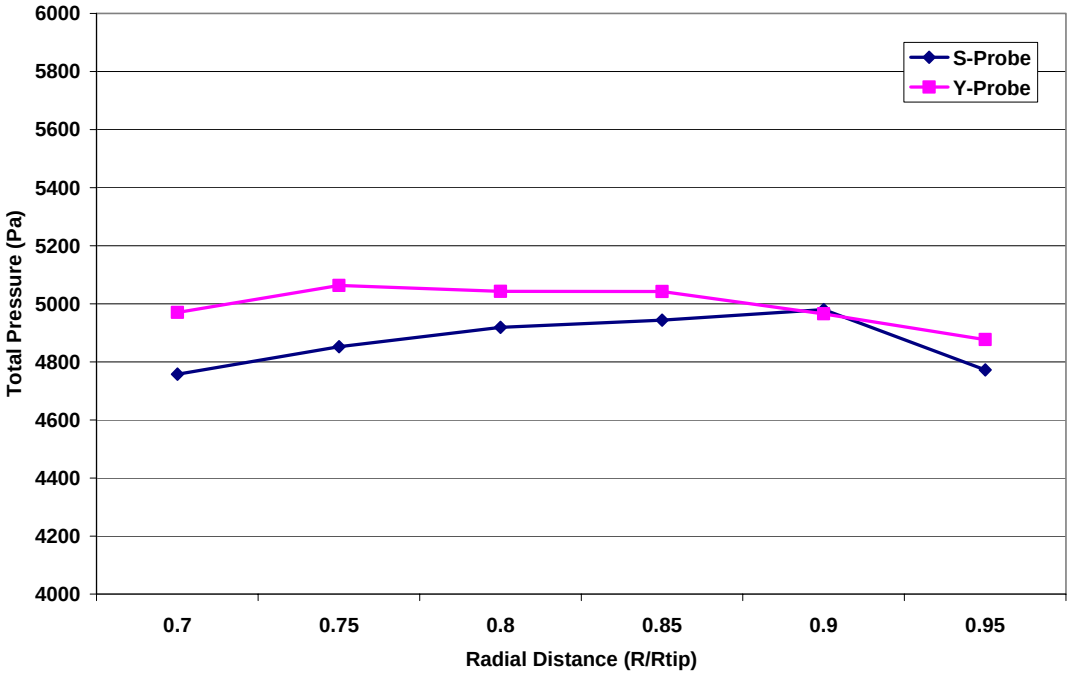

Figure 9. Total pressure versus radial distance for throttle setting 5+4

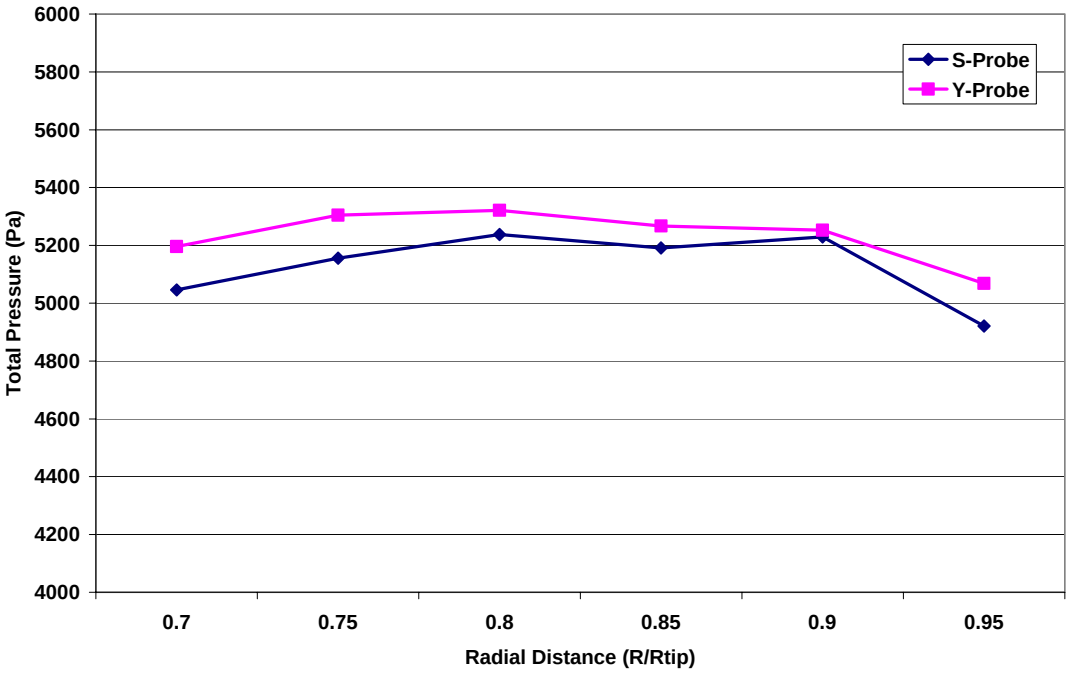

Figure 10. Total pressure vs radial distance for NOP (5+4+3)

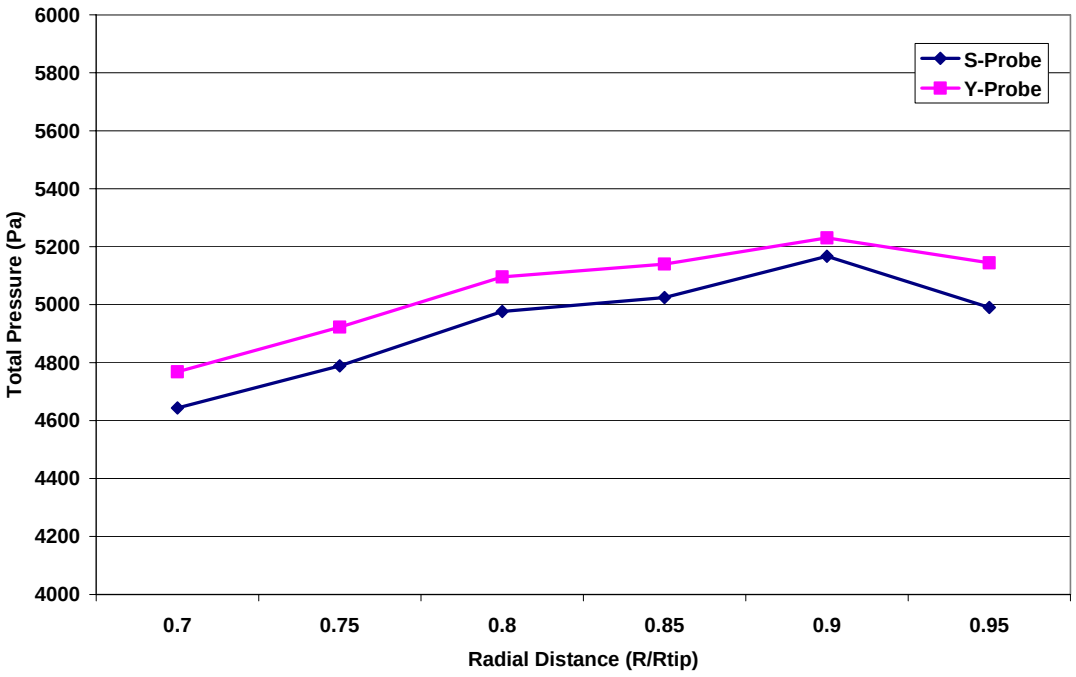

Figure 11. Total pressure vs radial distance for near stall

2. Velocity Distribution versus Radial Distance

The design data were taken from the information provided in Moyle's Lab #2 [Ref. 4] which originally came from his Doctoral Dissertation [Ref. 5].

a. Tangential Velocity Distribution

Figures 12-15 show the variation in the tangential velocity downstream of the stator (Y-probe) and the tangential velocity downstream of the rotor (S-probe). The design data (a symmetric diagram with tangential velocity increases with radius) most closely followed the variation of the Y-probe, which was downstream of the 2nd stage stator. The reason the rotor exit data (S-probe) deviated from the design was possibly because different inlet guide vanes (than required for the stage design) were used in the compressor for this experiment [Ref. 5].

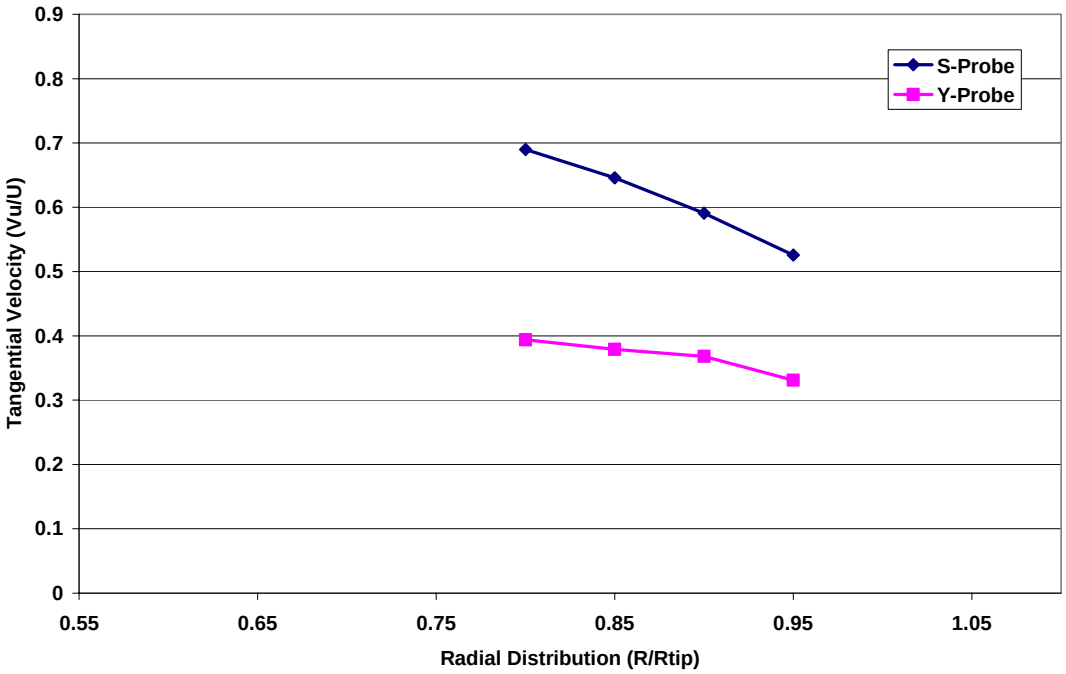

Figure 12. Tangential velocity vs radial distance at open throttle (5)

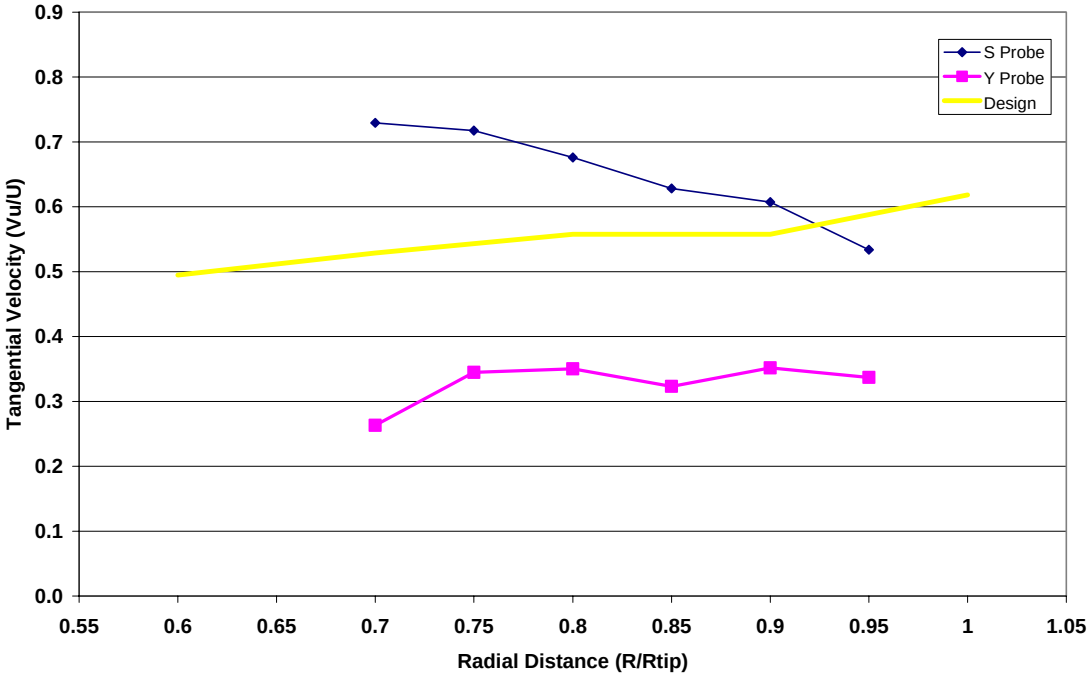

Figure 13. Tangential velocity vs radial distance for throttle 5+4

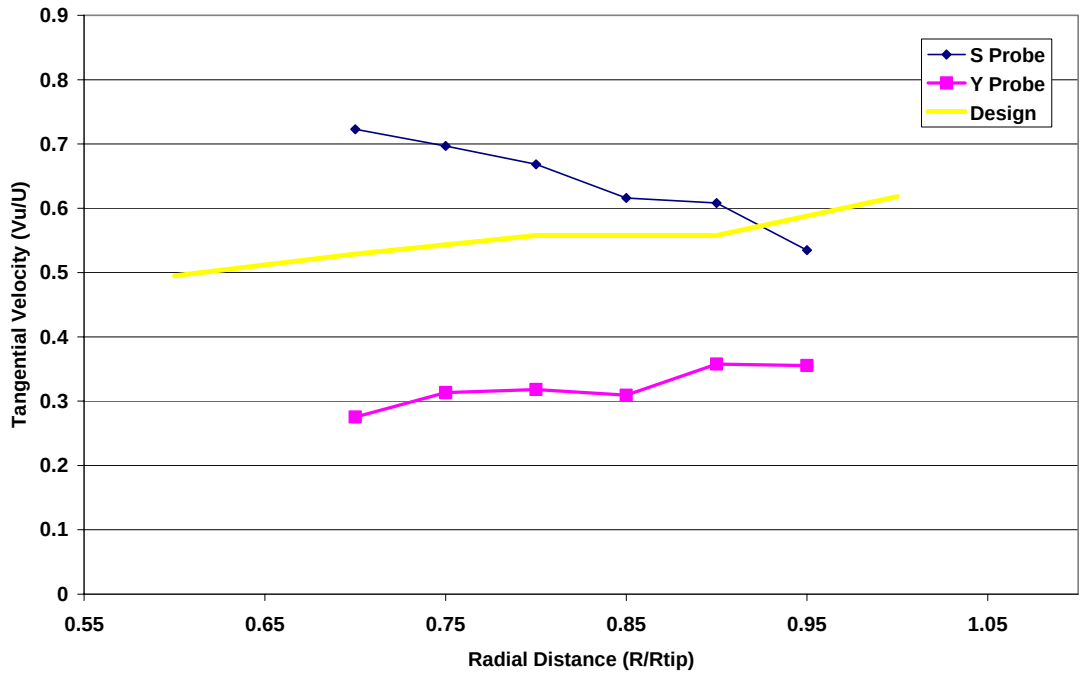

Figure 14. Tangential velocity vs radial distance for NOP (5+4+3)

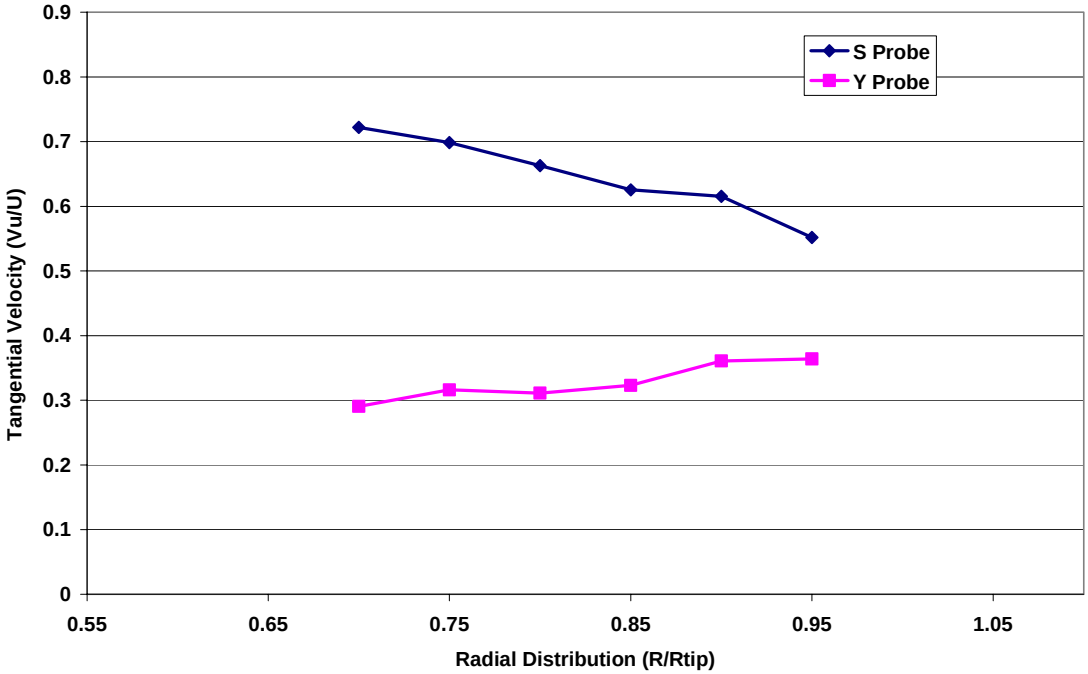

Figure 15. Tangential velocity vs radial distance at near stall

b. Axial Velocity Distribution

Figures 16-19 show that axial velocity downstream of the stator (Y-probe) and rotor (S-probe) decreased radially from the hub-to-tip. This matched the overall trend of the design data from Moyle's Lab #2 [Ref. 4] with the exception of the horizontal area in the middle. The horizontal line in the design data suggests a possible mistake in the design calculations. The expected trend was that the axial velocity would continue an upward trend from tip-to-hub as was observed from both radial probes. The figures show little change in the axial flow through the second stage which is characteristic of a repeating stage design.

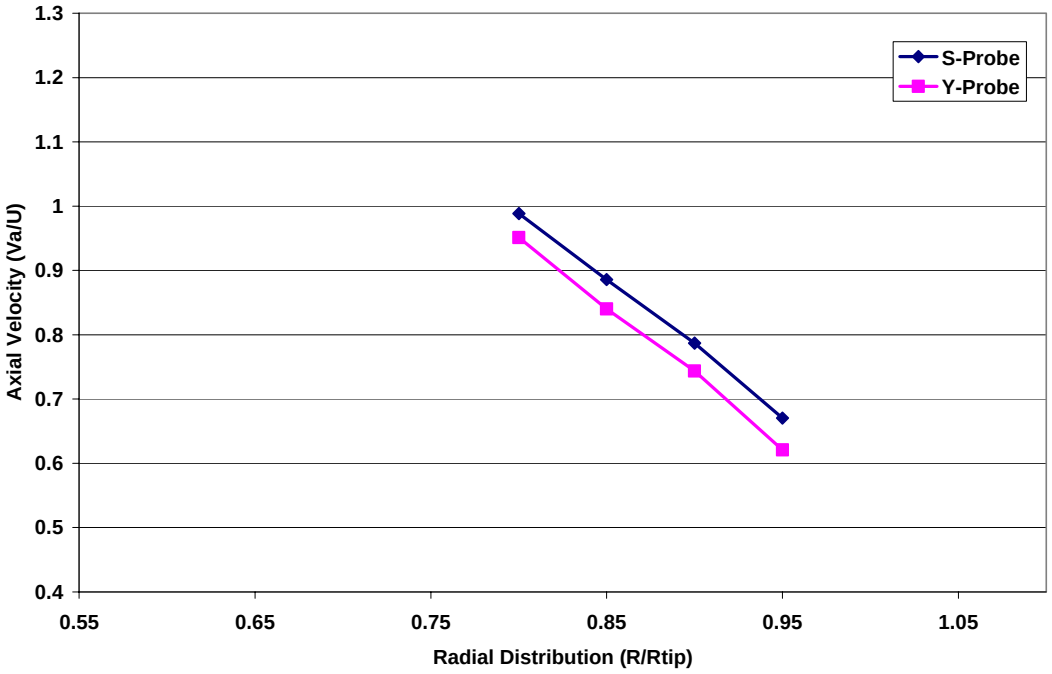

Figure 16. Axial velocity versus radial distance for open throttle (5)

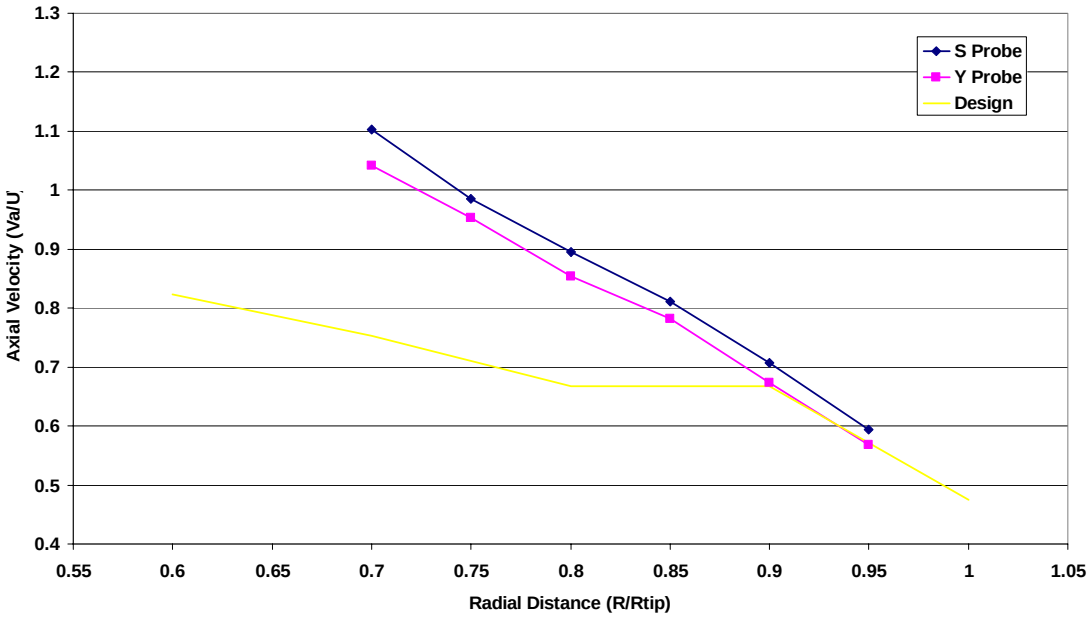

Figure 17. Axial velocity versus radial distance for throttle setting 5+4

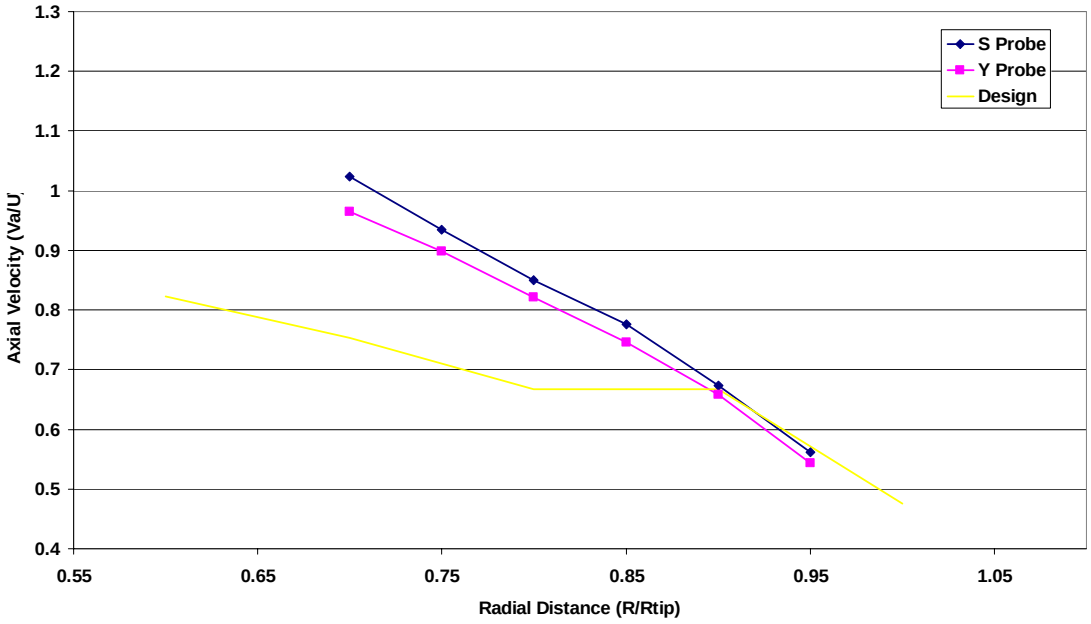

Figure 18. Axial velocity vs radial distance for NOP (5+4+3)

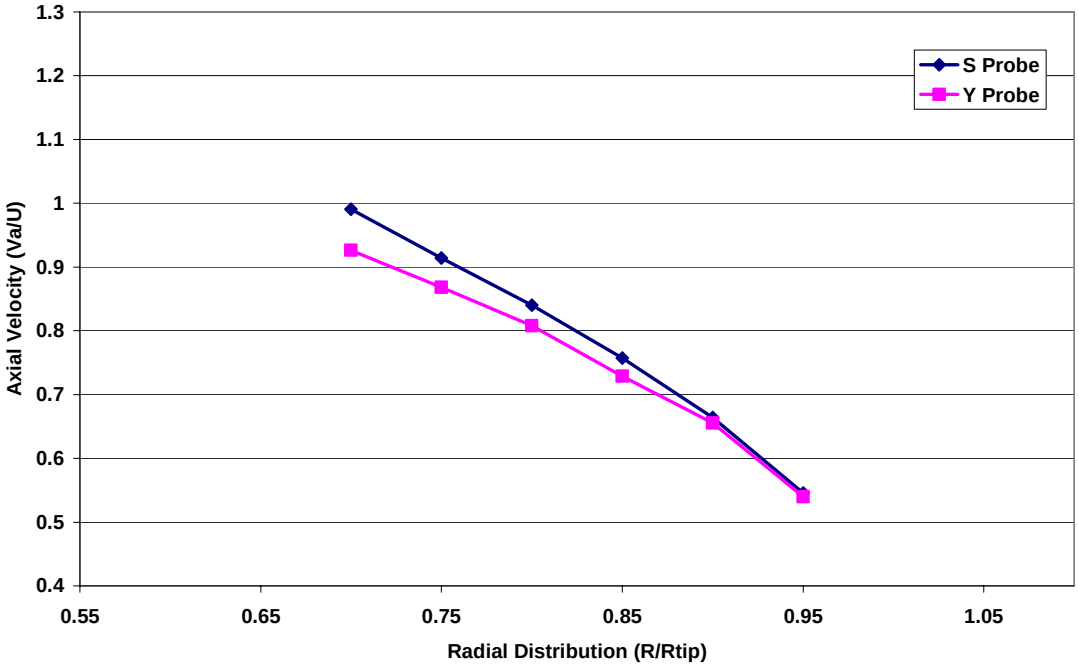

Figure 19. Axial velocity vs radial distance for near stall (5+4+3+2+1)

3. Flow Angle versus Radial Distance

Figures 20-23 show the plots of the flow yaw angle versus the radial distance for build #1 downstream of the stator (Y-probe) and downstream of the rotor (S-probe) for each throttle setting.

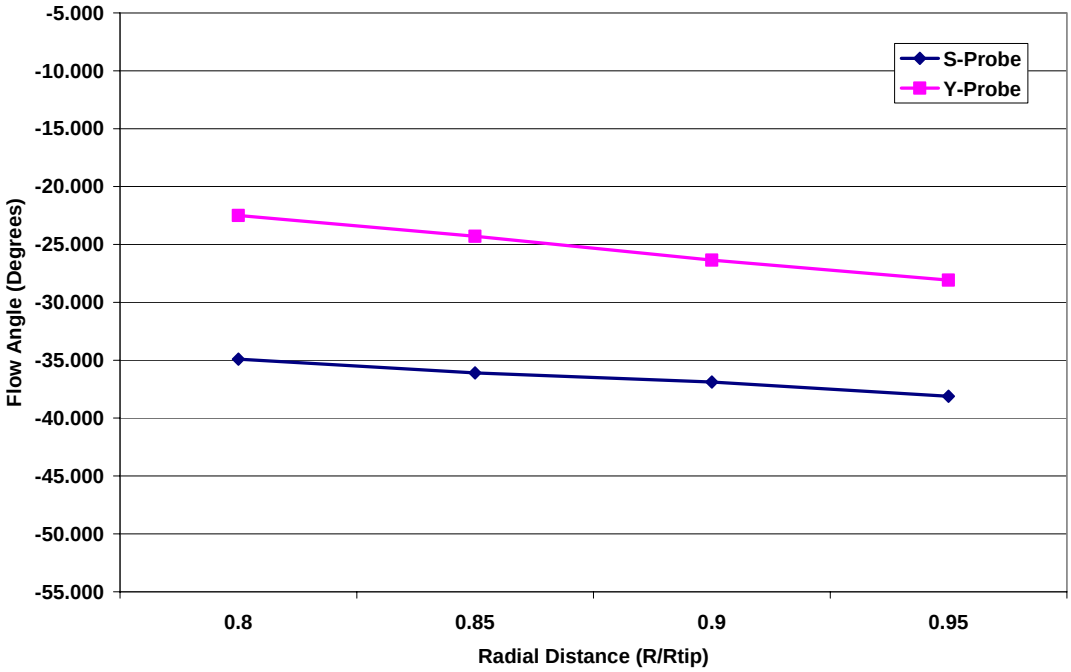

Figure 20. Flow angle versus radial distance for open throttle

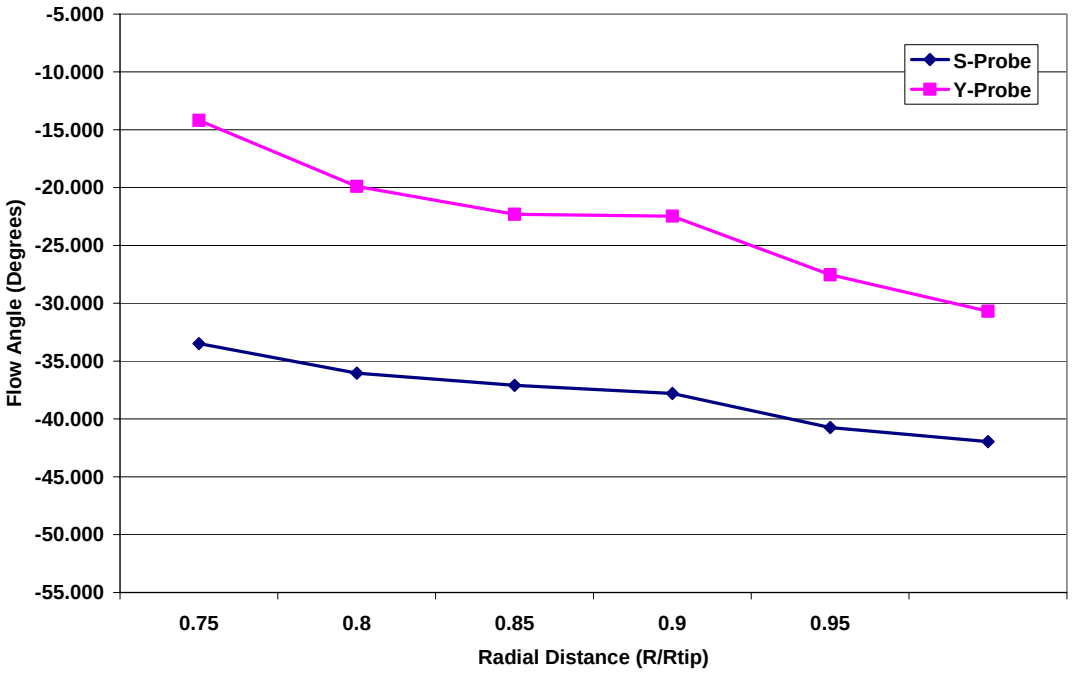

Figure 21. Flow angle versus radial distance for throttle setting 5+4

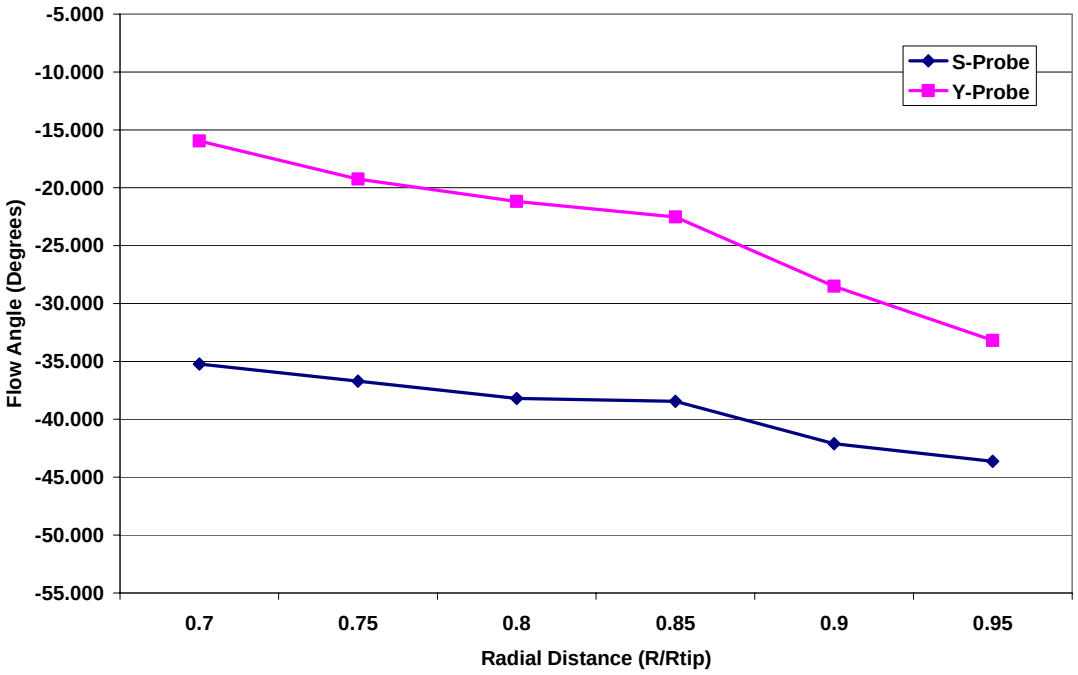

Figure 22. Flow angle versus radial distance for NOP (5+4+3)

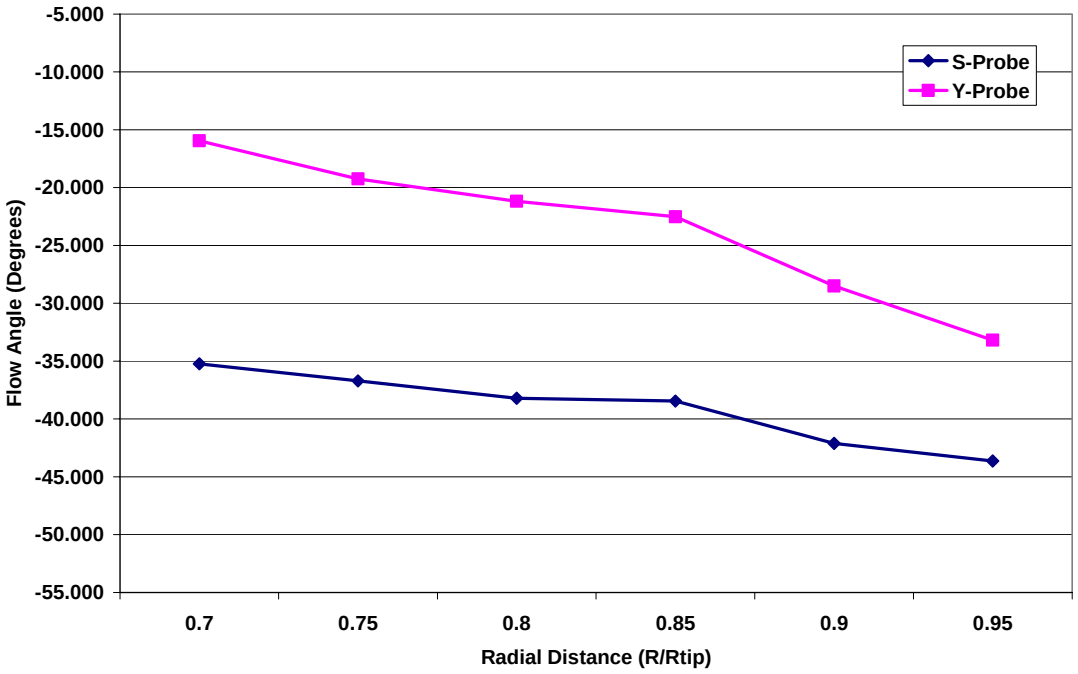

Figure 23. Flow angle vs radial distance for near stall (5+4+3+2+1)

C. VELOCITY TRIANGLES BUILD #1

Figures 24-25 show the velocity diagrams for point locations 2, 4, and 7 for each of the throttle settings. Location 2 was near the tip (R/Rtip = .95), while location 7 was the closest distance to the hub (R/Rtip = .7). Throttle setting 5 (open throttle) only had diagrams for point locations 2 and 4 because data were not gathered for location 7.

1. Point Location # 2

Figures 24a-d show the velocity diagrams for point location #2 for all throttle settings.

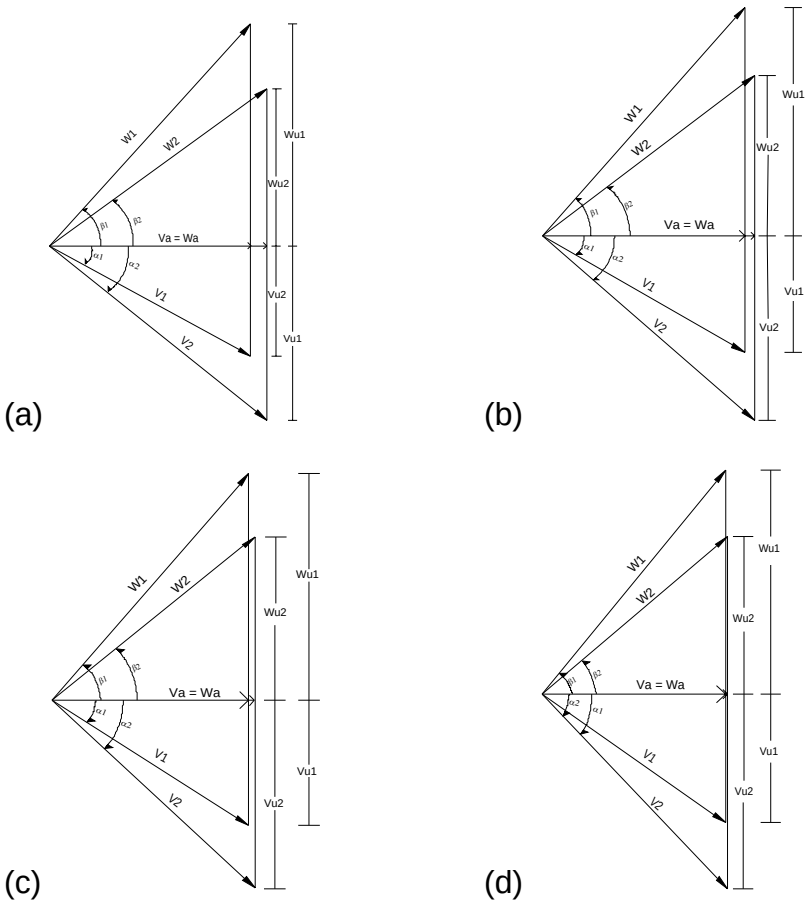

Figure 24. Point location #2 – (a) Open throttle (b) Throttle 5+4 (c) NOP (d) Near stall

2. Point Location # 4

Figures 25a-d show the velocity diagrams for point location # 4 at all throttle settings.

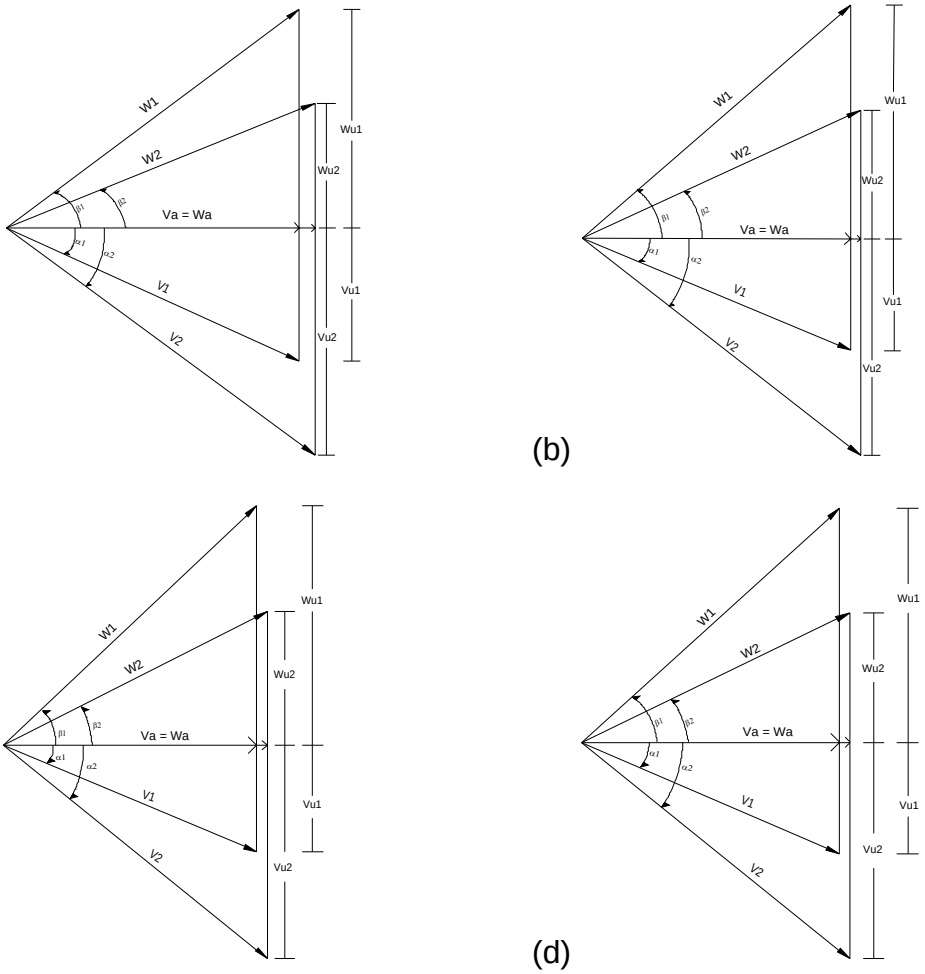

Figure 25. Point location #4 – (a) Open throttle (b) Throttle 5+4 (c) NOP (d) Near stall

3. Point Location # 7

Figures 26a-c show the velocity diagrams for point location # 7 at all throttle settings except open throttle (throttle 5).

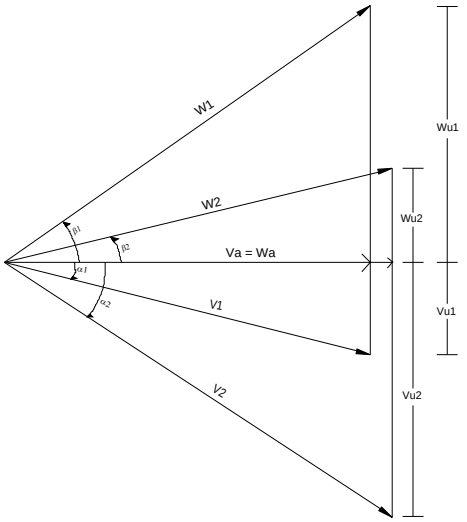

(a)

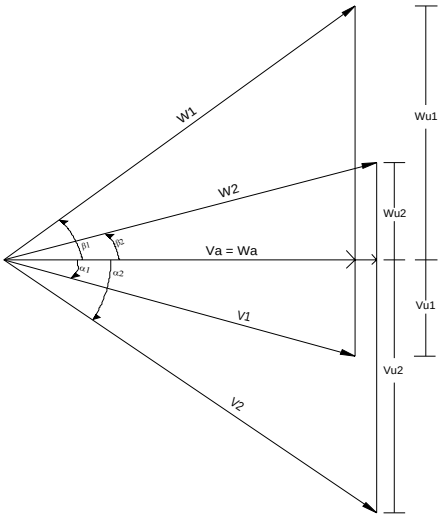

(b)

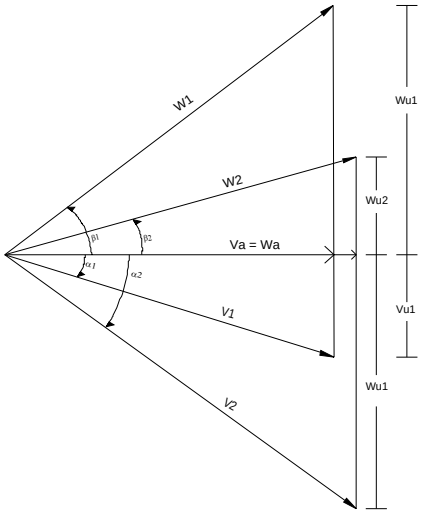

(c)

Figure 26. Point location #7 – (a) Throttle 5+4 (b) NOP (c) Near stall

D. PERFORMANCE RESULTS BUILD #2 AND COMPARISON WITH BUILD#1

From the test data, mass flow rate (Mflow), flow coefficient (Fco), and pressure-rise coefficient (Pco_e) were calculated and plotted for comparison with build #1. As shown in Figure 27 the rough-cast blades from build #2 produced very similar performance to that of the smooth-cast blades in build #1. Both smooth-cast and rough-cast blades showed the same trend in that the flow coefficient decreased and the pressure-rise coefficient increased as more throttle was applied.

Overall, the data between the two builds showed many similarities. The plots of pressure-rise coefficient versus flow coefficient showed that both blade configurations produced a similar pressure-rise for each throttle setting. As will be presented next, the velocity triangles showed the same trends at the different locations and different throttle settings. The largest differences were in the plots of total pressure and flow angle measured from the survey probes versus the radial distance along the blade. There was an increase in total pressure for the rough-cast blades as well as an increase in flow angles. But overall, the trends were similar to that of the smooth-cast blades.

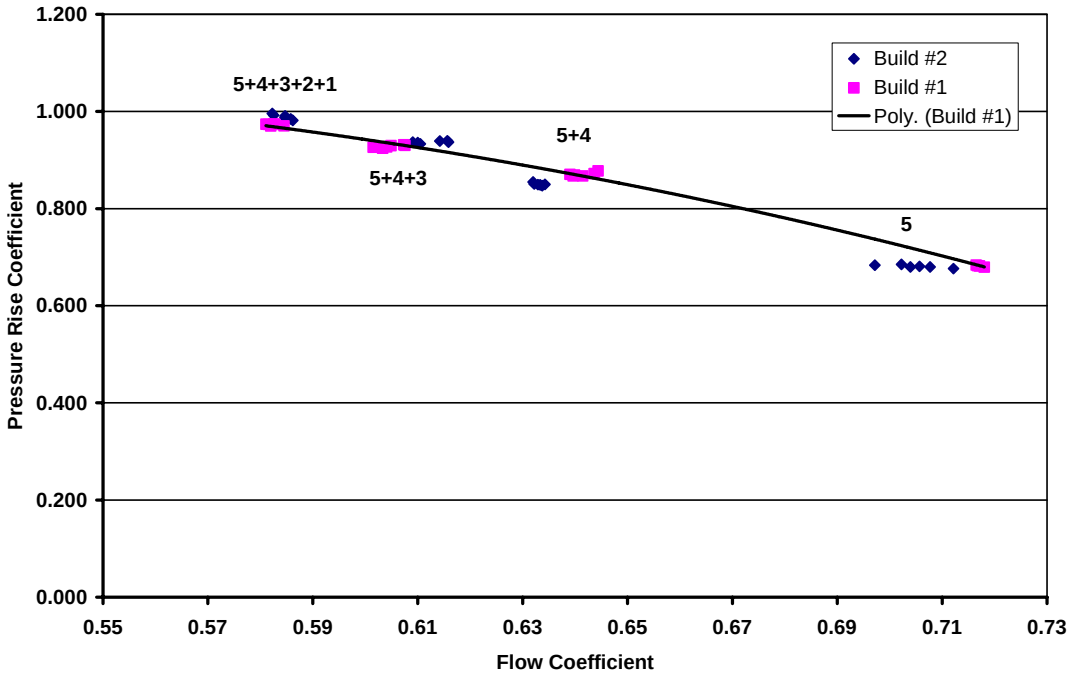

Figure 27. Pressure-rise coefficient versus flow coefficient for build #2

E. PROBE SURVEYS BUILD #2

1. Total Pressure versus Radial Distance

Figures 28-31 show the total pressure measured by the survey probes versus the radial distance (R/Rtip). The overall trend for build #2 showed an increase in pressure from both probes. A larger pressure loss at the tips was noted for build #2. The difference is due to the larger tip gap with the rough-cast blades.

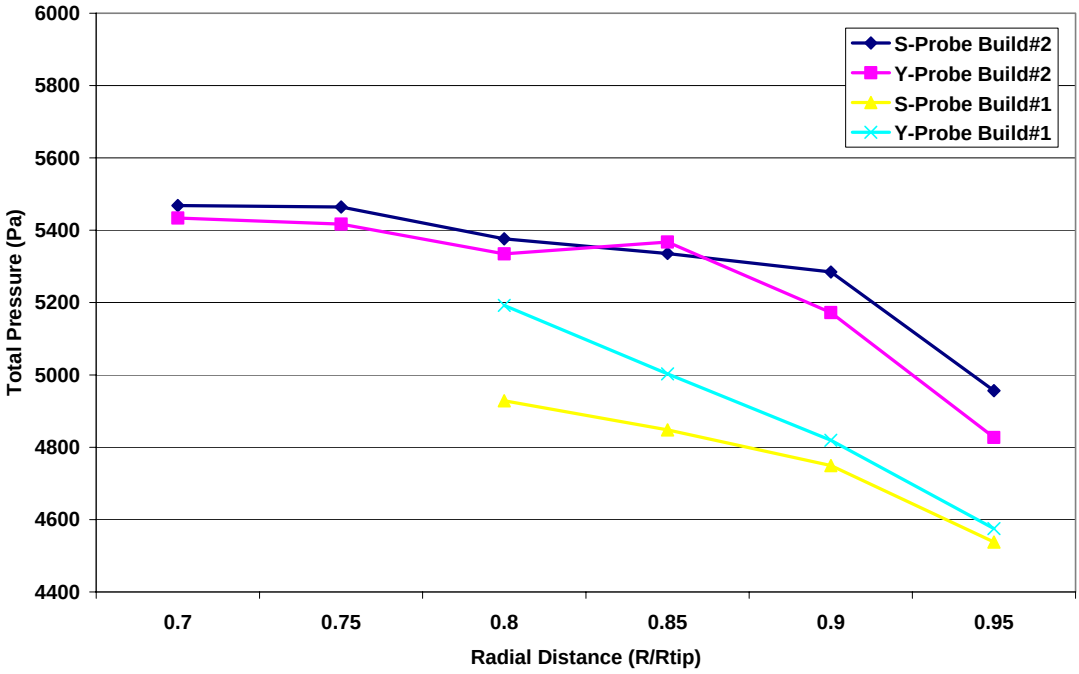

Figure 28. Total pressure versus radial distance at open throttle (5)

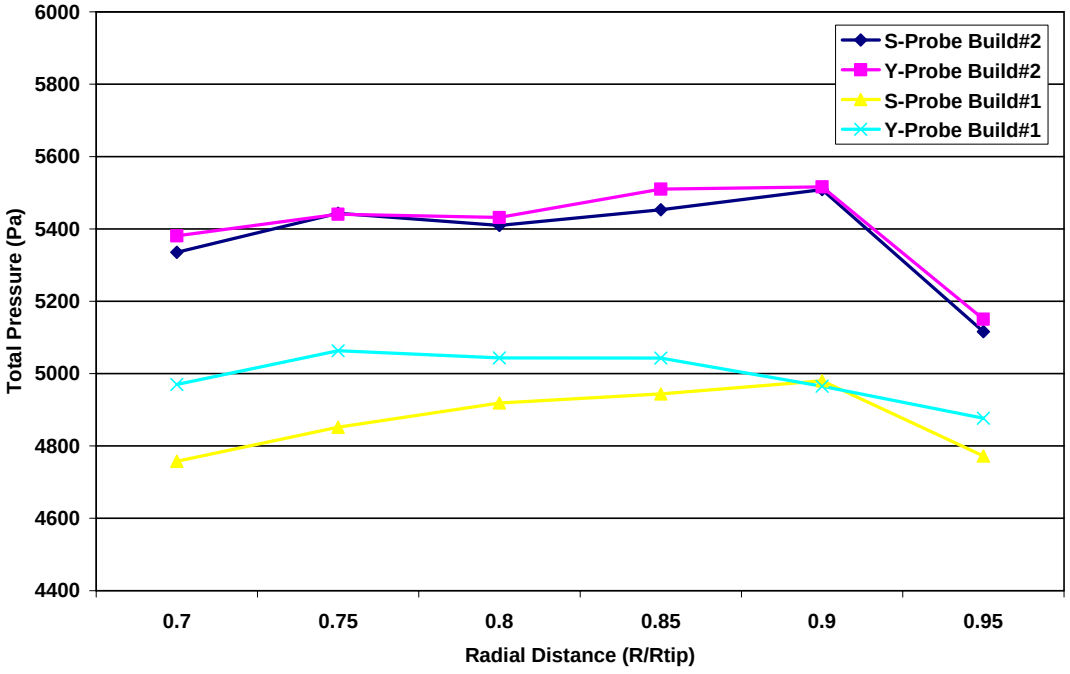

Figure 29. Total pressure versus radial distance for throttle setting 5+4

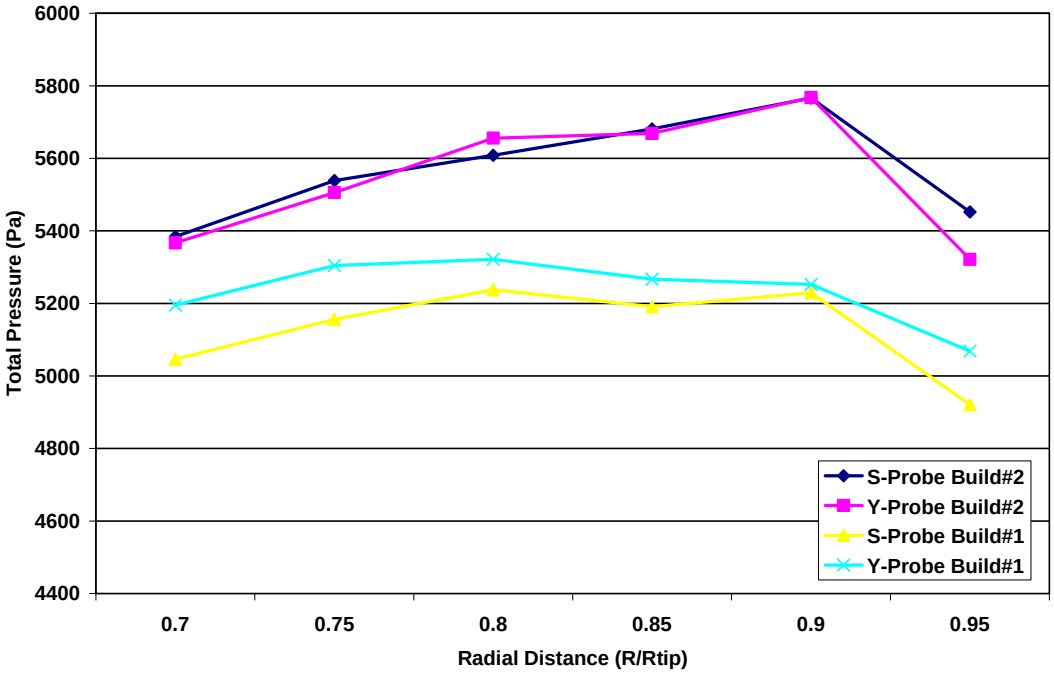

Figure 30. Total pressure vs radial distance for NOP

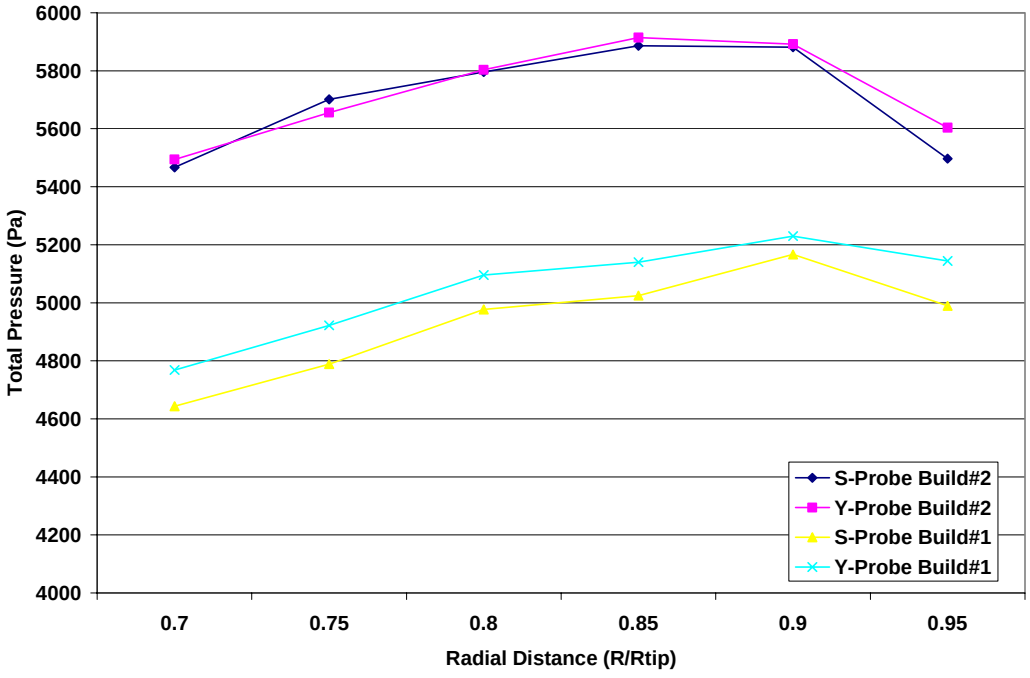

Figure 31. Total pressure vs radial distance at near stall

2. Velocity Distribution versus Radial Distance

a. Tangential Velocity Distribution

Figures 32-35 of the tangential velocity versus radial distance show the same overall trend as those for build #1.

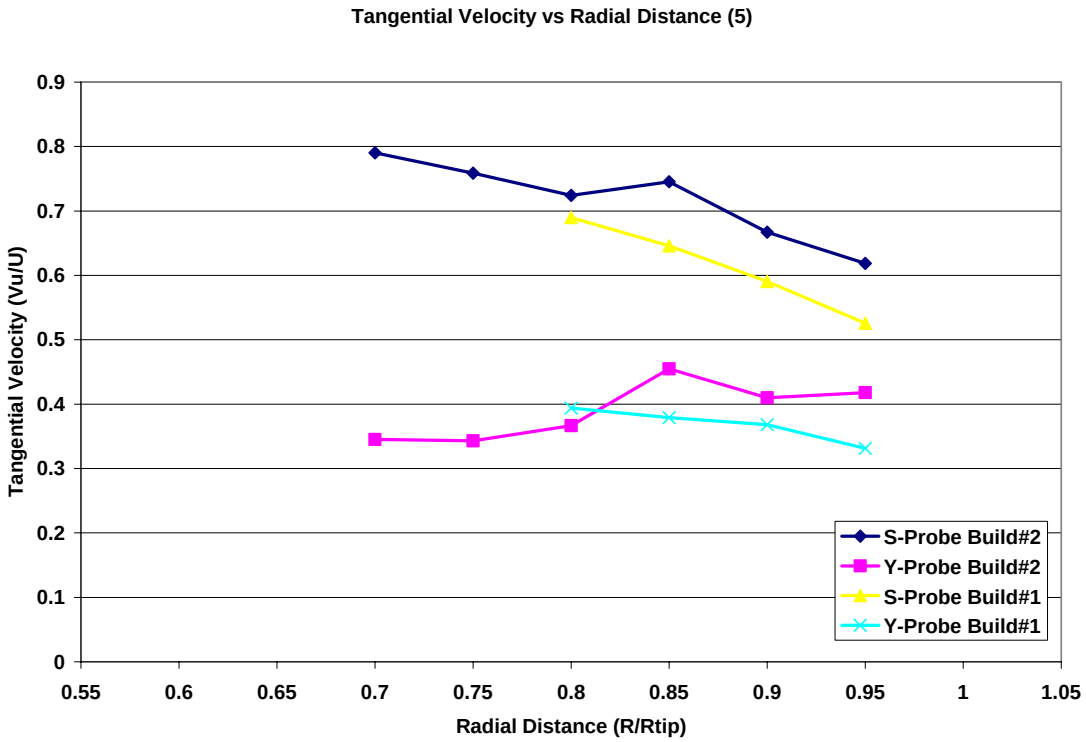

Figure 32. Tangential velocity vs radial distance at open throttle (5)

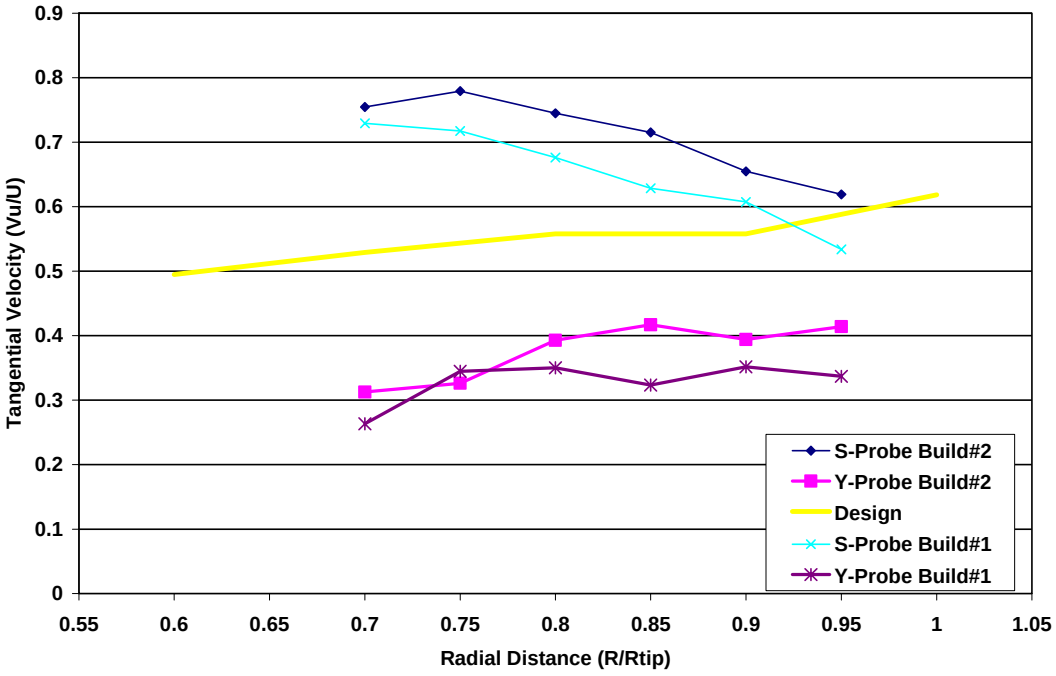

Figure 33. Tangential velocity vs radial distance for throttle setting 5+4

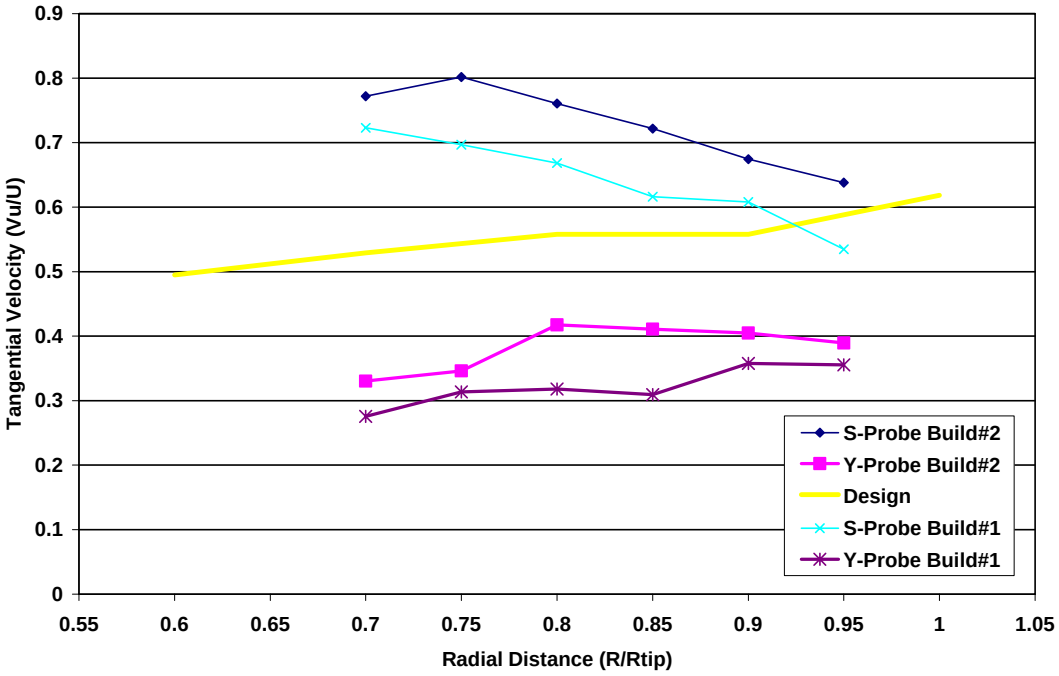

Figure 34. Tangential velocity vs radial distance for NOP (5+4+3)

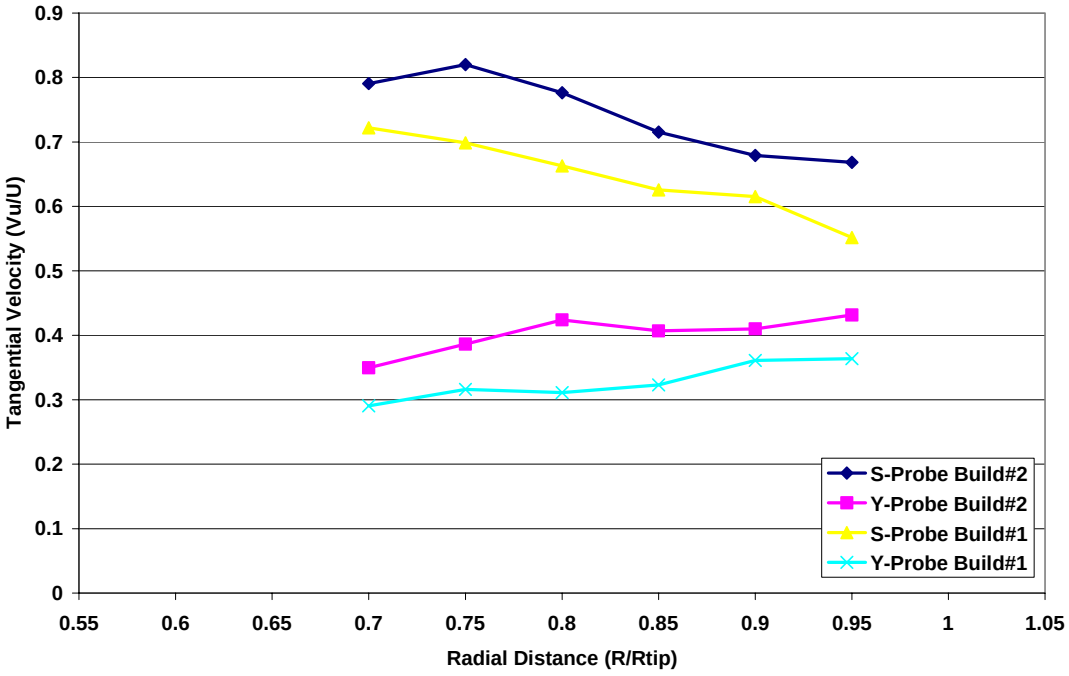

Figure 35. Tangential velocity vs radial distance at near stall

b. Axial Velocity Distribution

Figures 36-39 of axial velocity versus radial distance show the same trend as those of build #1.

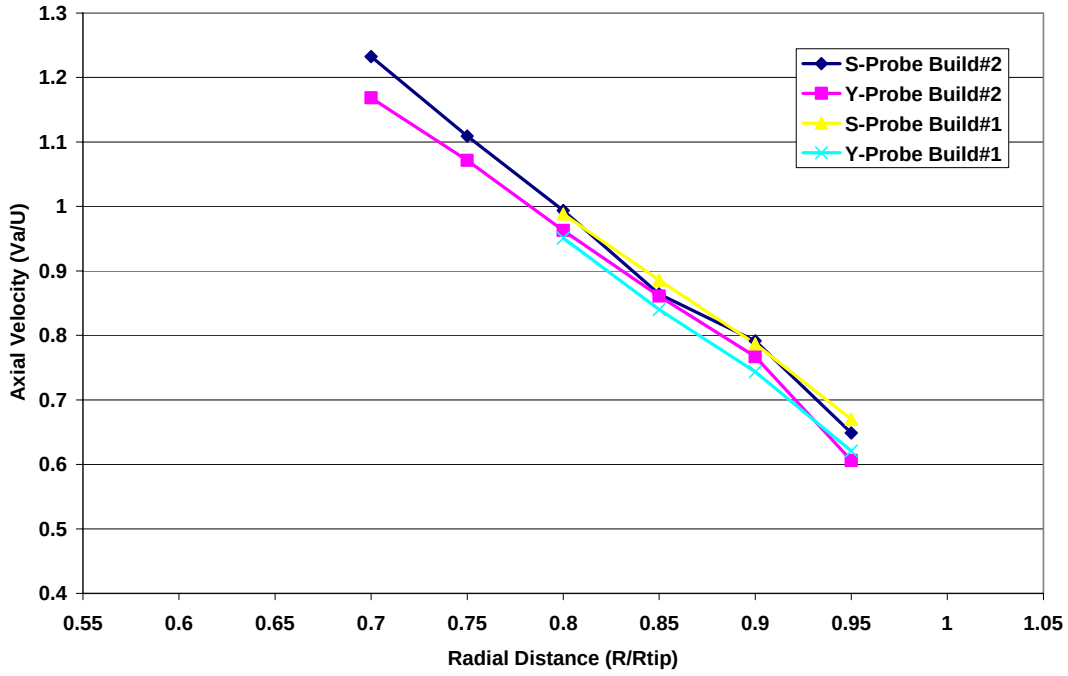

Figure 36. Axial velocity vs radial distance at open throttle (5)

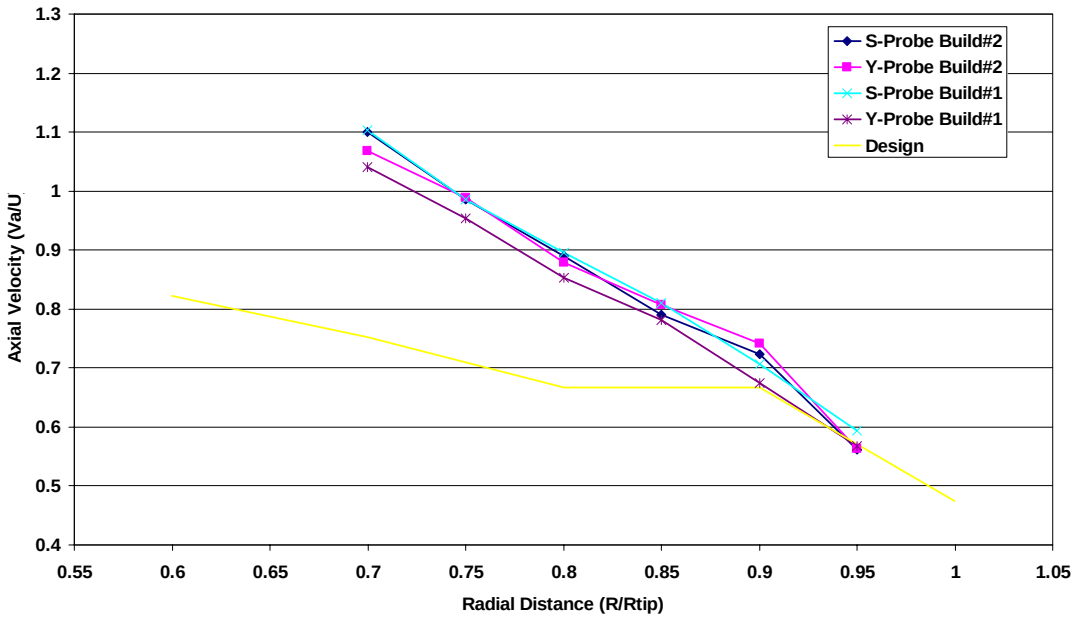

Figure 37. Axial velocity vs radial distance for throttle setting 5+4

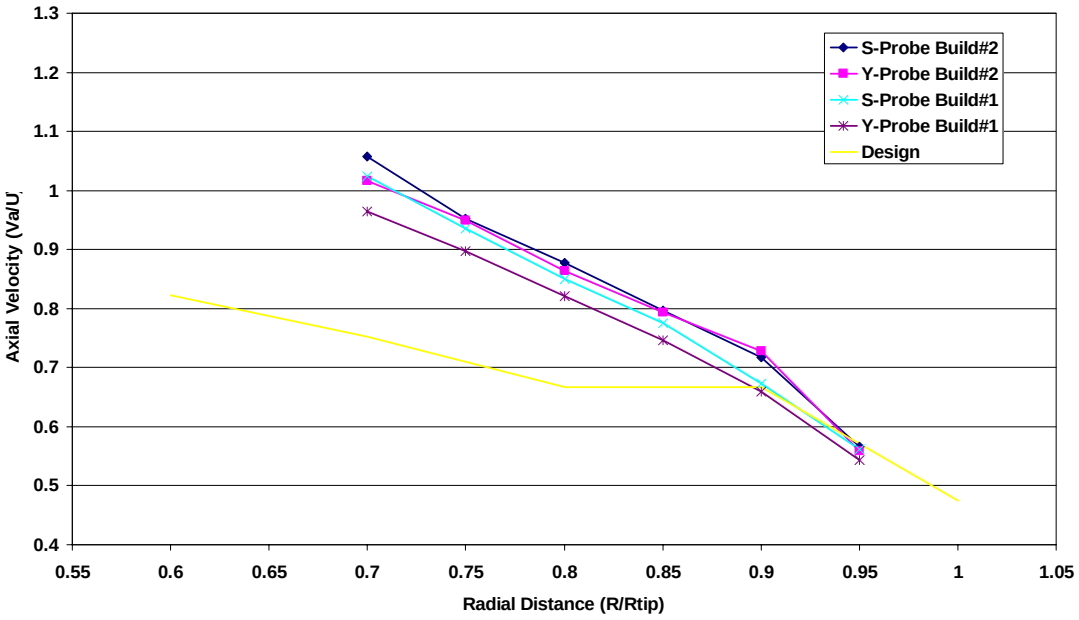

Figure 38. Axial velocity vs radial distance for NOP (5+4+3)

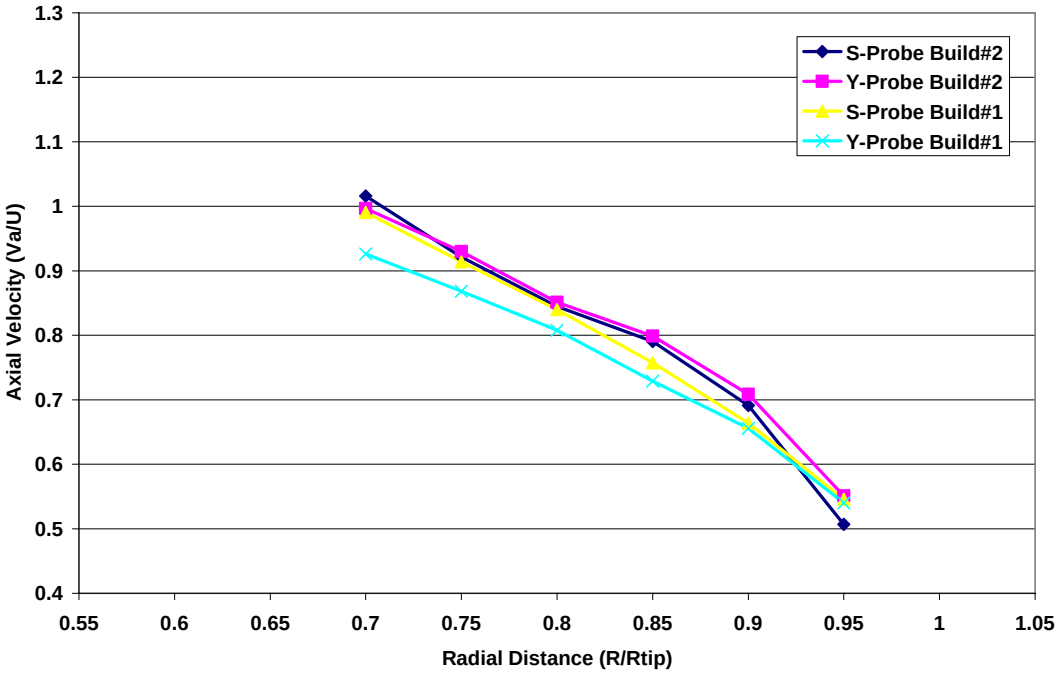

Figure 39. Axial velocity vs radial distance at near stall (5+4+3+2+1)

3. Flow Angle versus Radial Distance

Figures 40-43 show the flow angle measured from the survey probes versus the radial distance (R/Rtip). The flow angles for build #2 increased compared to those of build #1.

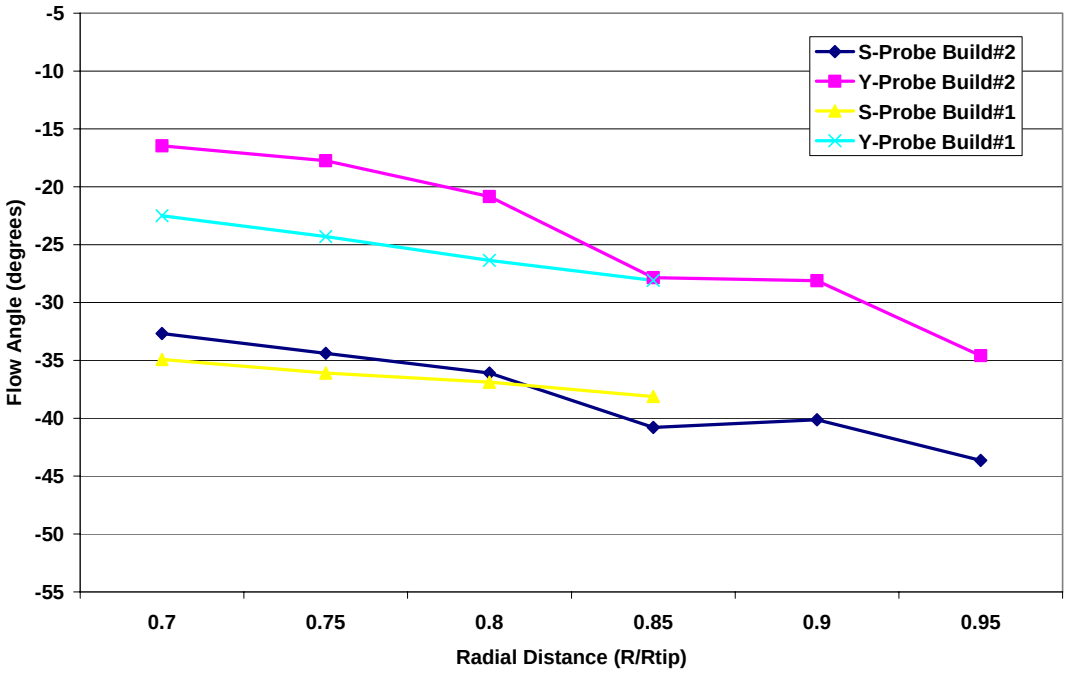

Figure 40. Flow angle versus radial distance at open throttle (5)

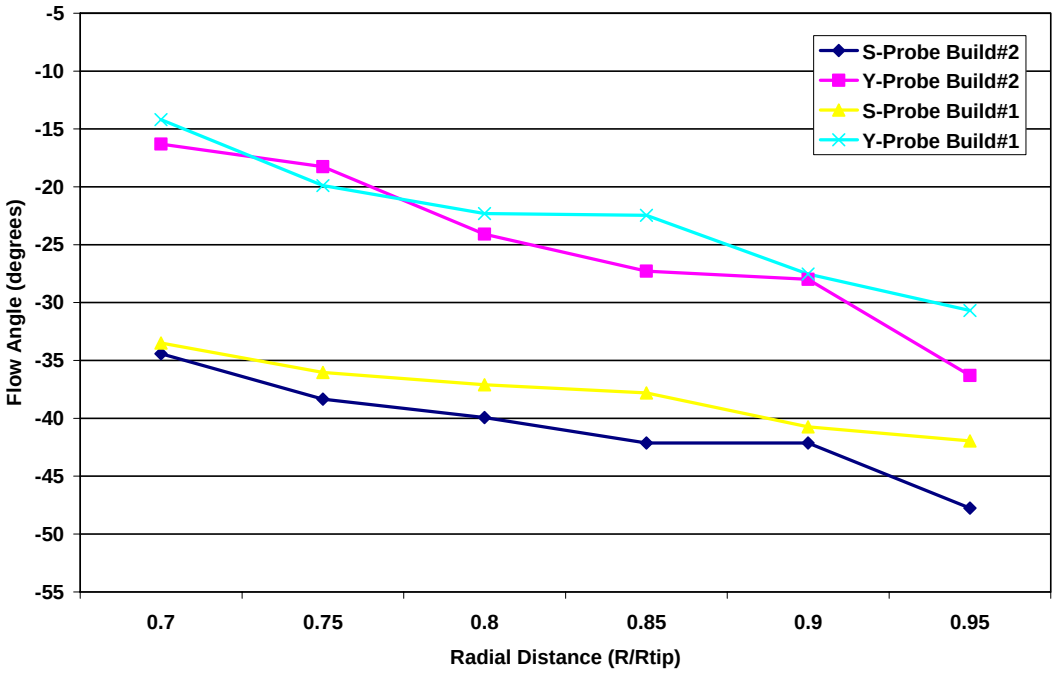

Figure 41. Flow angle versus radial distance for throttle setting 5+4

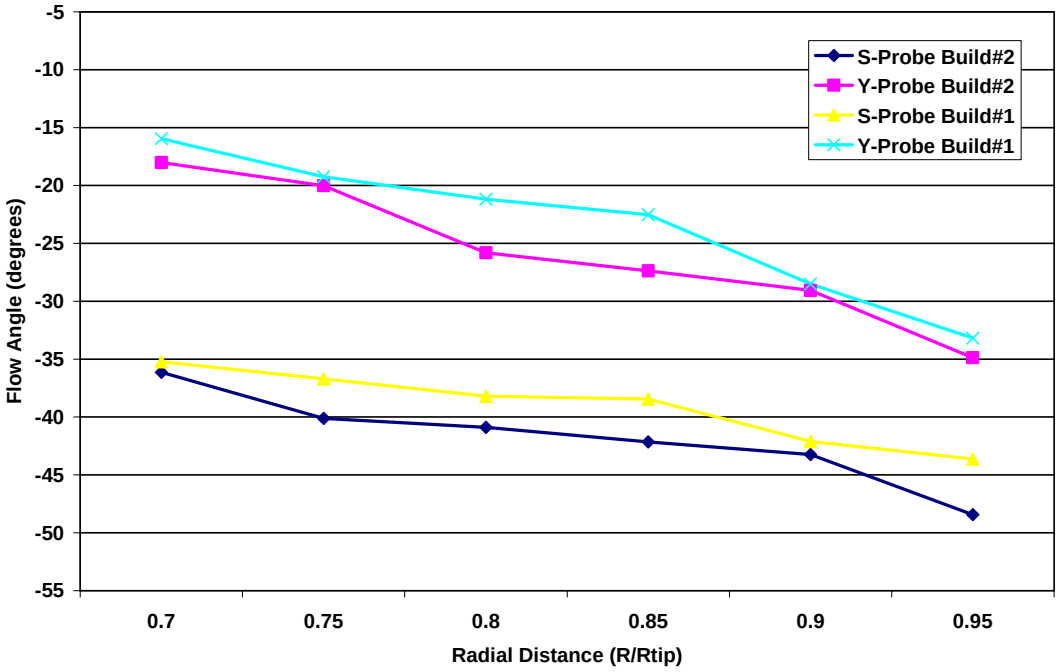

Figure 42. Flow angle versus radial distance for NOP (5+4+3)

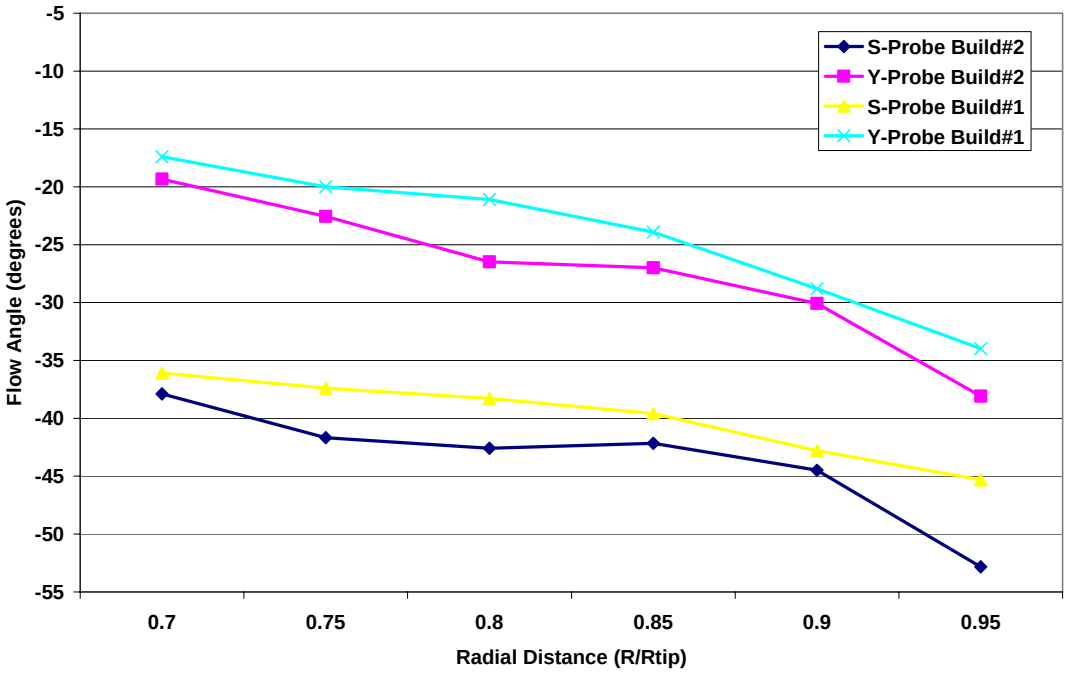

Figure 43. Flow angle vs radial distance at near stall (5+4+3+2+1)

F. VELOCITY TRIANGLES BUILD #2

The velocity triangles for build #2 show the same trends as the velocity triangles for build #1, as was expected. However, at the NOP the axial velocity showed less change through the second stage than build #1.

1. Point Location # 2

Figures 44a-d show the velocity diagrams for point location #2 for all throttle settings.

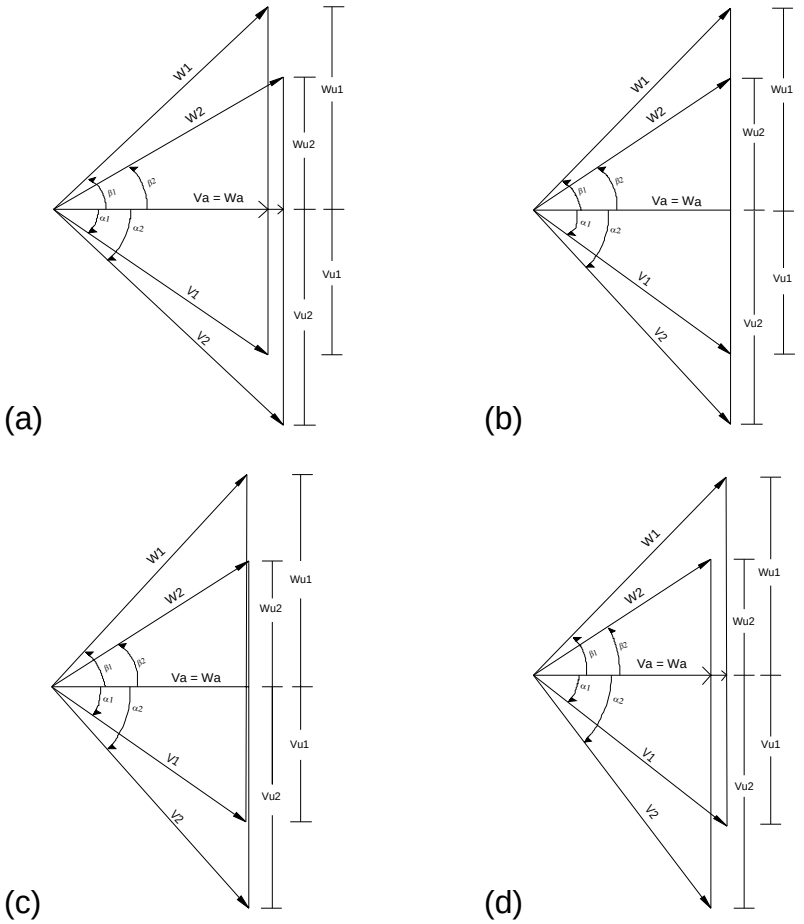

Figure 44. Point location #2 – (a) Open throttle (b) Throttle 5+4 (c) NOP (d) Near stall

2. Point Location # 4

Figures 45a-d show the velocity diagrams for point location # 4 for all throttle settings.

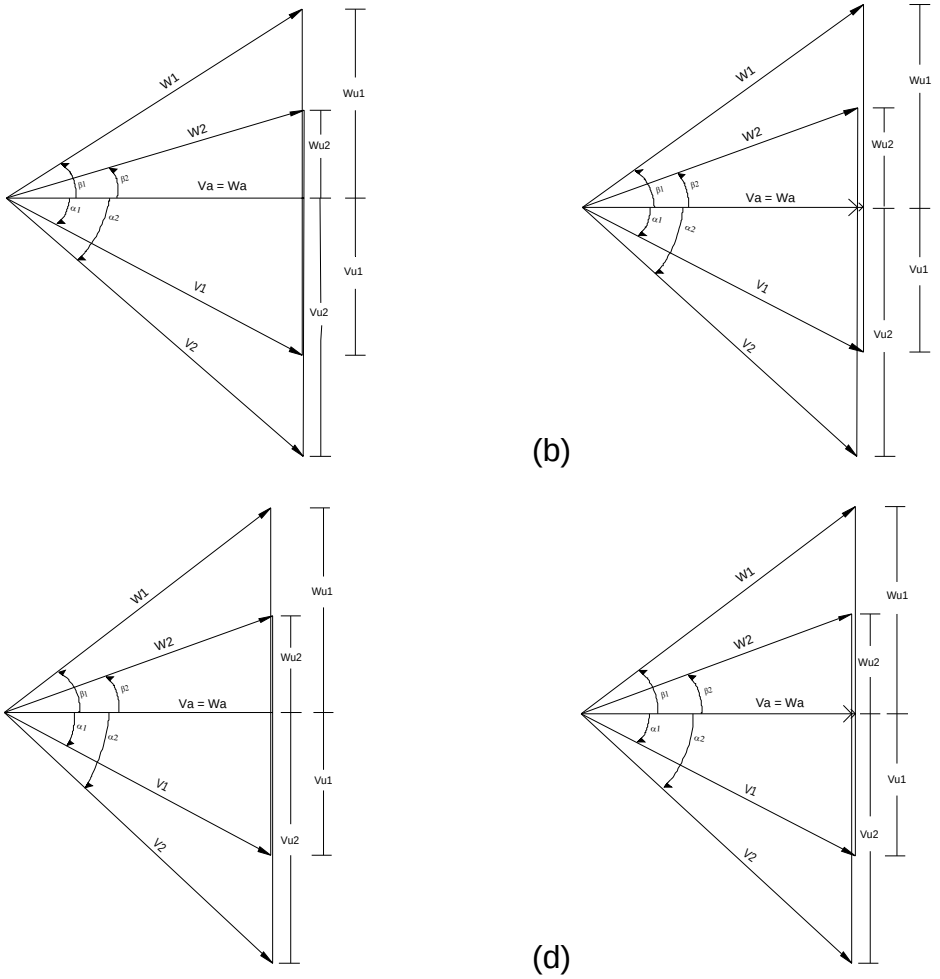

Figure 45. Point location #4 – (a) Open throttle (b) Throttle 5+4 (c) NOP (d) Near stall

3. Point Location # 7

Figures 46a-d show the velocity diagrams for point location # 7 for all throttle settings.

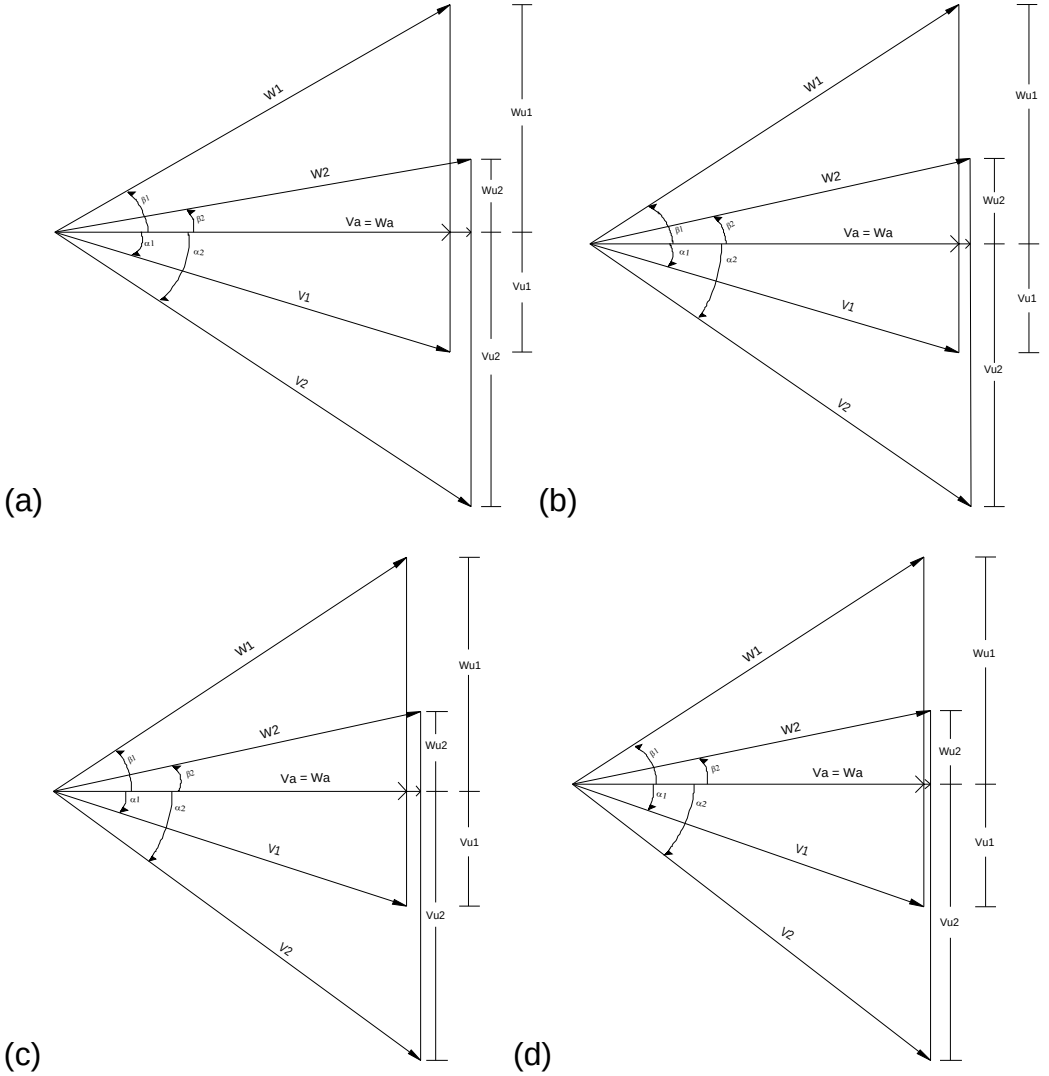

Figure 46. Point location #7 – (a) Open throttle (b) Throttle 5+4 (c) NOP (d) Near stall

THIS PAGE INTENTIONALLY LEFT BLANK

V. CONCLUSIONS AND RECOMMENDATIONS

A. CONCLUSIONS

Very few performance comparisons have been made between smooth and rough-cast blades. Completing the baseline performance of the compressor and reblading the compressor with the rough sand-cast aluminum blades and repeating the performance measurement, in the present study, was a success. The implementation of the high-temperature, deep-groove ball bearing was also successful, particularly for the long-term operation of the compressor.

The results for build #2 were better than expected since the rough-cast blades showed virtually no loss in pressure-rise despite the blade surface roughness and larger tip gap. A possible reason for this performance was that a different type of inlet guide vanes was installed for build #2.

The overall performance of the rough-cast blades was very similar to that of the smooth-cast blades. The similarities between results from the two builds showed that the rough-cast blades set up similar flow in the compressor to the smooth-cast blades. This suggests that rough-cast blades can be used to obtain an initial baseline performance of a low-speed multistage compressor design. Rough-cast blades could also be used as the initial stages of a compressor in order to set up an embedded-stage test of smooth blading. The new aluminum blades can also be used in the future for more severe testing involving stall due to inlet distortion.

B. RECOMMENDATIONS

A complete performance comparison should be made by measuring the efficiency at the various throttle settings for build #2. Also a study of how much the inlet guide vanes affect the performance of the compressor should be made. This would be accomplished by varying the angle of the IGVs and examining how it affects the performance results. It would also be beneficial to have the correct

IGVs sand cast and installed in the compressor. Computer modeling would be beneficial if it could be used to account for the performance differences found with the rough-cast blades and produce results to compare with the results of smooth-cast blades. Finally, a third stage should be added to examine the effects on the embedded stage and overall compressor performance.

APPENDIX A. PICTURES OF DISASSEMBLY / ASSEMBLY

A.1. SETUP OF THE MULTISTAGE COMPRESSOR

Figures A1-A3 show the setup of the probes on the compressor before disassembly.

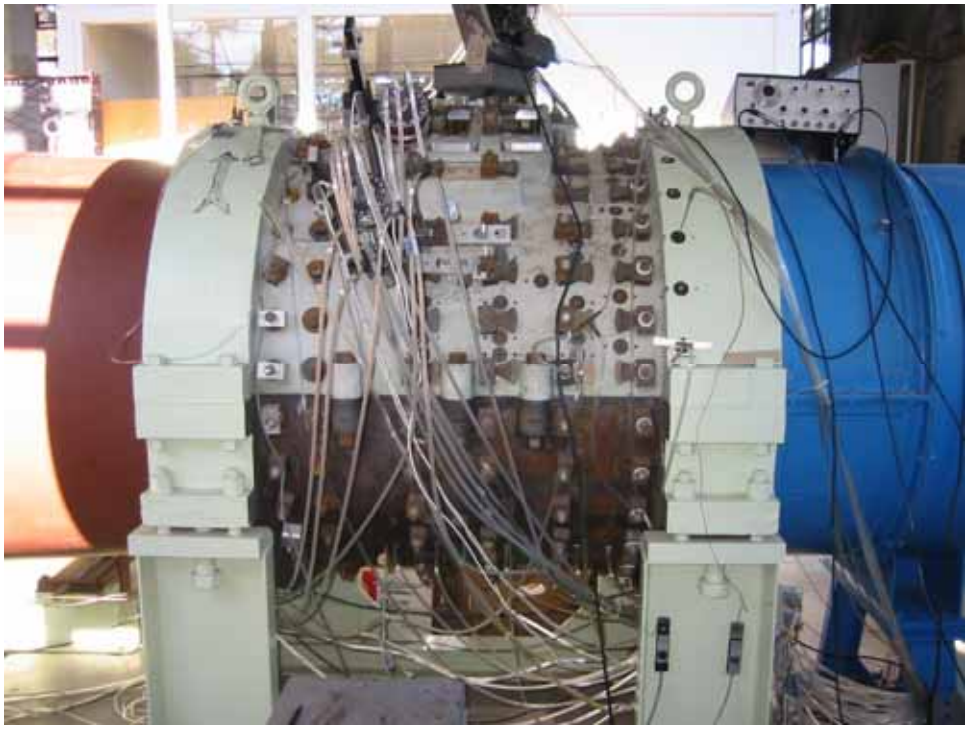

Figure A1. Probe survey setup of the LSMSC

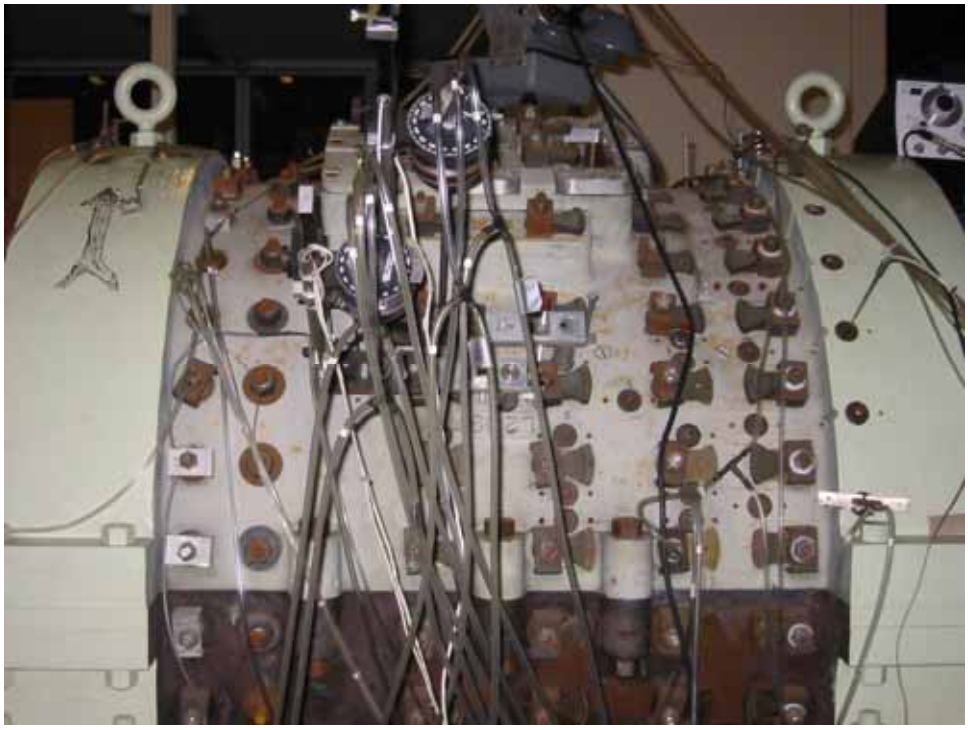

Figure A2. Close-up of probe survey setup for the LSMSC (south side)

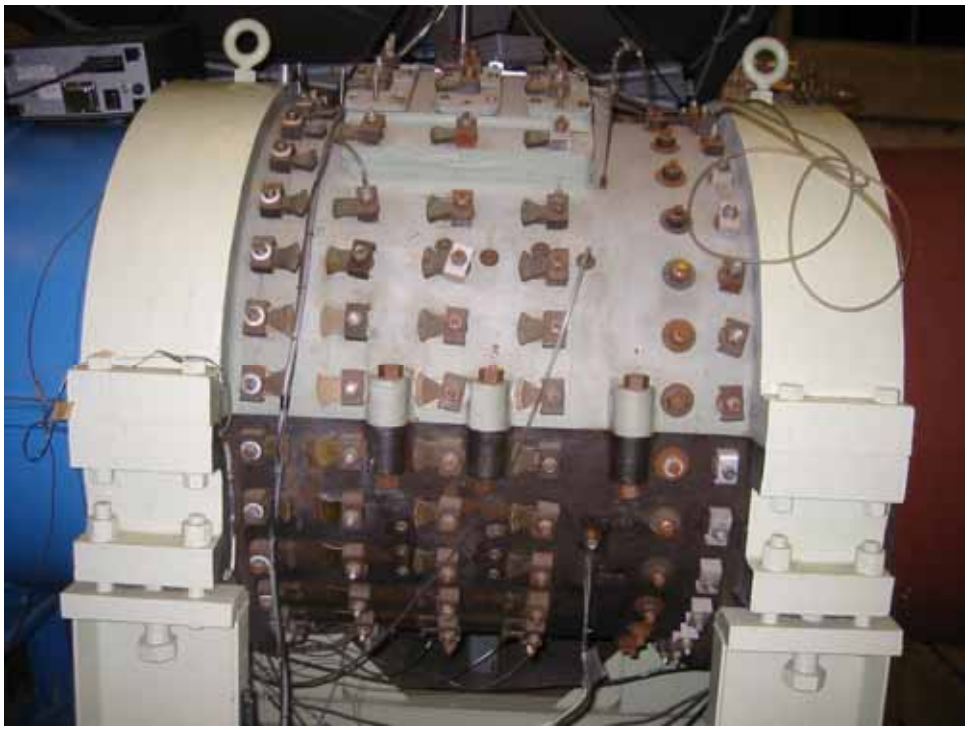

Figure A3. North side of the LSMSC

A.2. DISASSEMBLY OF THE MULTISTAGE COMPRESSOR

Figures A4-A15 show the disassembly of the compressor.

Figure A4. Top shell removed/blocks in place to guide rotor out of bottom shell

Figure A5. Rotor hub on blocks

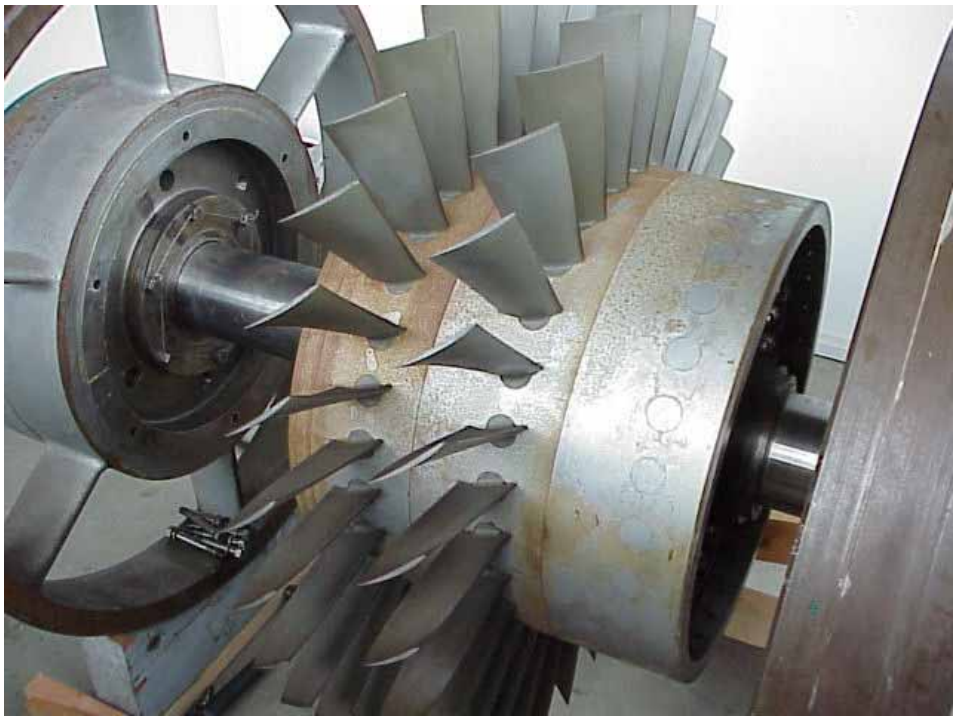

Figure A6. Close-up of smooth-cast (plastic) rotor blades and rotor hub

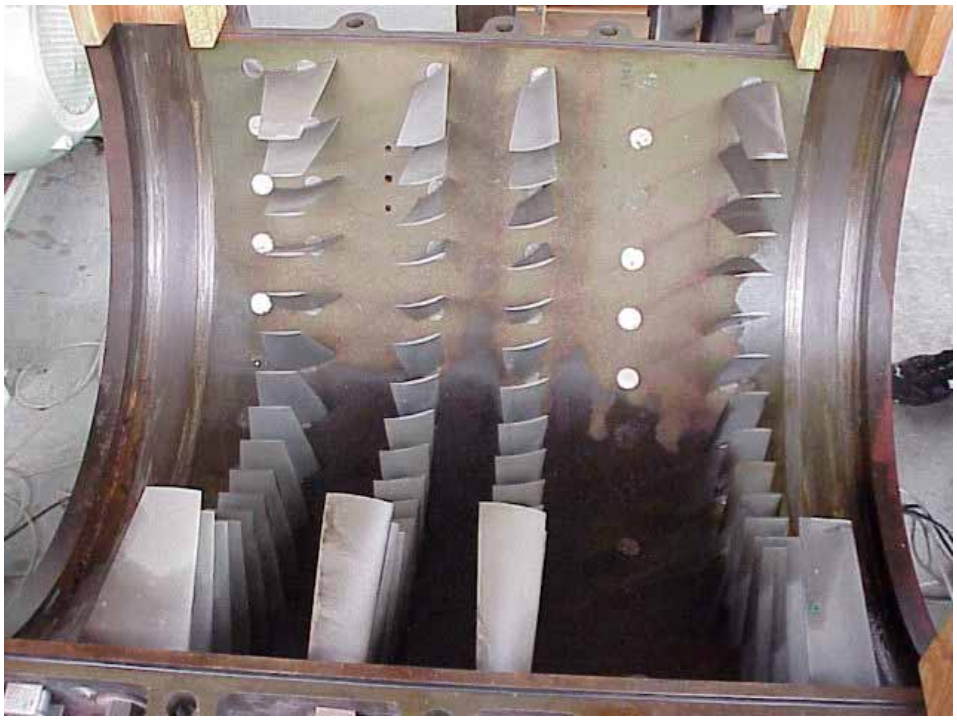

Figure A7. Bottom shell with smooth-cast blades: Inlet guide vanes (far right), Stator blades (middle two rows), Exit guide vanes (far left)

Figure A8. Close-up of smooth-cast stator blades

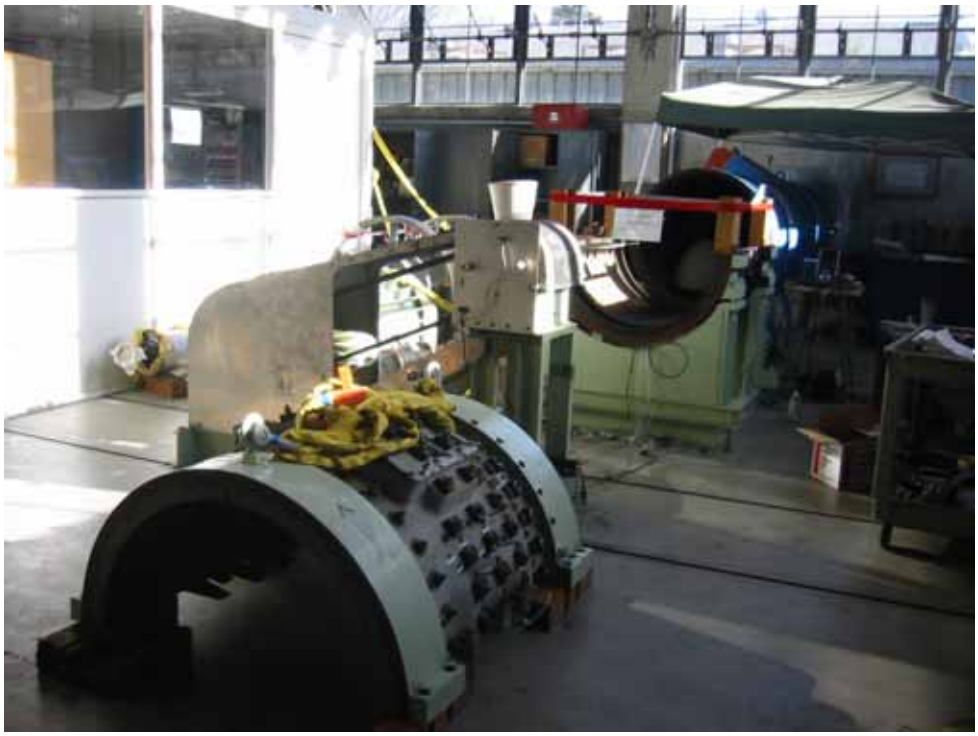

Figure A9. Upper casing foreground with LSMSC facility in background

Figure A10. Bottom shell of LSMSC with blades removed

Figure A11. Stator blades that were installed in LSMSC: Two longer stemmed stator blades were used in the top shell where it was raised up

Figure A12. Smooth-cast (top) and rough-cast (bottom) rotor blades

Figure A13. Smooth-cast (top) and rough-cast (bottom) stator blades

Figure A14. Smooth-cast inlet guide vane (IGV), all rough-cast IGVs were used

Figure A15. Smooth (top) and rough (bottom) cast exit guide vanes (EGVs)

A.3. ASSEMBLY OF THE MULTISTAGE COMPRESSOR

Figures A16-A26 show the assembly of the compressor with the new rough-cast blades.

Figure A16. Top shell with rough-cast blades: Inlet guide vanes (top), stator blades (middle two rows), exit guide vanes (bottom)

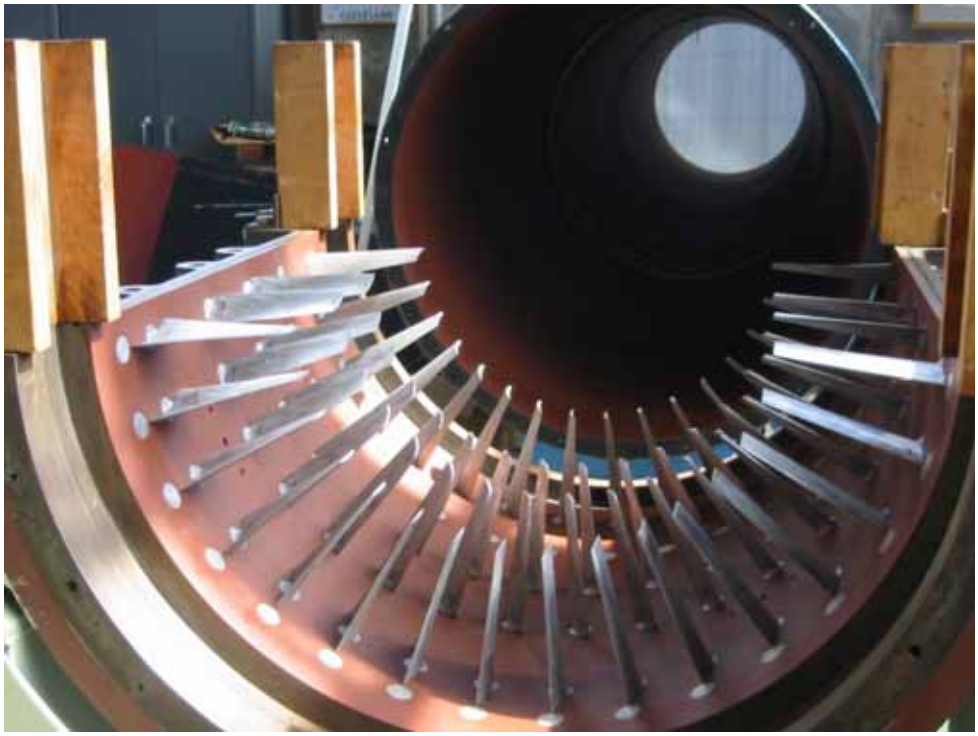

Figure A17. Bottom shell of LSMSC with new rough-cast (aluminum) blades

Figure A18. Bottom shell with rough-cast blades: Inlet guide vanes (far right), stator blades (middle two rows), exit guide vanes (far left)

Figure A19. Rotor hub completely assembled with rough-cast blades

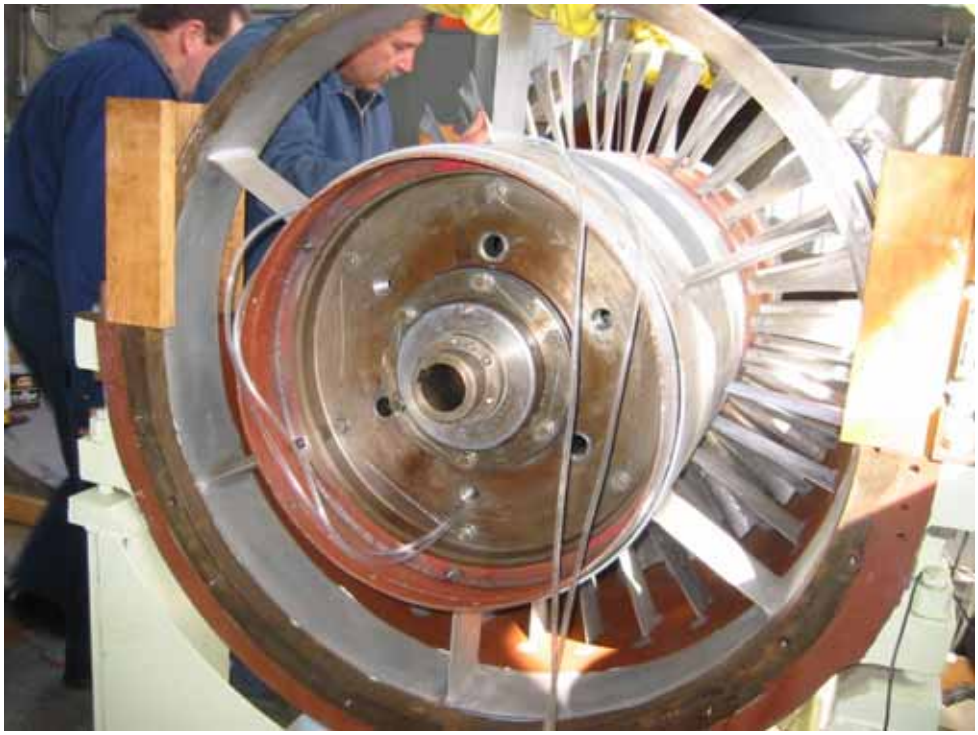

Figure A20. Rotor hub installed in bottom shell of LSMSC

Figure A21. Top shell being installed onto bottom shell using metal guide poles

Figure A22. Blade clearance of bottom shell with rotor hub

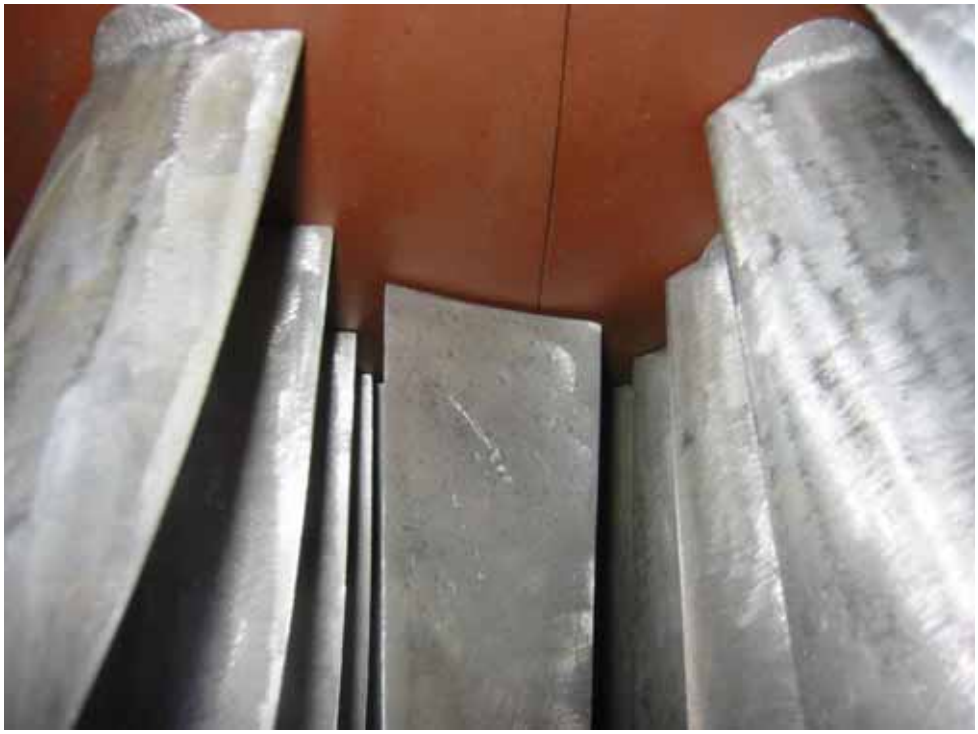

Figure A23. Stator blade clearance with hub

Figure A24. Inlet guide vane clearance with hub

Figure A25. Exit guide vane clearance with hub

Figure A26. Rotor blade clearance with shell

APPENDIX B. CHANGES TO HP VEE PROGRAM

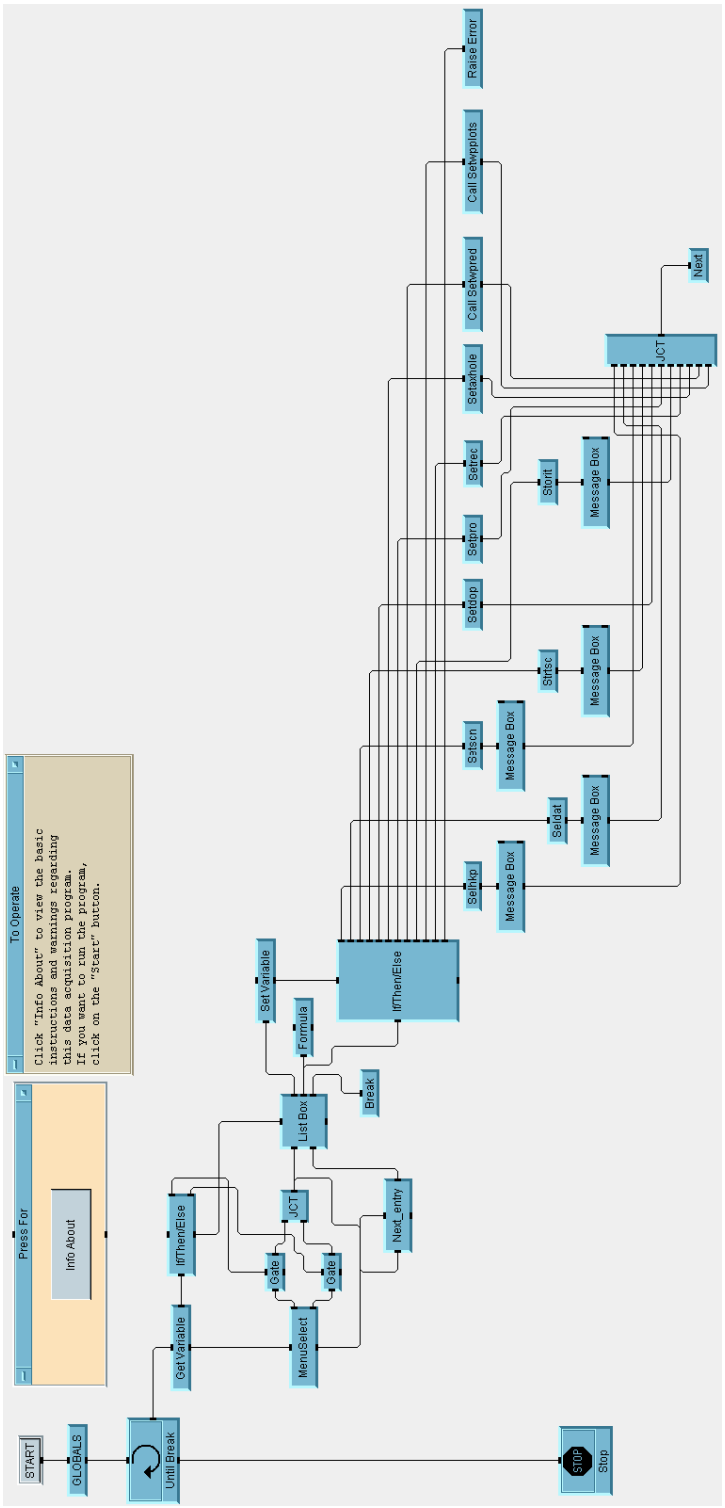

Figure B1. Main screen for HP Vee program

Figure B2 shows the screen SELHKP. Based on the operator's input, this screen will setup the program to run either Lab #1 (Lab1 cc), Lab #2 (Lab2 vd), or Lab #3 (Lab3 wp) [Ref. 4]. All work for this thesis was run on the setup for Lab #2.

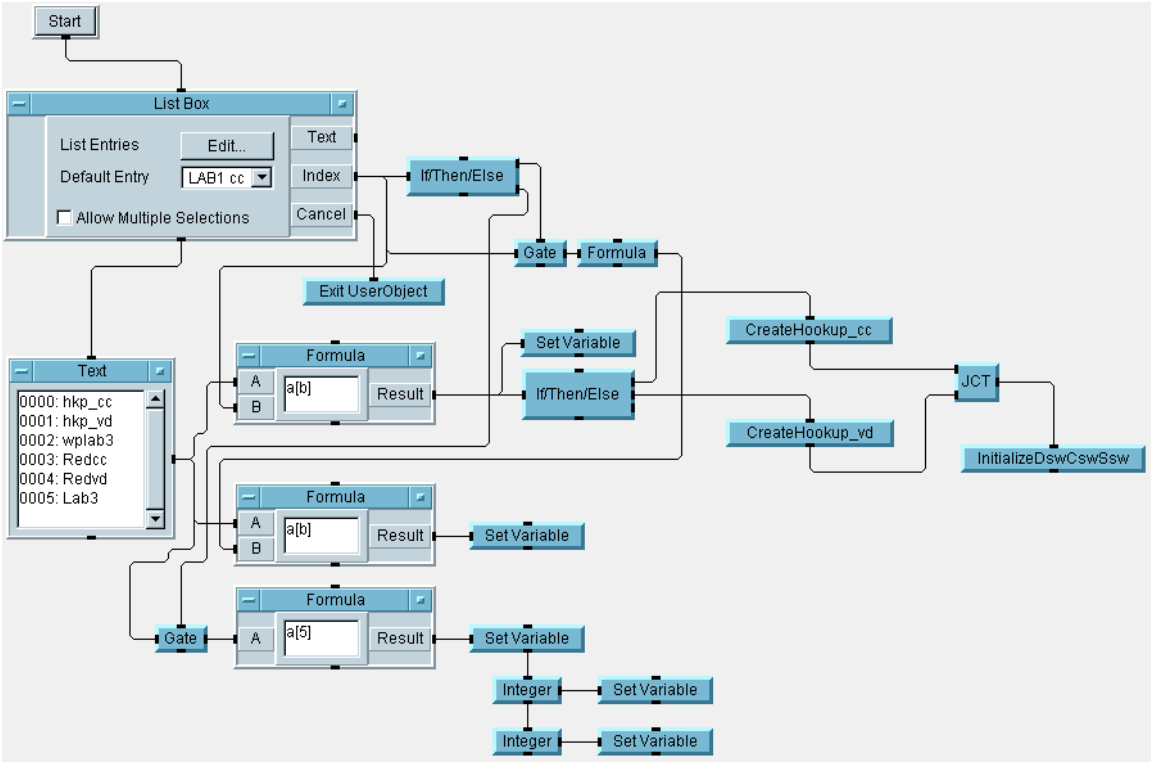

Figure B2. HP VEE screen display SELHKP

Figure B3 shows the screen for CreateHookup_vd which is the follow on screen after selecting Lab #2 in Figure B2.

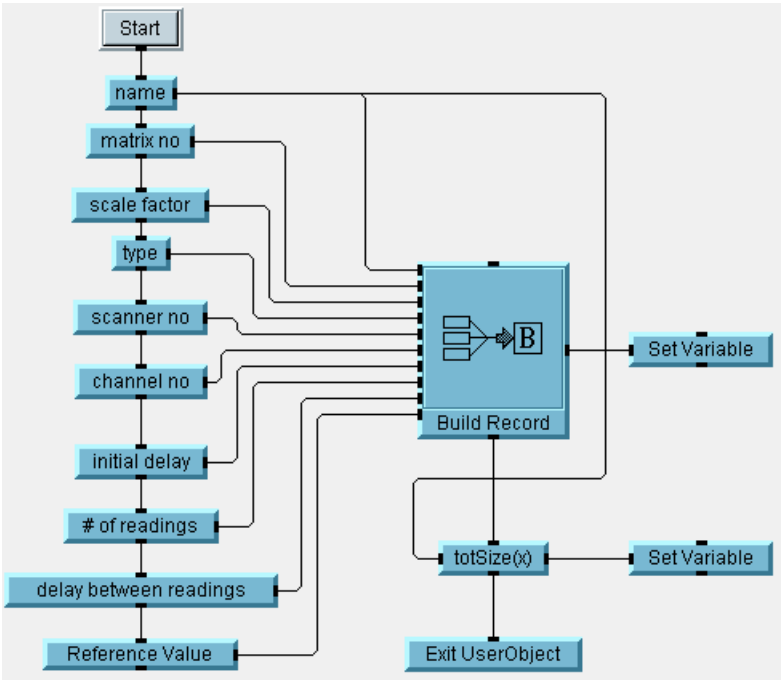

Figure B3. HP VEE screen display CreateHookup_vd

Table B1 shows the scale factors and scanivalve location for all pressure and temperature readings during the experiment. This table is an excel spreadsheet version of the same data found in the HP Vee screen “CreateHookup_vd in Figure B3.

Table B1. Reference sheet for all pressure and temperature readings

Line #	vbiname	vno	vscalf	t	sc	ch1	dely	mo	rdly	vrefval
0	PBAR	1	1	0	0	0	0.00E+00	0	0.00E+00	3.00E+01
1	Pabs	50	10000	1	1	204	1.00E+04	10	1.00E+04	3.00E+01
2	FBLD	7	1	0	0	0	0.00E+00	0	0.00E+00	8.05E+02
3	FBfv	11	10000	0	1	214	1.00E+04	9999	1.00E+04	8.05E+02
4	TRO	8	10000	0	1	101	1.00E+04	10	1.00E+04	0.00E+00
5	TWET	3	10000	0	1	102	1.00E+04	9999	1.00E+04	0.00E+00
6	P@21	191	10000	0	2	1	1.00E+04	9999	1.00E+04	0.00E+00
7	P#2	190	10000	0	2	2	1.00E+04	9999	1.00E+04	0.00E+00
8	P^2	196	10000	0	2	3	1.00E+04	9999	1.00E+04	0.00E+00
9	P0-T	12	10000	0	2	4	1.00E+04	9999	1.00E+04	0.00E+00
10	P0-S	13	10000	0	2	5	1.00E+04	9999	1.00E+04	0.00E+00
11	P2SW	84	10000	0	2	7	1.00E+04	9999	1.00E+04	0.00E+00
12	PE-S	89	10000	0	2	12	1.00E+04	9999	1.00E+04	0.00E+00
13	PR1-1	70	10000	0	2	13	1.00E+04	9999	1.00E+04	0.00E+00
14	PR1-2	71	10000	0	2	14	1.00E+04	9999	1.00E+04	0.00E+00
15	PR1-3	72	10000	0	2	15	1.00E+04	9999	1.00E+04	0.00E+00
16	PR1-4	73	10000	0	2	16	1.00E+04	9999	1.00E+04	0.00E+00
17	PR1-5	74	10000	0	2	17	1.00E+04	9999	1.00E+04	0.00E+00
18	PR1-6	75	10000	0	2	18	1.00E+04	9999	1.00E+04	0.00E+00
19	PR1-7	76	10000	0	2	19	1.00E+04	9999	1.00E+04	0.00E+00
20	PR1-8	77	10000	0	2	20	1.00E+04	9999	1.00E+04	0.00E+00
21	PR1-9	78	10000	0	2	21	1.00E+04	9999	1.00E+04	0.00E+00
22	PR1-0	79	10000	0	2	22	1.00E+04	9999	1.00E+04	0.00E+00
23	PR1-A	80	10000	0	2	23	1.00E+04	9999	1.00E+04	0.00E+00
24	PR1-B	81	10000	0	2	24	1.00E+04	9999	1.00E+04	0.00E+00
25	CS8	27	10000	0	2	45	1.00E+04	9999	1.00E+04	0.00E+00
26	P3-S	31	10000	0	2	46	1.00E+04	9999	1.00E+04	0.00E+00
27	P@22	192	10000	0	2	48	1.00E+04	9999	1.00E+04	0.00E+00
28	TAMB	2	1000	1	1	103	1.00E+04	10	1.00E+04	0.00E+00
29	P@31	194	10000	0	3	1	1.00E+04	9999	1.00E+04	0.00E+00
30	P#3	193	10000	0	3	2	1.00E+04	9999	1.00E+04	0.00E+00
31	P^3	197	10000	0	3	3	1.00E+04	9999	1.00E+04	0.00E+00
32	PX-1	33	10000	0	3	15	1.00E+04	9999	1.00E+04	0.00E+00
33	PX-2	34	10000	0	3	16	1.00E+04	9999	1.00E+04	0.00E+00
34	PX-3	113	10000	0	3	17	1.00E+04	9999	1.00E+04	0.00E+00
35	PX-4	35	10000	0	3	18	1.00E+04	9999	1.00E+04	0.00E+00
36	PX-5	36	10000	0	3	19	1.00E+04	9999	1.00E+04	0.00E+00
37	PY-1	37	10000	0	3	20	1.00E+04	9999	1.00E+04	0.00E+00
38	PY-2	38	10000	0	3	21	1.00E+04	9999	1.00E+04	0.00E+00
39	PY-3	114	10000	0	3	22	1.00E+04	9999	1.00E+04	0.00E+00
40	PY-4	39	10000	0	3	23	1.00E+04	9999	1.00E+04	0.00E+00
41	PY-5	40	10000	0	3	24	1.00E+04	9999	1.00E+04	0.00E+00
42	PS-1	45	10000	0	3	30	1.00E+04	9999	1.00E+04	0.00E+00
43	PS-2	116	10000	0	3	31	1.00E+04	9999	1.00E+04	0.00E+00
44	PS-3	117	10000	0	3	32	1.00E+04	9999	1.00E+04	0.00E+00
45	P@32	195	10000	0	3	48	1.00E+04	9999	1.00E+04	0.00E+00
46	RADX	56	1000	0	1	208	1.00E+04	9999	1.00E+04	0.00E+00
47	YAWX	62	10000	0	1	209	1.00E+04	9999	1.00E+04	0.00E+00
48	RADY	58	10	0	1	210	1.00E+04	9999	1.00E+04	0.00E+00
49	YAWY	57	1000	0	1	211	1.00E+04	9999	1.00E+04	0.00E+00
50	RADS	63	10	0	1	212	1.00E+04	9999	1.00E+04	0.00E+00
51	YAWS	64	1000	0	1	213	1.00E+04	9999	1.00E+04	0.00E+00
52	TORQ	6	10000	0	1	215	1.00E+04	20	1.00E+04	0.00E+00

Figure B4, shows the screen the tells the program to store the raw data collected from the scanivalves and saves it to a text file so that it can later be converted into an excel spreadsheet.

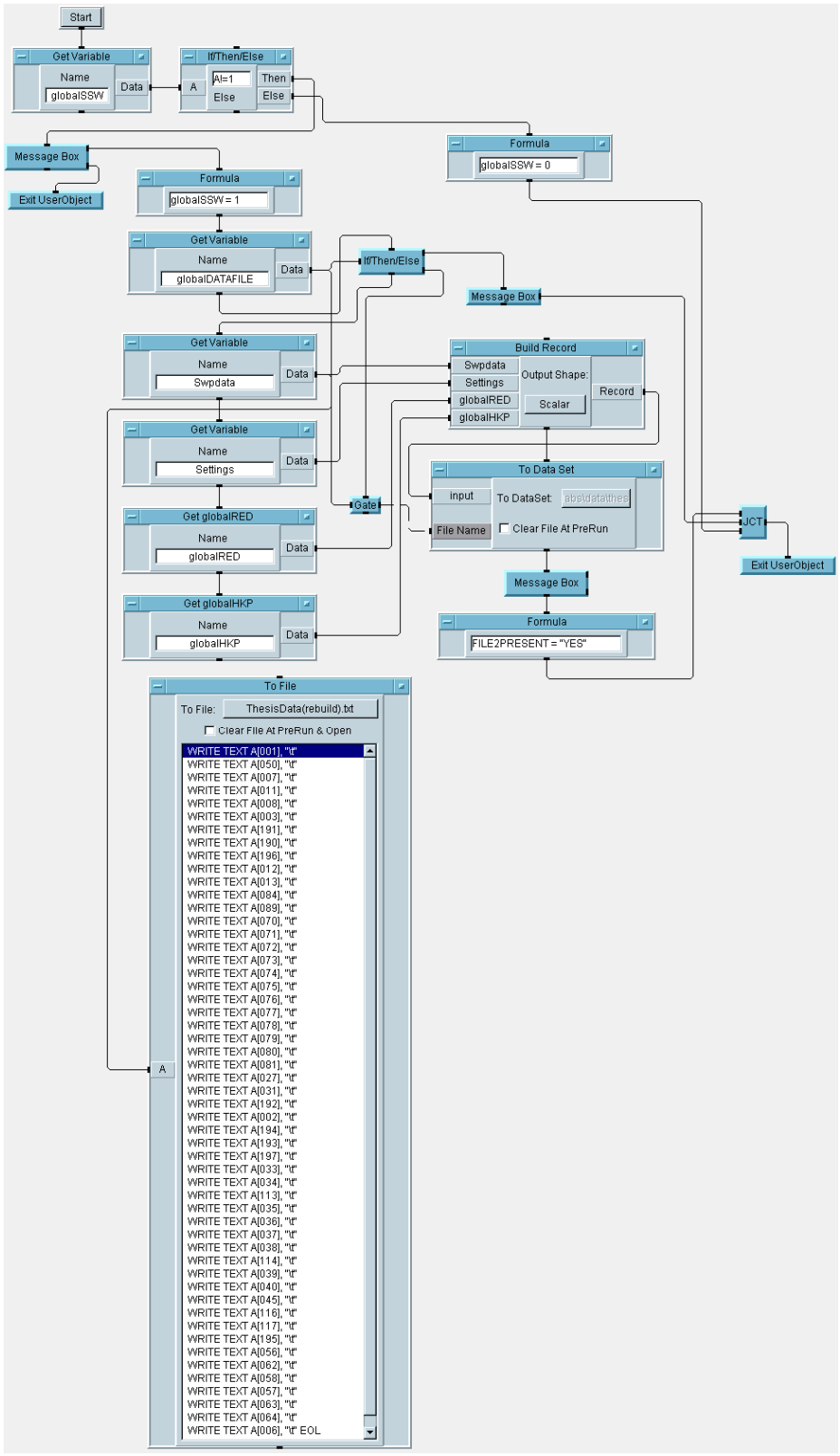

Figure B4. HP VEE screen display STORIT

The screen below, Figure B5, controls the raw data processing and is dependant upon which lab is used. Call Red_lab is the screen that is used to process the data for this experiment.

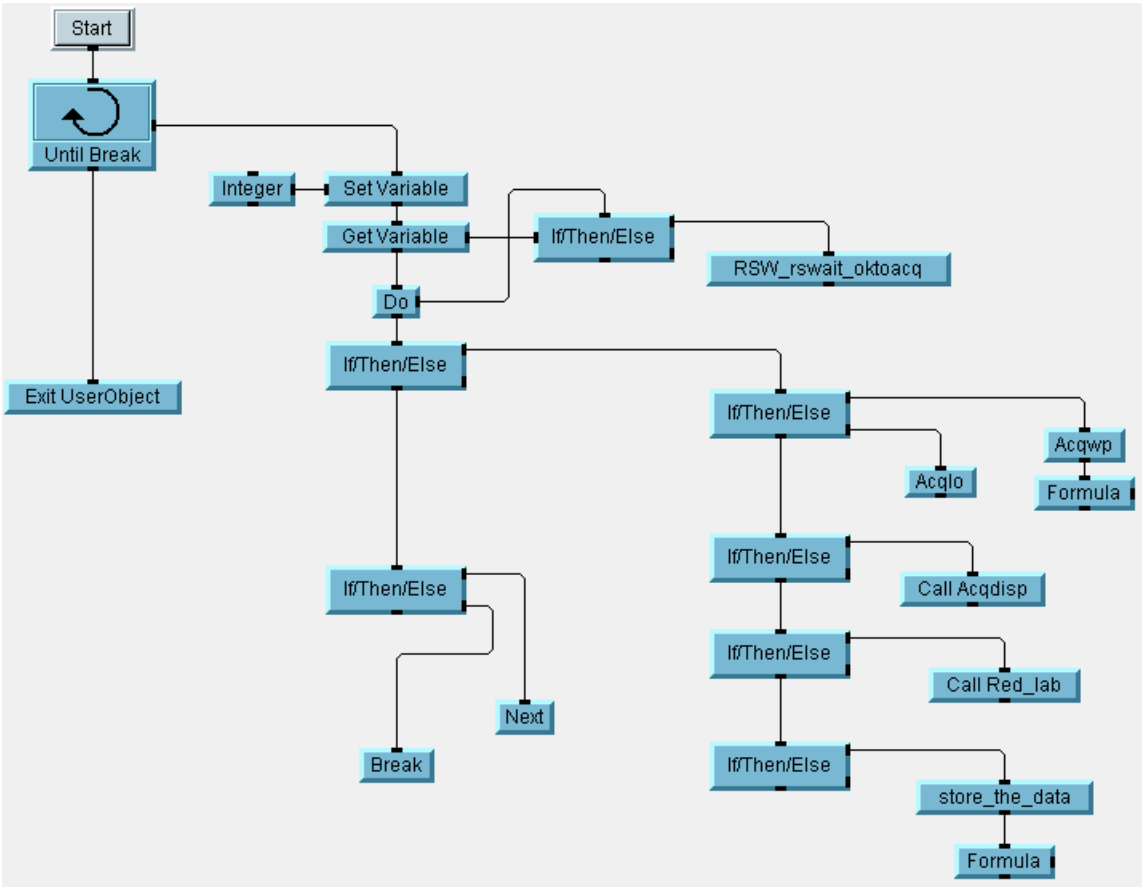

Figure B5. HP VEE screen display SETPRO

Figure B6 shows the screen for Call Red_lab. This screen was modified from the original program so that the data processing for Lab #1 (Red_lab_Redcc) would be accessed as well as the data processing for Lab #2 (Red_lab_Redvd).

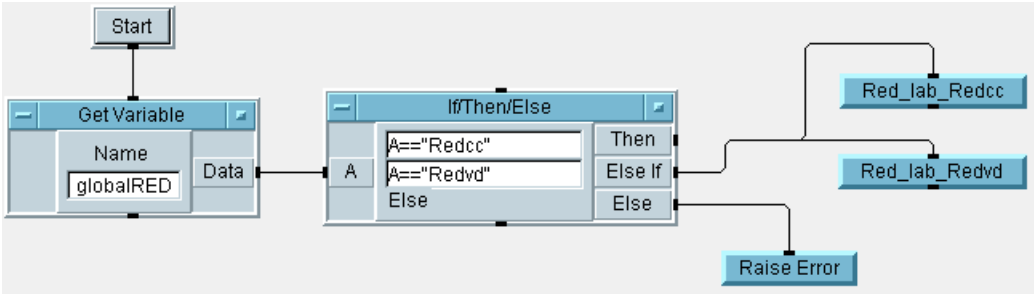

Figure B6. HP VEE screen display Call_Red_lab.

Figure B7 shows the screen Red_lab_Redcc which processes the data for Lab #1. This screen also saves the processed data for this portion into a text file which can be converted to an excel spreadsheet.

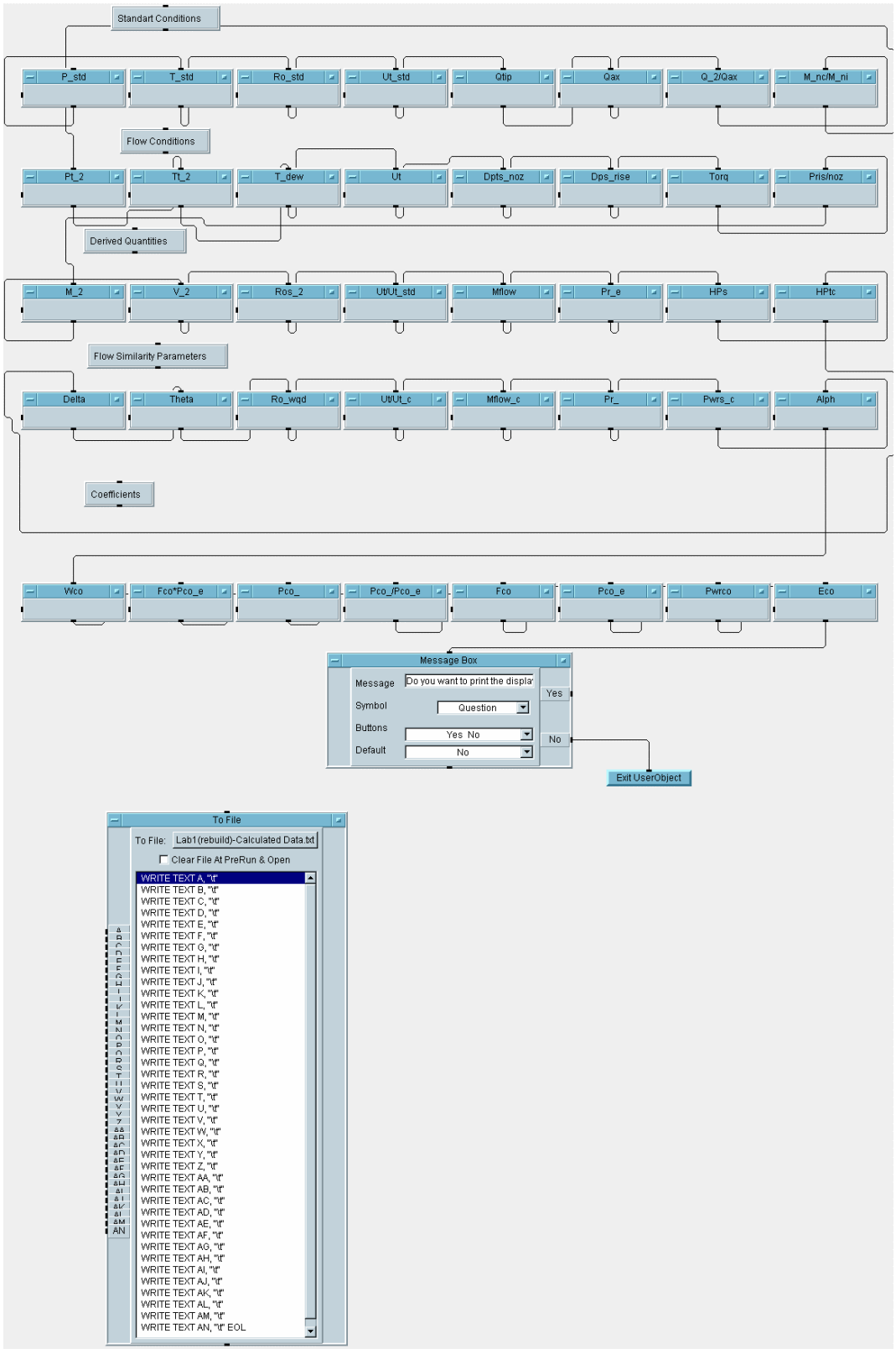

Figure B7. HP VEE screen display Red_lab_Redcc

Figure B8 below shows the printout display screen for the processed data for Lab #1 from Red_lab_Redcc.

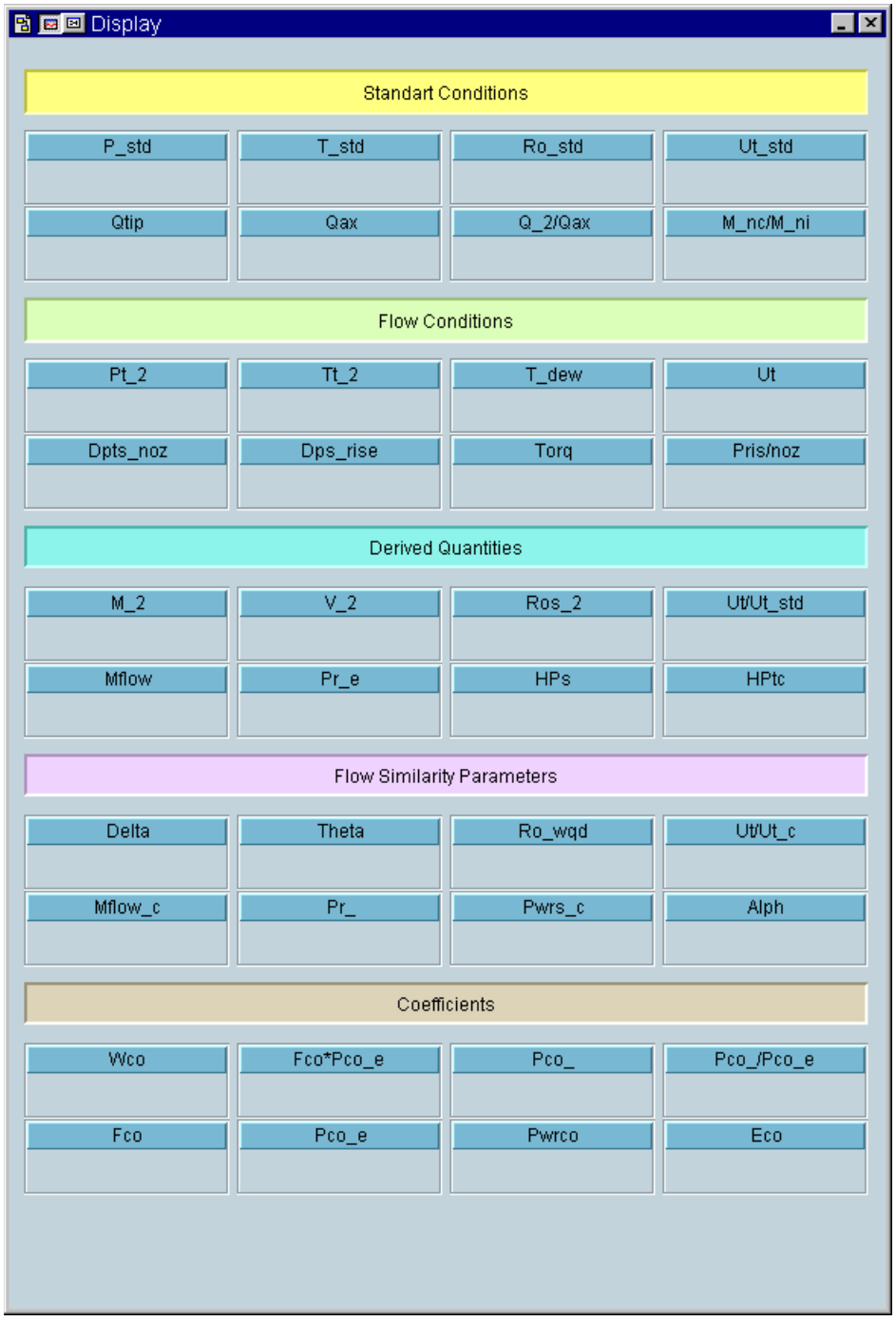

Figure B8. HP VEE screen display Red_lab_Redcc

Figure B9 shows the screen Red_lab_Redvd which processes the data for Lab #2. This data is also saved into a text file.

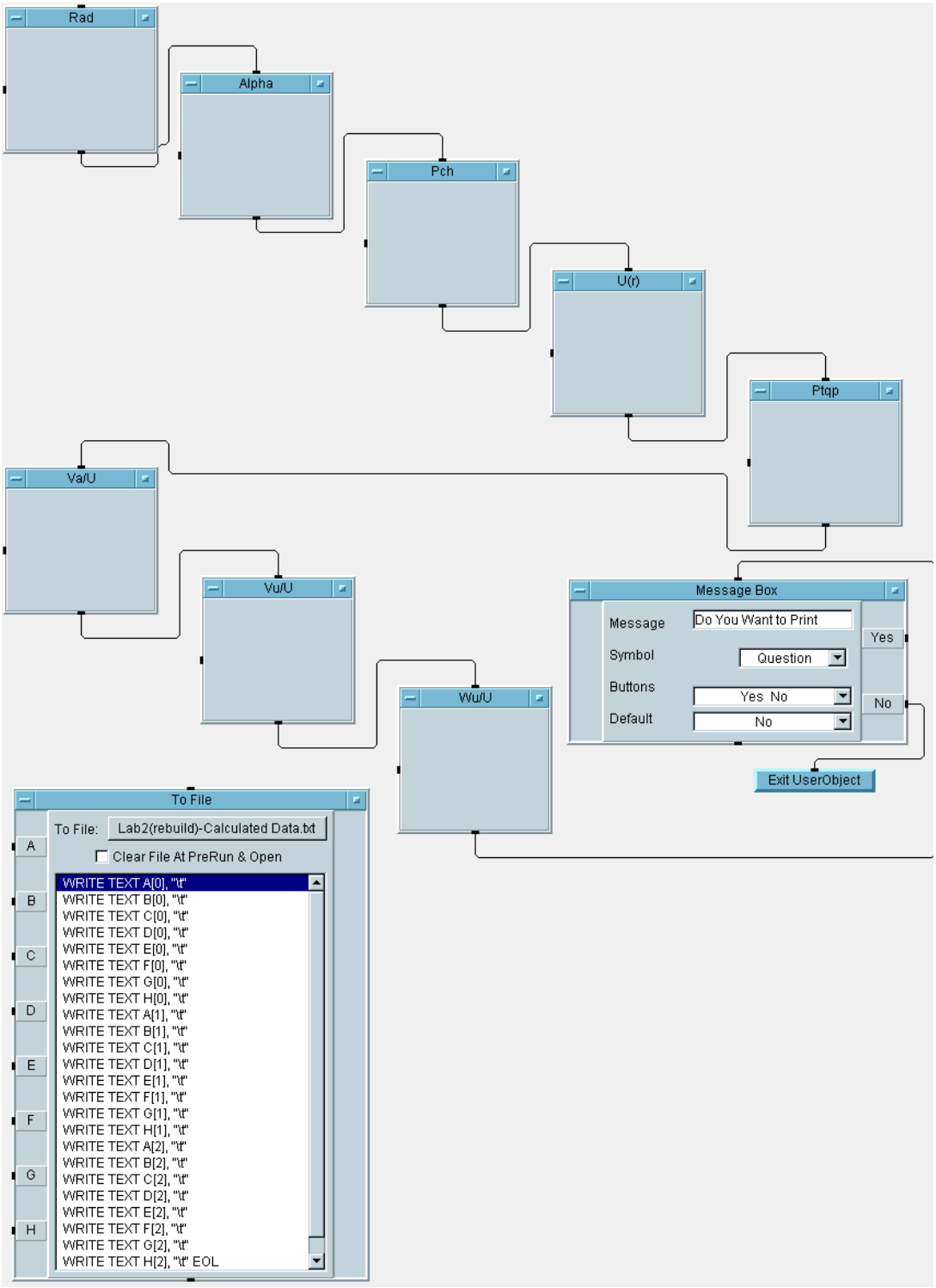

Figure B9. HP VEE screen display Red_lab_Redvd

Figure B10 shows the printout display screen for the processed data for Lab #2 from Red_lab_Redvd.

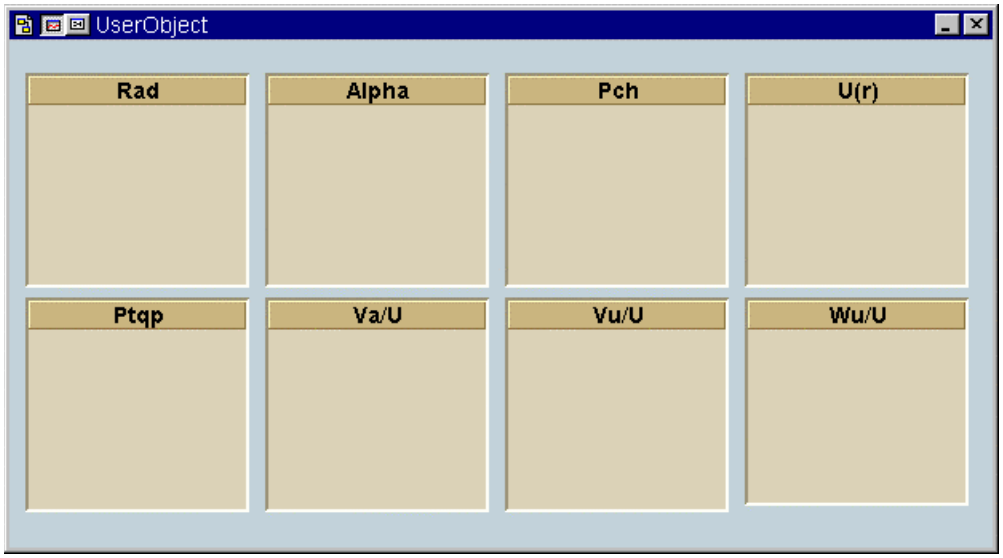

Figure B10. HP VEE screen display Red_lab_Redvd

THIS PAGE INTENTIONALLY LEFT BLANK

APPENDIX C. RAW DATA AND PROCESSED RESULTS

C.1. DATA FOR BUILD #1

Table C1. Raw data for build #1

	PBAR	Pabs	FBLD	FBfv	TRO	TWET	P@21	P#2	P*2
5+4	29.92	9.90E+37	806	1.61526	-9.47E-05	-9.55E-05	2.27E-06	0.001649	0.001652
	29.92	9.90E+37	805	1.614082	-9.66E-05	-9.56E-05	1.53E-06	0.001644	0.001646
	29.92	9.90E+37	806	1.615386	-7.13E-05	-6.96E-05	1.54E-06	0.001642	0.001643
	29.92	9.90E+37	806	1.619711	-7.31E-05	-7.01E-05	1.89E-07	0.001636	0.001636
	29.92	9.90E+37	806	1.602227	-8.77E-05	-8.24E-05	-1.17E-06	0.0016	0.0016
	29.92	9.90E+37	806	1.592318	-9.10E-05	-8.72E-05	-2.42E-06	0.001625	0.001627
	29.92	9.90E+37	806	1.602676	-9.60E-05	-8.98E-05	-3.25E-06	0.001623	0.001624
5+4+3	29.92	9.90E+37	806	1.630501	-1.52E-05	-1.71E-05	2.51E-06	0.001651	0.001654
	29.92	9.90E+37	806	1.628497	-4.54E-05	-4.32E-05	1.52E-06	0.001648	0.001649
	29.92	9.90E+37	806	1.628786	-6.73E-05	-6.30E-05	8.54E-07	0.001644	0.001646
	29.92	9.90E+37	806	1.606742	-8.05E-05	-7.46E-05	4.30E-08	0.001642	0.001643
	29.92	9.90E+37	806	1.604837	-9.48E-05	-8.78E-05	-4.17E-07	0.001637	0.001639
	29.92	9.90E+37	805	1.604586	-0.0001049	-9.82E-05	-5.73E-07	0.001646	0.001646
5+4+3+2+1	29.92	9.90E+37	806	1.621823	-3.51E-05	-3.75E-05	4.45E-06	0.001694	0.001696
	29.92	9.90E+37	805	1.619402	-4.51E-05	-4.41E-05	2.88E-06	1.69E-03	1.69E-03
	29.92	9.90E+37	805	1.619386	-5.75E-05	-5.51E-05	1.83E-06	1.69E-03	1.69E-03
	29.92	9.90E+37	805	1.618811	-7.03E-05	-6.66E-05	5.96E-07	1.68E-03	1.68E-03
	29.92	9.90E+37	805	1.624466	-8.01E-05	-7.60E-05	-1.64E-06	1.68E-03	1.68E-03
	29.92	9.90E+37	806	1.238004	-8.87E-05	-8.39E-05	-2.95E-06	1.67E-03	1.68E-03
5	29.92	9.90E+37	806	1.625809	-2.99E-05	-3.24E-05	4.50E-06	0.001536	0.001537
	29.92	9.90E+37	807	1.627084	-4.33E-05	-4.14E-05	2.72E-06	0.001529	0.001531
	29.92	9.90E+37	806	1.634604	-0.0001053	-0.0001033	3.61E-07	0.001527	0.001528
	29.92	9.90E+37	806	1.634496	-9.07E-05	-8.72E-05	-1.08E-06	0.001524	0.001525

PO-T	PO-S	P2SW	PE-S	PR1-1	PR1-2	PR1-3	PR1-4	PR1-5	PR1-6
0.001634	0.001389	0.000040	0.001307	0.0006598	0.0006954	0.0006966	0.000698	0.000698	0.000699
0.001627	0.001382	0.000040	0.001302	0.000655	0.0006913	0.0006925	0.0006947	0.000694	0.000696
0.001624	0.001379	0.000040	0.001299	0.0006516	0.0006887	0.0006872	0.0006876	0.000688	0.000693
0.001616	0.001375	0.000039	0.001294	0.0006488	0.0006844	0.0006832	0.000683	0.000683	0.000691
0.0016	0.0014	0.000037	0.0013	0.00065	0.00068	0.00068	0.00068	0.000683	0.000685
0.00161	0.001367	0.000036	0.001286	0.0006436	0.0006779	0.0006764	0.0006772	0.000679	0.000685
0.001606	0.001364	0.000034	0.001285	0.000638	0.0006785	0.0006768	0.0006779	0.000677	0.000681
0.001637	0.001419	0.000037	0.001378	0.0005734	0.0006133	0.0006129	0.0006148	0.000616	0.000616
0.001632	0.001416	0.000036	0.001376	0.0005733	0.0006108	0.0006121	0.0006121	0.000614	0.000615
0.001629	0.001414	0.000034	0.00137	0.0005726	0.0006086	0.0006097	0.0006101	0.000613	0.000613
0.001627	0.001413	0.000035	0.00137	0.0005797	0.0006077	0.0006083	0.0006089	0.00061	0.000611
0.001623	0.001408	0.000033	0.001366	0.0005656	0.0006044	0.0006063	0.0006085	0.000609	0.000608
0.001629	0.001412	0.000031	0.001371	0.0005686	0.0006083	0.0006094	0.0006094	0.000611	0.000613
0.00168	0.001481	0.000034	0.001438	0.00054	0.0005699	0.0005701	0.0005723	0.000572	0.000575
1.67E-03	1.47E-03	0.000033	0.0014	5.38E-04	5.67E-04	5.67E-04	5.68E-04	0.00057	0.000575
1.67E-03	1.47E-03	0.000032	0.0014	5.30E-04	5.65E-04	5.66E-04	5.56E-04	0.000569	0.00057
1.67E-03	1.47E-03	0.000030	0.0014	5.32E-04	5.64E-04	5.65E-04	5.66E-04	0.000568	0.000568
1.67E-03	1.46E-03	0.000029	0.0014	5.23E-04	5.58E-04	5.59E-04	5.62E-04	0.000564	0.000564
1.66E-03	1.46E-03	0.000026	0.0014	5.23E-04	5.54E-04	5.54E-04	5.57E-04	0.000558	0.000562
0.001512	0.001208	0.000056	0.0010	0.0008363	0.0008609	0.0008595	0.000862	0.000863	0.000866
0.001509	0.001204	0.000053	0.0010	0.0008333	0.0008574	0.0008564	0.000857	0.000859	0.000863
0.001503	0.0012	0.000049	0.0010	0.0008281	0.0008535	0.000853	0.0008513	0.000854	0.000856
0.001502	0.001199	0.000050	0.0010	0.000816	0.0008457	0.0008471	0.0008483	0.000848	0.000852

PR1-7	PR1-8	PR1-9	PR1-0	PR1-A	PR1-B	CS8	P3-S	P@22	TAMB
0.000702	0.00071	0.000717	0.000712	0.000672	0.000607	0.001286	0.001321	4.29E-06	-9.02E-05
0.000699	0.000704	0.000712	0.000709	0.000664	0.0006	0.001283	0.001321	3.95E-06	-9.57E-05
0.000698	0.000708	0.000717	0.000724	0.000687	0.000607	0.001277	0.001318	3.42E-06	-5.66E-05
0.000697	0.000703	0.000708	0.000717	0.00068	0.000608	0.001274	0.001312	2.28E-06	-5.87E-05
0.000691	0.000697	0.000701	0.000711	0.000678	0.000601	0.00127	0.001309	9.01E-07	-7.05E-05
0.000688	0.000693	0.000697	0.000705	0.000678	0.0006	0.001265	0.001306	-1.99E-08	-7.92E-05
0.000686	0.000697	0.000706	0.000712	0.000674	0.000596	0.001264	0.001306	-7.29E-07	-7.98E-05
0.000621	0.000625	0.000633	0.000638	0.000605	0.000539	0.001351	0.001375	4.75E-06	-5.59E-06
0.000617	0.000619	0.000627	0.000634	0.000605	0.000536	0.00135	0.001375	4.17E-06	-3.62E-05
0.000616	0.000618	0.000625	0.000631	0.0006	0.000535	0.001348	0.001375	3.52E-06	-5.79E-05
0.000611	0.000618	0.000623	0.000629	0.000597	0.000537	0.001344	0.001368	2.84E-06	-6.71E-05
0.00061	0.000618	0.000626	0.000626	0.000598	0.000535	0.001342	0.001368	2.23E-06	-8.09E-05
0.000615	0.000619	0.000626	0.00063	0.000599	0.000535	0.001346	0.001372	1.65E-06	-9.56E-05
0.000576	0.00058	0.000588	0.000597	0.000563	0.000502	0.001418	0.001435	5.70E-06	-1.86E-05
0.000576	0.000583	0.00059	0.000596	0.000561	0.000501	0.001413	0.001427	4.34E-06	-3.08E-05
0.000573	0.000575	0.000581	0.000594	0.0006	0.000497	0.00141	0.001431	3.81E-06	-4.47E-05
0.00057	0.000574	0.000579	0.00059	0.000557	0.000496	0.001408	0.001426	1.98E-06	-5.46E-05
0.000568	0.000572	0.000582	0.000584	0.000551	0.000486	0.001404	0.001422	1.23E-07	-7.76E-05
0.000565	0.000569	0.000578	0.000582	0.000548	0.000486	0.001402	0.001421	-9.70E-07	-7.19E-05
0.000871	0.000878	0.00088	0.000876	0.00083	0.000743	0.001024	0.001081	5.58E-06	-1.49E-05
0.000865	0.000872	0.000879	0.000867	0.000818	0.000737	0.001021	0.001078	4.07E-06	-3.15E-05
0.000865	0.000864	0.000872	0.000866	0.000821	0.000729	0.001019	0.001077	2.08E-06	-8.25E-05
0.000856	0.00086	0.000865	0.000856	0.000803	0.000722	0.00102	0.001081	9.60E-07	-7.65E-05

P@31	P#3	P*3	PX-1	PX-2	PX-3	PX-4	PX-5	PY-1	PY-2
1.44E-05	0.001642	0.001643	0.001362	-0.00036	0.000673	0.001061	0.001237	0.001391	0.001364
2.42E-05	0.001644	0.001646	0.001326	-0.000346	0.000681	0.001068	0.001243	0.001958	0.00133
1.26E-05	0.00162	0.00162	0.001258	-0.000349	0.000662	0.001043	0.00122	0.001993	0.001239
-8.17E-06	0.001597	0.001596	0.001237	-0.000371	0.000639	0.001018	0.001197	0.002024	0.001191
-3.11E-05	0.001569	0.00157	0.00121	-0.000394	0.000616	0.000994	0.001176	0.002025	0.001156
-4.67E-05	0.001551	0.001551	0.00119	-0.000402	0.000598	0.000975	0.001157	0.002033	0.001103
-6.10E-05	0.001535	0.001535	0.001204	-0.000416	0.000583	0.000967	0.00114	0.001995	0.001083
6.94E-05	0.001692	0.001692	0.001306	-0.000268	0.000823	0.001086	0.001255	0.002035	0.001423
8.11E-05	0.0017	0.0017	0.001356	-0.000256	0.000828	0.001093	0.001259	0.002109	0.001381
8.66E-05	0.001701	0.001703	0.001346	-0.00025	0.000833	0.001095	0.001265	0.002114	0.001359
8.94E-05	0.001703	0.001703	0.001361	-0.000251	0.000835	0.001094	0.00126	0.002136	0.001342
9.00E-05	0.001702	0.001703	0.001369	-0.000255	0.000837	0.001103	0.001262	0.00213	0.001315
8.47E-05	0.001702	0.001703	0.001335	-0.000266	0.000832	0.001095	0.001267	0.002086	0.001299
2.92E-05	0.001704	0.001703	0.001285	-0.000283	0.000858	0.001042	0.001213	0.002065	0.00145
7.44E-06	0.001677	0.001678	0.001266	-0.000303	0.000836	0.001024	0.001188	0.0021	0.001375
-1.37E-05	0.001655	0.001654	0.001259	-0.000328	0.000814	0.000999	0.001166	0.002064	0.001332
-4.22E-05	0.001626	0.001627	0.001229	-0.000355	0.000786	0.000968	0.001138	0.002046	0.00128
-8.54E-05	0.001581	0.001579	0.001165	-0.000394	0.000744	0.000924	0.001094	0.001976	0.001215
-9.27E-05	0.001573	0.001573	0.001169	-0.000402	0.00074	0.000916	0.001088	0.001914	0.001176
1.83E-05	0.001542	0.001541	0.001381	-0.000198	0.000368	0.001064	0.001248	0.001837	0.001119
1.04E-05	0.001532	0.001532	0.001357	-0.000221	0.000371	0.001055	0.001231	0.001935	0.001033
1.48E-05	0.001535	0.001534	0.001363	-0.00022	0.000375	0.001059	0.001231	0.002008	0.001012
1.04E-06	0.001517	0.001517	0.001354	-0.000234	0.000366	0.001037	0.001221	0.002084	0.00097

PY-3	PY-4	PY-5	PS-1	PS-2	PS-3	P@32	RADX	YAWX	RADY
0.001384	0.002104	0.001475	0.000986	0.00098	0.000986	-1.42E-05	0.001735	0.002585	-0.000296
0.001332	0.002228	0.001705	0.001916	0.001483	0.001467	-4.86E-06	0.001735	0.002585	0.091991
0.001256	0.002629	0.001811	0.001999	0.001465	0.001465	-1.68E-05	0.001737	0.002586	0.187395
0.001206	0.002731	0.001829	0.001985	0.001412	0.001405	-3.75E-05	0.001737	0.002586	0.278758
0.001152	0.002774	0.00179	0.001975	0.001373	0.001367	-5.87E-05	0.001737	0.002585	0.369074
0.001109	0.002878	0.001776	0.001948	0.001335	0.001324	-7.44E-05	0.001737	0.002585	0.459526
0.001089	0.002902	0.001773	0.00191	0.001286	0.001281	-8.86E-05	0.001737	0.002585	0.54525
0.001423	0.002819	0.001894	0.001976	0.001567	0.00155	4.19E-05	0.001737	0.002586	0.088221
0.001383	0.002934	0.001947	0.002099	0.001593	0.001583	5.32E-05	0.001737	0.002585	0.187114
0.001367	0.003033	0.001971	0.002084	0.001547	0.001543	5.84E-05	0.001737	0.002586	0.278217
0.001346	0.00308	0.001963	0.002103	0.001545	0.001535	6.10E-05	0.001737	0.002585	0.368453
0.001322	0.003107	0.001939	0.00207	0.001505	0.001499	6.17E-05	0.001737	0.002585	0.45919
0.0013	0.002948	0.001909	0.002026	0.001468	0.001456	5.56E-05	0.001737	0.002586	0.54564
0.001452	0.002258	0.001921	0.002003	0.001592	0.001578	-1.75E-06	0.001742	0.00259	0.088734
0.001382	0.002348	0.001938	0.002074	0.001572	0.001561	-2.24E-05	0.00174	0.002588	0.187523
0.00134	0.002368	0.001918	0.002017	0.001493	0.001486	-4.48E-05	0.001739	0.002587	0.278798
0.001291	0.002366	0.00188	0.001998	0.001453	0.001445	-7.49E-05	0.001739	0.002587	0.368822
0.00122	0.002384	0.001803	0.001922	0.001377	0.001369	-1.13E-04	0.001739	0.002587	0.459532
0.001187	0.00238	0.00174	0.001864	0.001329	0.001322	-1.20E-04	0.001738	0.002586	0.545609
0.00112	0.002547	0.001675	0.001822	0.001326	0.001312	-5.47E-06	0.00175	0.002594	0.089113
0.001038	0.002664	0.001752	0.001907	0.001309	0.001301	-1.39E-05	0.001745	0.002591	0.187382
0.001019	0.002706	0.001803	0.001946	0.001292	0.001283	-9.81E-06	0.001739	0.002587	0.279079
0.000982	0.002684	0.001832	0.001979	0.001286	0.001274	-2.41E-05	0.001739	0.002587	0.368541

YAWY	RADS	YAWS	TORQ
-2.13E-05	-0.000371	4.79E-05	0.003911
-0.0306888	0.091101	-0.0419576	0.003916
-0.0275406	0.183835	-0.0407345	0.003915
-0.0224576	0.280345	-0.0377916	0.003914
-2.23E-02	0.376856	-3.71E-02	0.003912
-0.0198884	0.474752	-0.0360435	0.003907
-0.0141831	0.568907	-0.0334905	0.003903
-0.0331822	0.091444	-0.0436308	0.003901
-0.0285048	0.183964	-0.0421163	0.003896
-0.0225204	0.280433	-0.0384579	0.003892
-0.0211759	0.377111	-0.0381996	0.003888
-0.019249	0.474402	-0.0367028	0.003887
-0.015942	0.569167	-0.0352298	0.003908
-0.0339875	0.091186	-0.0453138	0.003896
-2.88E-02	0.183822	-4.28E-02	0.003895
-2.39E-02	0.280208	-3.96E-02	0.003892
-2.11E-02	0.376789	-3.83E-02	0.003887
-2.00E-02	0.473925	-3.74E-02	0.003887
-1.74E-02	0.56884	-3.61E-02	0.003884
-0.0280827	0.091072	-0.0381146	0.003713
-0.0263514	0.183847	-0.0368812	0.003715
-0.0242887	0.2804	-0.0360992	0.003715
-0.0225041	0.376934	-0.0349075	0.00372

Table C2. Lab 1 processed results for build #1

	P_std	T_std	Ro_std	Ut_std	Qtip	Qax	Q_2/Qax	M_nc/M_ni	Pt_2
5+4	2115.594	518.67	0.002367	252.8982	16.16619	6.177415	0.992555	0.997638	397.9047
	2115.594	518.67	0.002367	252.8982	16.12845	6.178947	0.992554	0.997637	397.9621
	2115.594	518.67	0.002367	252.8982	16.16915	6.178904	0.992554	0.997637	397.9991
	2115.594	518.67	0.002367	252.8982	16.17013	6.090216	0.99266	0.99767	397.9585
	2115.594	518.67	0.002367	252.8982	16.17115	6.107006	0.99264	0.997664	397.983
	2115.594	518.67	0.002367	252.8982	16.17176	6.136538	0.992604	0.997652	398.016
	2115.594	518.67	0.002367	252.8982	16.17205	6.101062	0.992647	0.997666	397.9937
5+4+3	2115.594	518.67	0.002367	252.8982	16.15298	5.511985	0.993353	0.997895	397.175
	2115.594	518.67	0.002367	252.8982	16.15495	5.463587	0.993411	0.997913	397.163
	2115.594	518.67	0.002367	252.8982	16.15558	5.448666	0.993429	0.997919	397.1489
	2115.594	518.67	0.002367	252.8982	16.15644	5.401964	0.993485	0.997936	397.1253
	2115.594	518.67	0.002367	252.8982	16.15805	5.433939	0.993447	0.997924	397.1753
	2115.594	518.67	0.002367	252.8982	16.11562	5.494418	0.993374	0.997901	397.1512
5+4+3+2+1	2115.594	518.67	0.002367	252.8982	16.13058	5.049314	0.993907	0.998075	396.2766
	2115.594	518.67	0.002367	252.8982	16.09232	5.062504	0.993891	0.998069	396.3204
	2115.594	518.67	0.002367	252.8982	16.093	5.066421	0.993887	0.998068	396.3293
	2115.594	518.67	0.002367	252.8982	16.09323	5.044118	0.993913	0.998076	396.3079
	2115.594	518.67	0.002367	252.8982	16.09407	5.095352	0.993851	0.998056	396.3565
	2115.594	518.67	0.002367	252.8982	16.1333	5.064414	0.993888	0.998068	396.308
5	2115.594	518.67	0.002367	252.8982	16.23698	7.635122	0.990817	0.997065	400.7423
	2115.594	518.67	0.002367	252.8982	16.27772	7.672954	0.990772	0.99705	400.7679
	2115.594	518.67	0.002367	252.8982	16.23894	7.626682	0.990826	0.997067	400.7187
	2115.594	518.67	0.002367	252.8982	16.2387	7.62016	0.990834	0.99707	400.721

Tt_2	T_dew	Ut	Dpts_noz	Dps_rise	Torq	Pris/noz	M_2	V_2	Ros_2
458.5753	-35.77142	253.2124	2.446041	12.67413	391.0571	5.181488	0.149532	155.9416	0.00261
458.5734	-35.77142	252.8982	2.447036	12.62566	391.6297	5.159572	0.149539	155.9494	0.002611
458.5987	-35.77098	253.2124	2.447267	12.58072	391.512	5.140723	0.149532	155.9459	0.002611
458.5969	-35.77099	253.2124	2.4123	12.5542	391.4061	5.204243	0.148454	154.8263	0.002611
458.5823	-35.7712	253.2124	2.419121	12.53761	391.153	5.182711	0.148655	155.0331	0.002611
458.579	-35.77128	253.2124	2.430978	12.5031	390.7381	5.143239	0.149011	155.4018	0.002611
458.574	-35.77132	253.2124	2.416967	12.50774	390.3053	5.174973	0.14858	154.9539	0.002611
458.6548	-35.77011	253.2124	2.180737	13.41184	390.143	6.150142	0.141317	147.4227	0.002608
458.6246	-35.77054	253.2124	2.161729	13.40558	389.5507	6.201324	0.140693	146.7694	0.002608
458.6027	-35.77087	253.2124	2.155833	13.36353	389.2056	6.198775	0.140502	146.5673	0.002608
458.5895	-35.77107	253.2124	2.137422	13.358	388.7762	6.249583	0.139898	145.9381	0.002609
458.5752	-35.77129	253.2124	2.15027	13.33147	388.7046	6.199906	0.140306	146.3592	0.002609
458.5651	-35.77146	252.8982	2.17388	13.39714	390.8392	6.162776	0.141095	147.1768	0.002608
458.6349	-35.77045	253.2124	1.99447	14.0407	389.6215	7.039817	0.13537	141.2372	0.002604
458.6249	-35.77056	252.8982	1.999936	14.0152	389.4515	7.007827	0.13554	141.4127	0.002605
458.6125	-35.77074	252.8982	2.001556	14.00474	389.1872	6.996927	0.135591	141.4641	0.002605
458.5997	-35.77093	252.8982	1.992781	14.00262	388.6824	7.026674	0.135294	141.1533	0.002605
458.5899	-35.77109	252.8982	2.013212	13.95815	388.7377	6.933273	0.135976	141.8602	0.002605
458.5813	-35.77122	253.2124	2.000897	13.98722	388.4134	6.990478	0.135568	141.4349	0.002605
458.6401	-35.77036	253.2124	3.038249	9.834469	371.2876	3.236887	0.165802	172.8372	0.002622
458.6267	-35.77051	253.5265	3.053449	9.823441	371.4841	3.217162	0.166211	173.2586	0.002622
458.5647	-35.77155	253.2124	3.035036	9.84023	371.5093	3.242212	0.165715	172.732	0.002622
458.5793	-35.77128	253.2124	3.032586	9.855893	371.9737	3.249997	0.165642	172.66	0.002622

Ut/Ut_std	Mflow	Pr_e	HPs	HPtc	Delta	Theta	Ro_wqd	Ut/Ut_c	Mflow_c
1.001242	1.841406	1.016357	120.0248	0	0.973511	0.884137	1.012714	1.071592	1.767305
1	1.841767	1.016229	120.0514	0	0.973652	0.884133	1.012712	1.070264	1.767394
1.001242	1.841786	1.016114	120.1645	0	0.973742	0.884182	1.012711	1.07156	1.767307
1.001242	1.828674	1.016271	120.1319	0	0.973643	0.884179	1.01271	1.071562	1.754902
1.001242	1.831238	1.016187	120.0543	0	0.973703	0.88415	1.012709	1.07158	1.757221
1.001242	1.835663	1.016025	119.9269	0	0.973784	0.884144	1.012709	1.071585	1.761314
1.001242	1.830406	1.016126	119.7941	0	0.973729	0.884134	1.012709	1.071591	1.756358
1.001242	1.739364	1.019913	119.7443	0	0.971726	0.88429	1.012716	1.071492	1.672606
1.001242	1.731877	1.02002	119.5625	0	0.971697	0.884232	1.012715	1.071529	1.665393
1.001242	1.729567	1.019952	119.4566	0	0.971662	0.88419	1.012715	1.071557	1.663184
1.001242	1.722237	1.020056	119.3248	0	0.971605	0.884164	1.012714	1.071574	1.656207
1.001242	1.727384	1.019907	119.3028	0	0.971727	0.884137	1.012714	1.071592	1.660917
1	1.736783	1.019922	119.8091	0	0.971668	0.884117	1.012716	1.070276	1.670032
1.001242	1.664079	1.022709	119.5842	0	0.969528	0.884252	1.01273	1.071524	1.603787
1	1.666331	1.022609	119.3837	0	0.969635	0.884233	1.012729	1.070207	1.60576
1	1.667011	1.022572	119.3027	0	0.969657	0.884209	1.012729	1.070223	1.606354
1	1.663376	1.022624	119.148	0	0.969605	0.884184	1.012729	1.070239	1.602911
1	1.671797	1.022381	119.1649	0	0.969724	0.884165	1.012729	1.070252	1.610808
1.001242	1.666708	1.022534	119.2134	0	0.969605	0.884148	1.012729	1.071592	1.606083
1.001242	2.049825	1.005533	113.9571	0	0.980454	0.884262	1.012671	1.071486	1.953612
1.002484	2.054882	1.005411	114.1589	0	0.980517	0.884236	1.012671	1.072833	1.958272
1.001242	2.048855	1.005569	114.0252	0	0.980396	0.884116	1.012671	1.071583	1.952612
1.001242	2.047966	1.005624	114.1677	0	0.980402	0.884145	1.012671	1.071564	1.951791

Pr_	Pwrs_c	Alph	Wco	Fco*Pco_e	Pco_	Pco_/Pco_e	Fco	Pco_e	Pwrco	Eco
1.032354	114.7667	1.000015	1.116877	0.5074683	0.904262	1.162894721	0.652612	0.777595	0.728888	0.696223
1.032225	115.2036	1.000015	1.121073	0.5073881	0.900674	1.158522675	0.652645	0.777433	0.731663	0.693473
1.032107	114.8766	1.000013	1.117945	0.5036795	0.897384	1.162732162	0.652613	0.771789	0.729586	0.690364
1.032036	114.857	1.000013	1.125656	0.4990399	0.895383	1.162706145	0.648032	0.770085	0.729461	0.684121
1.031993	114.7735	1.000014	1.123354	0.4990209	0.894182	1.162725433	0.648888	0.76904	0.728931	0.684593
1.031905	114.6418	1.000015	1.119457	0.4988137	0.891713	1.162697889	0.6504	0.766934	0.728095	0.685095
1.031915	114.5206	1.000015	1.121429	0.4975712	0.892014	1.16271444	0.64857	0.767182	0.727325	0.684112
1.034243	114.7204	1.000007	1.179636	0.5080703	0.957058	1.163459976	0.617643	0.822596	0.728593	0.69733
1.034223	114.5453	1.00001	1.182937	0.5055671	0.956522	1.163527511	0.614979	0.822088	0.727482	0.694955
1.034116	114.4447	1.000012	1.183468	0.5033065	0.95352	1.163539587	0.614163	0.819499	0.726843	0.692456
1.0341	114.3233	1.000014	1.187193	0.500947	0.953069	1.163565842	0.611587	0.819094	0.726072	0.689941
1.034031	114.2858	1.000015	1.183438	0.5013476	0.951133	1.163573535	0.613326	0.817424	0.725833	0.69072
1.034206	115.2044	1.000016	1.18644	0.5085381	0.956024	1.159347101	0.616692	0.824622	0.731668	0.69504
1.035888	114.823	1.000009	1.231356	0.5102574	1.003052	1.164191898	0.59223	0.861587	0.729246	0.699706
1.03582	115.0441	1.00001	1.232211	0.5118214	1.001152	1.159860899	0.592958	0.863166	0.73065	0.700502
1.035793	114.9616	1.000012	1.230872	0.5116128	1.000392	1.159881329	0.593178	0.862495	0.730126	0.700719
1.035787	114.8169	1.000013	1.231962	0.5104249	1.000239	1.159911316	0.591906	0.862341	0.729206	0.699973
1.035674	114.8177	1.000014	1.225931	0.5113228	0.997068	1.159890627	0.594822	0.859623	0.729212	0.7012
1.03575	114.4501	1.000015	1.225602	0.5089853	0.99919	1.164271784	0.593078	0.85821	0.726877	0.700236
1.025016	108.2045	1.000009	0.952595	0.4349379	0.699186	1.159704335	0.72141	0.6029	0.687211	0.632903
1.024989	107.9849	1.00001	0.948399	0.4338741	0.698423	1.164049751	0.72313	0.599994	0.685816	0.632639
1.025032	108.265	1.000016	0.953615	0.4349125	0.699622	1.159902335	0.721041	0.603174	0.687595	0.632512
1.025071	108.4018	1.000015	0.955222	0.4354198	0.70072	1.159880926	0.720737	0.604131	0.688464	0.632451

Table C3. Lab 2 processed results for build #1

S Probe

	Rad	Alpha	Pch	U(r)	Ptqp	Va/U	Vu/U	Wu/U
5+4	-0.003712	-0.047899	0	253.2646	0.053889	0.060414	-5.05E-05	1.000051
	0.911008	41.95759	0	240.0986	0.116544	0.593619	0.533702	0.466298
	1.837664	40.6722	0	227.3613	0.137825	0.706684	0.607248	0.392752
	2.803448	37.7916	0	213.7753	0.152302	0.810452	0.628461	0.371539
	3.768563	37.05939	0	200.1987	0.172779	0.895314	0.676123	0.323877
	4.747521	36.0435	0	186.4273	0.196532	0.985946	0.717476	0.282524
	5.689073	33.4905	0	173.1822	0.223325	1.10253	0.729486	0.270514
5+4+3	0.914436	43.63081	0	240.3487	0.119926	0.560964	0.534774	0.465226
	1.839643	42.11634	0	227.3335	0.142449	0.672614	0.608102	0.391898
	2.804334	38.45792	0	213.7628	0.159938	0.775785	0.616157	0.383843
	3.77111	38.19962	0	200.1628	0.184042	0.849411	0.668411	0.331589
	4.744021	36.70277	0	186.4765	0.208745	0.934852	0.696887	0.303113
	5.691668	35.22982	0	172.9308	0.237547	1.023751	0.722975	0.277025
5+4+3+2+1	0.911859	45.3138	0	240.3849	0.121573	0.545769	0.55178	0.44822
	1.838216	42.81968	0	227.0715	0.141071	0.663961	0.615259	0.384741
	2.802078	39.55375	0	213.5293	0.155148	0.757312	0.625474	0.374526
	3.767891	38.28411	0	199.9597	0.175236	0.839984	0.663002	0.336998
	4.739253	37.39313	0	186.3122	0.19421	0.91397	0.698609	0.301391
	5.688396	36.08816	0	173.1917	0.217957	0.990662	0.72209	0.27791
5	0.910716	38.11456	0	240.401	0.110547	0.670203	0.525781	0.474219
	1.838467	36.88118	0	227.6321	0.129044	0.787086	0.590557	0.409443
	2.804	36.09923	0	213.7675	0.149354	0.885739	0.645874	0.354126
	3.76934	34.90749	0	200.1877	0.173133	0.988458	0.68975	0.31025

Y Probe

Rad	Alpha	Pch	U(r)	Ptqp	Va/U	Vu/U	Wu/U
-0.00296	0.021295	0	253.254	0.076066	0.18371	6.83E-05	0.999932
0.919909	30.68883	0	239.9736	0.119219	0.567713	0.336934	0.663066
1.874134	27.56149	0	226.8483	0.137989	0.674052	0.351809	0.648191
2.787576	22.45763	0	213.9985	0.155017	0.781936	0.323211	0.676789
3.690736	22.30136	0	201.2935	0.175224	0.853333	0.350001	0.649999
4.595259	19.8884	0	188.5692	0.200457	0.953015	0.344769	0.655231
5.452502	14.18313	0	176.5101	0.224595	1.041086	0.263109	0.736891
0.882212	33.18224	0	240.802	0.123055	0.543571	0.355462	0.644538
1.871136	28.50481	0	226.8904	0.14363	0.658585	0.357654	0.642346
2.782171	22.52041	0	214.0746	0.161796	0.746115	0.309363	0.690637
3.684531	21.17585	0	201.3808	0.184729	0.820964	0.318033	0.681967
4.591901	19.24898	0	188.6165	0.209918	0.897614	0.313443	0.686557
5.4564	15.94199	0	176.2363	0.23551	0.9646	0.275538	0.724462
0.887342	33.9875	0	240.7298	0.124978	0.539925	0.364012	0.635988
1.875228	28.82782	0	226.5514	0.143456	0.655741	0.360911	0.639089
2.787981	23.90683	0	213.7274	0.158416	0.728849	0.323086	0.676914
3.688218	21.05768	0	201.0791	0.177433	0.807789	0.311015	0.688985
4.595322	20.00515	0	188.3344	0.195378	0.868397	0.316159	0.683841
5.456092	17.41581	0	176.4596	0.215601	0.926207	0.290536	0.709464
0.891125	28.0827	0	240.6766	0.111192	0.620904	0.331291	0.668709
1.873823	26.35137	0	227.1341	0.131502	0.74345	0.368265	0.631735
2.790787	24.28874	0	213.9534	0.153856	0.840153	0.379145	0.620855
3.685415	22.50412	0	201.3683	0.180266	0.95099	0.393993	0.606007

C.2. GRAPHS FOR BUILD #1

Power coefficient was also calculated and plotted for build #1. In the future data should be obtained so that the power coefficient and efficiency can be calculated for build #2.

1. Power Coefficient versus Flow Coefficient

The power coefficient is a non-dimensional measure of the shaft work input. The plot below, Figure C1, of power coefficient versus flow coefficient shows the relationship between the shaft input power and the amount of flow through the compressor. The required power was largest at open throttle, but varied less than 1% over the full range of throttle variation.

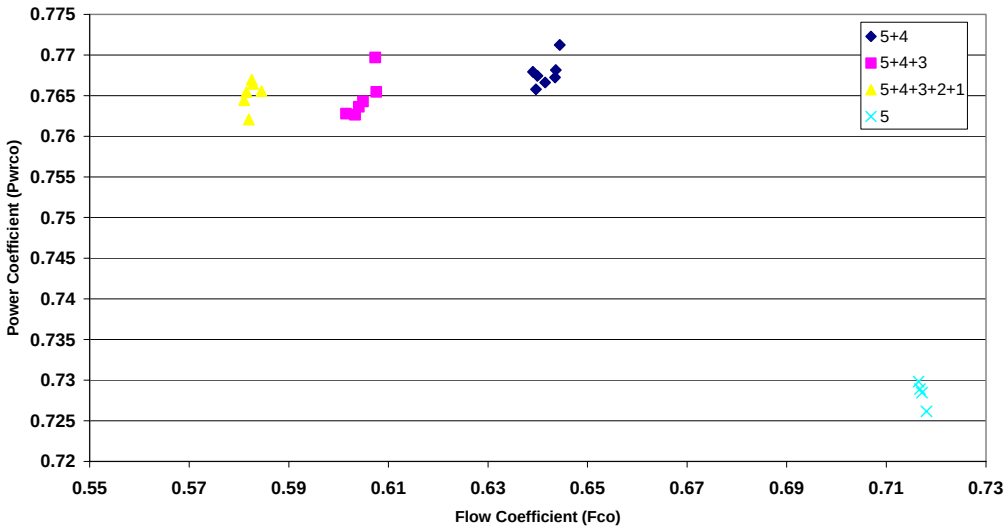

Figure C1. Power coefficient versus flow coefficient for build #1

C.3. DATA FOR BUILD #2

Table C4. Raw data for build #2

	PBAR	Pabs	FBLD	FBfv	TRO	TWET	P@21	P#2	P*2
5+4	29.92	9.90E+37	803	1.57282	-9.85E-05	-0.0001068	-3.24E-06	0.00171	0.001714
	29.92	9.90E+37	803	1.571519	-9.32E-05	-9.93E-05	-4.31E-06	0.001708	0.001715
	29.92	9.90E+37	803	1.572385	-9.12E-05	-9.88E-05	-5.12E-06	0.001709	0.001714
	29.92	9.90E+37	803	1.575328	-9.93E-05	-0.0001068	-5.44E-06	0.001707	0.001712
	29.92	9.90E+37	803	1.567454	-0.0001148	-0.0001211	-5.81E-06	0.001709	0.001712
	29.92	9.90E+37	803	1.569403	-0.0001187	-0.0001243	-5.92E-06	0.001707	0.00171
5+4+3	29.92	9.90E+37	802	1.572025	1.10E-05	5.64E-06	-7.29E-08	0.001809	0.001812
	29.92	9.90E+37	802	1.586211	-3.29E-05	-3.21E-05	-1.27E-06	0.001804	0.001808
	29.92	9.90E+37	802	1.60416	-5.60E-05	-5.79E-05	-1.91E-06	0.001801	0.001804
	29.92	9.90E+37	802	1.601965	-7.56E-05	-7.68E-05	-2.35E-06	0.001795	0.001799
	29.92	9.90E+37	802	1.608625	-0.0001061	-0.0001028	-3.01E-06	0.001789	0.001793
	29.92	9.90E+37	802	1.607805	-0.0001007	-0.0001074	-3.30E-06	0.001786	0.00179
5+4+3+2+1	29.92	9.90E+37	802	1.575601	-2.85E-05	-3.37E-05	-9.27E-08	0.001818	0.001822
	29.92	9.90E+37	802	1.573761	-4.25E-05	-4.75E-05	-6.72E-07	0.001819	0.001823
	29.92	9.90E+37	802	1.572853	-7.00E-05	-7.02E-05	-1.18E-06	0.001814	0.001818
	29.92	9.90E+37	802	1.590317	-8.57E-05	-8.55E-05	-1.81E-06	0.001808	0.001812
	29.92	9.90E+37	802	1.605075	-9.74E-05	-9.69E-05	-2.15E-06	0.001806	0.001809
	29.92	9.90E+37	802	1.610221	-9.01E-05	-9.28E-05	-2.73E-06	0.001799	0.001803
5	29.92	9.90E+37	803	1.612664	-9.93E-05	-0.0001105	-2.69E-06	0.001652	0.001658
	29.92	9.90E+37	803	1.607538	-9.64E-05	-0.0001021	-3.09E-06	0.001647	0.00165
	29.92	9.90E+37	803	1.598185	-0.0001041	-0.000106	-4.01E-06	0.001645	0.001652
	29.92	9.90E+37	803	1.60407	-0.0001177	-0.000119	-3.60E-06	0.001643	0.001649
	29.92	9.90E+37	803	1.605361	-0.0001184	-0.0001207	-4.10E-06	0.001643	0.001647
	29.92	9.90E+37	803	1.594096	-0.0001274	-0.0001291	-4.35E-06	0.001644	0.001649

PO-T	PO-S	P2SW	PE-S	PR1-1	PR1-2	PR1-3	PR1-4	PR1-5	PR1-6
0.001697	0.001461	0.000204	0.001419	0.000796	0.0008	0.000805	0.000804	0.000806	0.000806
0.001698	0.001462	0.000202	0.001419	0.000798	0.000803	0.000802	0.000805	0.000804	0.000804
0.001696	0.001461	0.0002	0.001416	0.000797	0.000801	0.000803	0.000802	0.000803	0.000805
0.001694	0.001458	0.0002	0.001413	0.000794	0.000798	0.000799	0.000801	0.000801	0.000802
0.001695	0.001461	0.000199	0.001417	0.000795	0.0008	0.0008	0.000801	0.000803	0.000802
0.001693	0.001459	0.000197	0.001421	0.000792	0.000798	0.000801	0.000801	0.000802	0.000803
0.001797	0.001577	0.000192	0.001533	0.000746	0.000751	0.000751	0.000752	0.000754	0.000759
0.001793	0.001572	0.000191	0.001533	0.000746	0.000751	0.000752	0.000754	0.000754	0.000756
0.001789	0.001568	0.000189	0.001527	0.000745	0.00075	0.000752	0.000754	0.000753	0.000755
0.00178	0.001562	0.000188	0.001521	0.000738	0.000747	0.000748	0.000751	0.000751	0.000752
0.001776	0.001559	0.000184	0.001521	0.000736	0.00074	0.000741	0.000742	0.000744	0.000745
0.001774	0.001557	0.000183	0.001521	0.000727	0.000732	0.000732	0.000733	0.000733	0.000737
0.001809	0.001611	0.000169	0.001591	0.000667	0.00067	0.000669	0.00067	0.000673	0.000676
0.001809	0.001609	0.00017	0.001585	0.000674	0.000677	0.000679	0.00068	0.000682	0.000687
0.001803	0.001603	0.000168	0.001578	0.000672	0.000677	0.000677	0.000679	0.000678	0.00068
0.0018	0.001601	0.000166	0.001582	0.000664	0.000668	0.000671	0.000674	0.000673	0.000676
0.001796	0.001596	0.000168	0.001574	0.000673	0.000676	0.000677	0.000677	0.000677	0.000678
0.001791	0.00159	0.000167	0.001569	0.000672	0.000675	0.000677	0.000677	0.000679	0.000679
0.001638	0.001341	0.000256	0.001224	0.001002	0.001012	0.001013	0.001016	0.001014	0.001014
0.001632	0.001338	0.000255	0.001228	0.001003	0.00101	0.001014	0.001012	0.001011	0.00101
0.00163	0.001339	0.000254	0.001227	0.000992	0.001004	0.001003	0.001005	0.001005	0.001004
0.001627	0.001342	0.000251	0.00123	0.000993	0.001008	0.001004	0.001003	0.001004	0.001004
0.001628	0.001339	0.000249	0.001231	0.000987	0.001005	0.001003	0.001004	0.001002	0.001003
0.001628	0.001336	0.000251	0.001226	0.000993	0.001003	0.001002	0.001003	0.001003	0.001003

PR1-7	PR1-8	PR1-9	PR1-0	PR1-A	PR1-B	CS8	P3-S	P@22	TAMB
0.000809	0.00082	0.000825	0.000828	0.000789	0.000718	0.001422	0.00133	-2.67E-06	-9.46E-05
0.000805	0.000808	0.000817	0.000821	0.000785	0.000716	0.001419	0.001331	-3.70E-06	-9.21E-05
0.000806	0.000815	0.000826	0.000832	0.00079	0.000716	0.001416	0.001334	-4.14E-06	-9.20E-05
0.000802	0.000814	0.000823	0.000827	0.00079	0.00071	0.001417	0.001333	-4.76E-06	-9.92E-05
0.000806	0.00081	0.000823	0.000825	0.000784	0.000708	0.001414	0.001334	-5.01E-06	-0.00011247
0.000803	0.000809	0.000821	0.000826	0.000784	0.000708	0.001413	0.001337	-5.23E-06	-0.00012168
0.000761	0.000769	0.000777	0.000776	0.000742	0.000674	0.001545	0.001457	3.31E-07	4.39E-06
0.000759	0.000767	0.000773	0.000785	0.000742	0.000671	0.001538	0.001451	-7.35E-07	-3.50E-05
0.000759	0.000765	0.000772	0.000783	0.000741	0.000668	0.001535	0.001451	-1.33E-06	-5.37E-05
0.000752	0.000762	0.000767	0.000773	0.000732	0.000659	0.00153	0.001441	-1.83E-06	-6.98E-05
0.000748	0.000755	0.000761	0.000763	0.000725	0.000657	0.001531	0.001446	-2.24E-06	-0.00010559
0.000742	0.000743	0.000753	0.000763	0.000717	0.000652	0.001528	0.001448	-2.53E-06	-0.00010091
0.000682	0.000694	0.000703	0.000711	0.000668	0.000607	0.001596	0.001504	4.24E-07	-3.20E-05
0.000688	0.000702	0.000706	0.000716	0.000678	0.000616	0.001589	0.0015	-2.98E-08	-4.33E-05
0.000684	0.000692	0.000699	0.000711	0.000671	0.000607	0.001585	0.001496	-5.53E-07	-6.36E-05
0.00068	0.000686	0.000692	0.000704	0.000667	0.000599	0.001585	0.001497	-1.03E-06	-7.83E-05
0.000683	0.000692	0.000702	0.000705	0.000668	0.000602	0.001577	0.001493	-1.72E-06	-8.84E-05
0.000683	0.000693	0.000696	0.00071	0.000668	0.000604	0.001572	0.001488	-1.89E-06	-8.67E-05
0.001015	0.001021	0.001025	0.001019	0.000966	0.000884	0.001218	0.001113	-1.97E-06	-9.63E-05
0.001013	0.001019	0.00102	0.001011	0.000962	0.000886	0.001218	0.001119	-2.81E-06	-9.33E-05
0.001012	0.001015	0.00102	0.001013	0.000956	0.000874	0.001216	0.00112	-3.23E-06	-0.00010015
0.001004	0.001012	0.001016	0.001015	0.000953	0.000875	0.00122	0.001129	-3.22E-06	-0.00010907
0.001009	0.001014	0.001015	0.001012	0.000966	0.000874	0.001219	0.001135	-3.31E-06	-0.00011296
0.001005	0.001012	0.001013	0.001013	0.000965	0.000868	0.001216	0.001132	-3.63E-06	-0.00012068

P@31	P#3	P*3	PX-1	PX-2	PX-3	PX-4	PX-5	PY-1	PY-2
1.72E-06	0.001724	0.001725	0.001726	0.001695	0.001603	0.00094	0.00118	0.002068	0.001364
1.14E-06	0.001729	0.001729	0.001729	0.001632	0.00129	0.000947	0.001194	0.002215	0.001298
-6.60E-06	0.001711	0.001707	0.001707	0.00166	0.001335	0.000953	0.001193	0.002212	0.001249
-1.16E-05	0.001719	0.001717	0.001716	0.00169	0.001371	0.000953	0.001173	0.00218	0.001227
-7.30E-06	0.00172	0.001721	0.001721	0.001681	0.001372	0.000947	0.001184	0.002184	0.001202
-1.53E-05	0.001718	0.001718	0.001718	0.001677	0.001352	0.000945	0.001183	0.00216	0.00118
1.18E-05	0.001812	0.001814	0.001814	0.001531	0.001642	0.000998	0.00124	0.002136	0.001473
-3.47E-06	0.001808	0.00181	0.00181	0.001545	0.001682	0.000991	0.001245	0.002315	0.001414
-1.03E-07	0.001796	0.001792	0.001791	0.001541	0.001645	0.000986	0.001236	0.002276	0.001353
-9.65E-06	0.001792	0.001794	0.001795	0.001586	0.00173	0.000983	0.001238	0.00227	0.001326
-1.18E-05	0.001786	0.001789	0.001787	0.001613	0.001741	0.000983	0.00123	0.00221	0.001284
-1.50E-05	0.001783	0.001786	0.001785	0.001651	0.00179	0.00098	0.001227	0.002155	0.001258
6.62E-08	0.001872	0.001875	0.001877	0.001213	0.001303	0.001059	0.001276	0.00225	0.001558
8.24E-06	0.00187	0.001872	0.001872	0.001217	0.001293	0.001043	0.00129	0.002365	0.001496
4.83E-06	0.001863	0.001866	0.001864	0.001255	0.001343	0.001038	0.001285	0.002374	0.001449
-4.65E-06	0.001858	0.001861	0.001861	0.001283	0.001344	0.001041	0.001284	0.00233	0.001404
-7.12E-06	0.001851	0.001855	0.001854	0.001331	0.001386	0.001036	0.001279	0.00227	0.001366
-3.81E-06	0.001846	0.001847	0.001848	0.001378	0.001457	0.001031	0.001274	0.002206	0.001333
6.29E-06	0.001661	0.001664	0.001664	0.001575	0.001627	0.000892	0.001196	0.001938	0.001157
6.73E-06	0.001662	0.001662	0.00166	0.001598	0.001664	0.000894	0.001196	0.002077	0.001081
1.48E-06	0.00166	0.001664	0.001662	0.001619	0.001687	0.000896	0.001196	0.002155	0.001037
1.89E-06	0.001662	0.001665	0.001663	0.001616	0.001685	0.000897	0.001193	0.002142	0.001041
-5.65E-06	0.001656	0.001658	0.001654	0.001615	0.001671	0.000896	0.001186	0.002175	0.00101
-4.52E-06	0.001659	0.00166	0.00166	0.001621	0.001675	0.000896	0.001189	0.002182	0.000991

PY-3	PY-4	PY-5	PS-1	PS-2	PS-3	P@32	RADX	YAWX	RADY
0.001364	0.001805	0.00188	0.002054	0.001579	0.001567	-8.27E-06	0.001739	0.002584	0.089008
0.001307	0.001865	0.00198	0.002211	0.001633	0.001615	-1.14E-05	0.001739	0.002584	0.188944
0.001261	0.001882	0.001959	0.002189	0.001576	0.001563	-1.64E-05	0.00174	0.002584	0.27875
0.001236	0.001893	0.001945	0.002172	0.001535	0.001523	-1.44E-05	0.001739	0.002584	0.368724
0.001219	0.001858	0.001989	0.002185	0.001538	0.001525	-1.52E-05	0.001739	0.002584	0.459778
0.001188	0.001844	0.001951	0.002142	0.00151	0.001502	-1.74E-05	0.001739	0.002584	0.544923
0.001472	0.001395	0.001996	0.002189	0.001707	0.001672	1.83E-06	0.001741	0.002585	0.089324
0.001427	0.001314	0.002132	0.002315	0.001721	0.001716	-4.00E-06	0.00174	0.002585	0.188874
0.001365	0.001328	0.002092	0.002281	0.001658	0.001646	-8.96E-06	0.001739	0.002584	0.279549
0.001337	0.001294	0.002067	0.002252	0.001612	0.001605	-1.02E-05	0.001739	0.002584	0.368581
0.001312	0.001288	0.002015	0.002224	0.001585	0.001583	-1.11E-05	0.001739	0.002585	0.458786
0.001273	0.001326	0.001972	0.002162	0.001557	0.001545	-1.07E-05	0.001739	0.002584	0.54577
0.001531	0.000942	0.002086	0.002207	0.001744	0.001702	1.37E-06	0.001739	0.002585	0.088041
0.001505	0.001028	0.002184	0.002361	0.001788	0.001777	5.40E-06	0.00174	0.002585	0.187176
0.001448	0.001159	0.002186	0.002363	0.001749	0.001739	-3.37E-06	0.001739	0.002585	0.280249
0.001412	0.001168	0.002132	0.002327	0.001706	0.001691	-5.10E-06	0.001739	0.002585	0.369554
0.001365	0.001079	0.002079	0.002289	0.001666	0.001652	-7.37E-06	0.001739	0.002585	0.45978
0.001341	0.001179	0.002031	0.002195	0.001608	0.001599	-5.87E-06	0.001739	0.002585	0.545657
0.001157	0.001426	0.001752	0.00199	0.001444	0.001431	4.14E-06	0.001738	0.002584	0.088397
0.001103	0.001427	0.001866	0.002122	0.001467	0.001457	-1.40E-06	0.001738	0.002585	0.187749
0.001053	0.001431	0.001925	0.002142	0.001439	0.001428	-2.21E-06	0.001738	0.002585	0.279358
0.001045	0.001399	0.001935	0.002158	0.001442	0.001432	-2.39E-06	0.001738	0.002584	0.368961
0.001029	0.001375	0.001956	0.002194	0.001451	0.001439	-4.60E-06	0.001738	0.002585	0.459271
0.000995	0.001366	0.001954	0.002195	0.001436	0.001423	-4.41E-06	0.001738	0.002584	0.545921

YAWY	RADS	YAWS	TORQ
-0.036301	0.091659	-0.047767	0.5969
-0.02799	0.184178	-0.042136	0.615962
-0.027287	0.280168	-0.042137	0.622696
-0.024085	0.377043	-0.039934	0.632718
-0.01826	0.4744	-0.038337	0.634136
-0.016306	0.569547	-0.034425	0.656054
-0.034874	0.090876	-0.04843	0.544154
-0.029068	0.184099	-0.043246	0.524237
-0.027385	0.28057	-0.042151	0.541716
-0.025805	0.376972	-0.040893	0.553033
-0.020022	0.474295	-0.040115	0.567517
-0.018011	0.568587	-0.036141	0.575912
-0.038073	0.091063	-0.05283	0.519316
-0.030074	0.18401	-0.044497	0.511476
-0.026994	0.280112	-0.042157	0.515308
-0.026477	0.37673	-0.042588	0.527754
-0.022553	0.473893	-0.041668	0.537115
-0.019331	0.568598	-0.037884	0.532835
-0.034586	0.090738	-0.043644	0.594426
-0.028111	0.184229	-0.04012	0.613251
-0.02785	0.280917	-0.040787	0.624299
-0.020852	0.377281	-0.036084	0.582391
-0.017745	0.474234	-0.03438	0.598972
-0.016454	0.568787	-0.032673	0.615632

Table C5. Lab 1 processed results for build #2

	P_std	T_std	Ro_std	Ut_std	Qtip	Qax	Q_2/Qax	M_nc/M_ni	Pt_2
5+4	2115.594	518.67	0.002367	252.8982	16.08133	5.926357	0.99285868	0.99772842	398.598
	2115.594	518.67	0.002367	252.8982	16.07992	5.943987	0.99283727	0.997721696	398.5802
	2115.594	518.67	0.002367	252.8982	16.07891	5.918502	0.99286769	0.997731565	398.5388
	2115.594	518.67	0.002367	252.8982	16.08031	5.933598	0.9928496	0.997725544	398.5773
	2115.594	518.67	0.002367	252.8982	16.07949	5.905579	0.99288307	0.997736485	398.5233
	2115.594	518.67	0.002367	252.8982	16.07916	5.901556	0.99288782	0.997738081	398.509
5+4+3	2115.594	518.67	0.002367	252.8982	15.98939	5.577918	0.99327331	0.997869308	397.1536
	2115.594	518.67	0.002367	252.8982	15.99192	5.603159	0.99324292	0.997859379	397.1962
	2115.594	518.67	0.002367	252.8982	15.99362	5.606855	0.99317093	0.997857811	397.214
	2115.594	518.67	0.002367	252.8982	15.99595	5.509168	0.99335584	0.997894949	397.1926
	2115.594	518.67	0.002367	252.8982	15.99688	5.499864	0.99336693	0.997898478	397.1826
	2115.594	518.67	0.002367	252.8982	15.99678	5.482838	0.99338734	0.997904963	397.1726
5+4+3+2+1	2115.594	518.67	0.002367	252.8982	15.97058	5.019924	0.99394209	0.998085566	396.2542
	2115.594	518.67	0.002367	252.8982	15.97183	5.061638	0.99389196	0.998069467	396.3028
	2115.594	518.67	0.002367	252.8982	15.97438	5.060311	0.9938936	0.998069728	396.3416
	2115.594	518.67	0.002367	252.8982	15.97418	5.023796	0.99401582	0.998083699	396.3052
	2115.594	518.67	0.002367	252.8982	15.97753	5.07846	0.99387183	0.99806241	396.4091
	2115.594	518.67	0.002367	252.8982	15.97901	5.085131	0.99386388	0.998059607	396.4568
5	2115.594	518.67	0.002367	252.8982	16.14368	7.459917	0.99102786	0.997126648	401.236
	2115.594	518.67	0.002367	252.8982	16.14441	7.366726	0.9911393	0.997162468	401.1902
	2115.594	518.67	0.002367	252.8982	16.14412	7.289348	0.99123167	0.997192413	401.1212
	2115.594	518.67	0.002367	252.8982	16.14309	7.150523	0.99139763	0.99724641	400.9851
	2115.594	518.67	0.002367	252.8982	16.14308	7.254639	0.99127302	0.997206103	401.0582
	2115.594	518.67	0.002367	252.8982	16.14465	7.325644	0.99118816	0.997178369	401.14

Tt_2	T_dew	Ut	Dpts_noz	Dps_rise	Torq	Pris/noz	M_2	V_2	Ros_2
458.5715	-35.77161	252.2699	2.352098889	12.1529889	59690	5.1668699	0.146308	152.5956	0.002616
458.5768	-35.77148	252.2699	2.358985556	12.164381	61596.23	5.1566153	0.14653	152.8275	0.002616
458.5788	-35.77147	252.2699	2.348752222	12.1583539	62269.59	5.1765162	0.146221	152.5066	0.002615
458.5707	-35.77161	252.2699	2.354946667	12.1318952	63271.82	5.1516645	0.146402	152.6929	0.002616
458.5552	-35.77185	252.2699	2.343623333	12.1803743	63413.6	5.1972406	0.146063	152.3385	0.002616
458.5513	-35.7719	252.2699	2.341965556	12.2380246	65605.39	5.2255357	0.146016	152.2885	0.002616
458.681	-35.76973	251.9557	2.206662222	13.4126022	54415.36	6.0782308	0.14217	148.3128	0.002607
458.6371	-35.77036	251.9557	2.216864444	13.4192236	52423.75	6.053245	0.142486	148.634	0.002608
458.614	-35.77079	251.9557	2.218451111	13.3789574	54171.56	6.0307651	0.142525	148.671	0.002608
458.5944	-35.7711	251.9557	2.180038889	13.3290542	55303.31	6.114136	0.141278	147.3719	0.002608
458.5639	-35.77154	251.9557	2.176362222	13.3665392	56751.66	6.1416887	0.141159	147.244	0.002609
458.5693	-35.77162	251.9557	2.169643333	13.3793538	57591.24	6.1666144	0.140941	147.0178	0.002609
458.6415	-35.77038	251.9557	1.98308	14.2218998	51931.55	7.1716218	0.134976	140.8293	0.002604
458.6275	-35.77062	251.9557	1.999702222	14.1501756	51147.64	7.0761413	0.135531	141.4041	0.002605
458.6	-35.77099	251.9557	1.999406667	14.0952729	51530.82	7.0497279	0.135507	141.3744	0.002605
458.5843	-35.77125	251.9557	1.984933333	14.1662686	52775.37	7.1368989	0.135025	140.8715	0.002605
458.5726	-35.77144	251.9557	2.006921111	14.0627884	53711.45	7.0071456	0.135739	141.6122	0.002605
458.5799	-35.77137	251.9557	2.009801111	14.0180863	53283.45	6.9748625	0.135821	141.6981	0.002606
458.5707	-35.77167	252.2699	2.973641111	9.68512556	59442.55	3.2569921	0.163767	170.7159	0.002626
458.5736	-35.77153	252.2699	2.936621111	9.73387044	61325.1	3.3146498	0.16274	169.652	0.002626
458.5659	-35.77159	252.2699	2.90566	9.73102133	62429.86	3.3489883	0.161889	168.768	0.002626
458.5523	-35.77181	252.2699	2.84993	9.78605711	58239.07	3.4337886	0.160353	167.1725	0.002626
458.5516	-35.77184	252.2699	2.891521111	9.81231578	59897.19	3.3934789	0.161513	168.3747	0.002626
458.5426	-35.77198	252.2699	2.920131111	9.74787822	61563.15	3.3381646	0.162292	169.1812	0.002626

Ut/Ut_std	Mflow	Pr_e	HPs	HPtc	Delta	Theta	Ro_wqd	Ut/Ut_c	Mflow_c
0.997515528	1.805856	1.015648	18252.11	0	0.975208	0.88413	1.0126846	1.0675925	1.730189
0.997515528	1.80844	1.015634	18835	0	0.975164	0.88414	1.0126857	1.0675864	1.7327524
0.997515528	1.804529	1.015684	19040.9	0	0.975063	0.884144	1.0126862	1.0675841	1.729189
0.997515528	1.806894	1.015578	19347.36	0	0.975157	0.884128	1.0126855	1.067594	1.7312708
0.997515528	1.802612	1.015772	19390.72	0	0.975025	0.884098	1.0126863	1.0676141	1.727367
0.997515528	1.801986	1.015927	20060.93	0	0.97499	0.884091	1.0126867	1.0676191	1.7268198
0.996273292	1.749456	1.019751	16618.5	0	0.971674	0.884341	1.0127186	1.0661424	1.6824559
0.996273292	1.753536	1.019702	16010.26	0	0.971778	0.884256	1.0127182	1.0661977	1.6861043
0.996273292	1.754167	1.019592	16544.04	0	0.971822	0.884211	1.0127178	1.0662267	1.6865856
0.996273292	1.739099	1.019711	16889.68	0	0.971769	0.884174	1.0127155	1.0662503	1.672148
0.996273292	1.7377	1.019829	17332.01	0	0.971745	0.884115	1.0127156	1.0662889	1.6707797
0.996273292	1.735019	1.019905	17588.42	0	0.97172	0.884125	1.0127154	1.066282	1.6682553
0.996273292	1.659241	1.023242	15859.94	0	0.969473	0.884264	1.0127295	1.0661981	1.5992278
0.996273292	1.666148	1.022953	15620.54	0	0.969592	0.884238	1.0127293	1.0662157	1.6056595
0.996273292	1.666073	1.022816	15737.56	0	0.969687	0.884185	1.0127281	1.0662498	1.6053747
0.996273292	1.660131	1.023088	16117.65	0	0.969598	0.884154	1.0127282	1.0662698	1.5997639
0.996273292	1.669213	1.022684	16403.52	0	0.969852	0.884132	1.0127267	1.0662837	1.6080709
0.996273292	1.670377	1.022552	16272.81	0	0.969969	0.884146	1.0127254	1.0662738	1.6090147
0.997515528	2.028131	1.005589	18176.44	0	0.981662	0.884128	1.01265	1.0675753	1.9304053
0.997515528	2.01558	1.005942	18752.09	0	0.98155	0.884134	1.0126485	1.0675708	1.9186871
0.997515528	2.005045	1.006128	19089.91	0	0.981381	0.884119	1.0126483	1.0675805	1.9089681
0.997515528	1.985969	1.006612	17808.44	0	0.981048	0.884093	1.0126483	1.0675977	1.8914147
0.997515528	2.000249	1.006418	18315.46	0	0.981227	0.884091	1.0126492	1.0675991	1.9046648
0.997515528	2.010029	1.00608	18824.88	0	0.981427	0.884074	1.0126489	1.0676103	1.913566

Pr_	Pwrs_c	Alph	Wco	Fco*Pco_e	Pco_	Pco_/Pco_e	Fco	Pco_e	Pwrco	Eco
1.030949	17618.32	1	175.1346	0.480829532	0.864996	1.149370987	0.638906	0.752582	111.8946	0.004297
1.03098	18181.89	1	180.4694	0.482036376	0.865885	1.149371673	0.639853	0.753355	115.4739	0.004174
1.030966	18382.6	1	182.8377	0.48083055	0.865491	1.149361476	0.638537	0.753019	116.7486	0.004119
1.030897	18676.48	1	185.5373	0.480336576	0.863556	1.149353424	0.639306	0.751341	118.6151	0.00405
1.031023	18720.49	1	186.3947	0.48116278	0.867065	1.149443501	0.637864	0.754334	118.8945	0.004047
1.03117	19368.13	1	192.9043	0.483270608	0.871191	1.149512683	0.637662	0.757879	123.0077	0.003929
1.034252	16162.07	1	165.2169	0.518918866	0.957325	1.146165139	0.62128	0.835242	102.6459	0.005055
1.034267	15567.99	1	158.7996	0.520225299	0.957755	1.146280499	0.622627	0.835533	98.87292	0.005262
1.034163	16085.84	1	164.035	0.518785981	0.954846	1.146296367	0.622805	0.832983	102.1618	0.005078
1.034029	16422.39	1	168.9129	0.512330847	0.9511	1.146289228	0.617474	0.829721	104.2992	0.004912
1.034125	16852.24	1	173.4761	0.51330095	0.953777	1.146403688	0.616968	0.831973	107.0293	0.004796
1.034157	17102.1	1	176.3146	0.513007913	0.954674	1.146402961	0.616036	0.832756	108.6161	0.004723
1.036351	15458.49	1	166.2486	0.523037256	1.015979	1.147112593	0.590546	0.885684	98.17747	0.005327
1.036167	15223	1	163.0602	0.522500518	1.010837	1.147074043	0.592921	0.881231	96.68188	0.005404
1.036023	15335.02	1	164.2892	0.520323168	1.006812	1.147083953	0.592816	0.877714	97.3933	0.005342
1.036204	15706.51	1	168.8593	0.521065975	1.011884	1.147195808	0.590744	0.88205	99.75265	0.005224
1.035935	15980.68	1	170.9193	0.519915673	1.004365	1.14711595	0.593812	0.875556	101.4939	0.005123
1.035817	15851.58	1	169.4392	0.518542879	1.001067	1.147049276	0.59416	0.872732	100.674	0.005151
1.024594	17430.2	1	155.2942	0.427287284	0.6874	1.146783992	0.71284	0.599415	110.6999	0.00386
1.024715	17984.35	1	161.2099	0.426765321	0.690777	1.146823417	0.708513	0.60234	114.2193	0.003736
1.024708	18311.31	1	164.9764	0.424464786	0.690561	1.146839413	0.704924	0.602143	116.2958	0.00365
1.024847	17087.61	1	155.3802	0.422904839	0.694463	1.146929507	0.698442	0.605497	108.5241	0.003897
1.024916	17570.88	1	158.6631	0.427031925	0.69638	1.146959975	0.703335	0.607153	111.5933	0.003827
1.024751	18055.7	1	162.2827	0.426214538	0.691788	1.146915902	0.706622	0.603172	114.6725	0.003717

Table C6. Lab 2 processed results for build #2

S Probe

	Rad	Alpha	Pch	U(r)	Ptqp	Va/U	Vu/U	Wu/U
5+4	0.91659	47.76725	0	239.4239	0.125646	0.561928	0.619008	0.380992
	1.84178	42.13622	0	226.4574	0.151219	0.723633	0.654684	0.345316
	2.801678	42.13668	0	213.0044	0.169197	0.790532	0.71522	0.28478
	3.770434	39.93386	0	199.4273	0.19148	0.88958	0.744698	0.255302
	4.744002	38.33721	0	185.7827	0.222031	0.985318	0.779197	0.220803
	5.695468	34.42477	0	172.4479	0.252566	1.1009	0.754501	0.245499
5+4+3	0.908763	48.43041	0	239.2353	0.134118	0.565748	0.637899	0.362101
	1.840993	43.24554	0	226.1864	0.158681	0.716996	0.674378	0.325622
	2.805702	42.15115	0	212.6828	0.17681	0.797276	0.721689	0.278311
	3.76972	40.89289	0	199.1889	0.199008	0.878178	0.760511	0.239489
	4.742954	40.11472	0	185.566	0.226454	0.95157	0.801714	0.198286
	5.685866	36.14075	0	172.3676	0.255137	1.057221	0.772091	0.227909
5+4+3+2+1	0.910629	52.83008	0	239.2092	0.135244	0.506766	0.668368	0.331632
	1.840101	44.49737	0	226.1988	0.161826	0.691144	0.679123	0.320877
	2.801118	42.15723	0	212.747	0.183087	0.790188	0.715425	0.284575
	3.767303	42.58786	0	199.2228	0.205575	0.844677	0.77639	0.22361
	4.738928	41.66803	0	185.6224	0.232958	0.92142	0.820033	0.179967
	5.685984	37.88365	0	172.3659	0.259031	1.015995	0.790465	0.209535
5	0.907382	43.64378	0	239.5529	0.121601	0.648604	0.618602	0.381398
	1.842291	40.11972	0	226.4502	0.145082	0.791525	0.666991	0.333009
	2.809172	40.7866	0	212.8994	0.165735	0.864139	0.745552	0.254448
	3.772806	36.084	0	199.394	0.190374	0.993842	0.724297	0.275703
	4.74234	34.37991	0	185.806	0.222822	1.109027	0.758796	0.241204
	5.687871	32.67272	0	172.5544	0.258556	1.232224	0.790245	0.209755

Y Probe

Rad	Alpha	Pch	U(r)	Ptqp	Va/U	Vu/U	Wu/U
0.890079	36.30117	0	239.7954	0.126097	0.56362	0.414037	0.585963
1.889442	27.99022	0	225.7894	0.152325	0.741152	0.393915	0.606085
2.787498	27.28714	0	213.2031	0.170645	0.807975	0.416797	0.583203
3.687241	24.08541	0	200.5932	0.19003	0.878968	0.392913	0.607087
4.597775	18.25998	0	187.8321	0.217095	0.988142	0.326031	0.673969
5.449225	16.30585	0	175.899	0.244831	1.06817	0.312473	0.687527
0.893244	34.87404	0	239.4525	0.130663	0.558535	0.389263	0.610737
1.888742	29.06776	0	225.518	0.159646	0.728021	0.404675	0.595325
2.795495	27.38534	0	212.8257	0.176179	0.792843	0.410714	0.589286
3.685813	25.80508	0	200.3634	0.198329	0.863463	0.417509	0.582491
4.587856	20.02163	0	187.737	0.219914	0.94954	0.34601	0.65399
5.457702	18.01135	0	175.5613	0.245138	1.015889	0.330305	0.669695
0.880414	38.07336	0	239.6321	0.137383	0.551047	0.431662	0.568338
1.871756	30.07427	0	225.7558	0.162758	0.708298	0.410161	0.589839
2.802485	26.99412	0	212.7278	0.183985	0.798737	0.406873	0.593127
3.695538	26.47736	0	200.2273	0.203788	0.85137	0.424057	0.575943
4.597799	22.55315	0	187.5979	0.226236	0.930032	0.386243	0.613757
5.456571	19.33133	0	175.5772	0.250905	0.996612	0.349621	0.650379
0.883974	34.58632	0	239.881	0.118098	0.605898	0.417768	0.582232
1.87749	28.11135	0	225.9569	0.14263	0.767327	0.40991	0.59009
2.793579	27.85039	0	213.1179	0.166364	0.861127	0.454989	0.545011
3.68961	20.85178	0	200.56	0.186716	0.962659	0.366676	0.633324
4.592711	17.74471	0	187.9031	0.215978	1.071416	0.342854	0.657146
5.459211	16.45358	0	175.7591	0.247649	1.168656	0.345142	0.654858

THIS PAGE INTENTIONALLY LEFT BLANK

APPENDIX D. EQUATIONS

D.1. EQUATIONS USED TO CHECK HP VEE PROGRAM

The equations below are the equations that were used to calculate mass flow rate, flow coefficient, pressure-rise coefficient, power coefficient, and efficiency coefficient from the pressure data obtained during the experiment. These calculations were used to check the HP Vee program which also calculated these results which can be found in Appendix C.

Mass flow rate: mflow

$$\dot{m} = \rho A_o \sqrt{\frac{2}{\rho}(p_{ot} - p_{os})}$$

Flow coefficient: Fco

$$\phi = \frac{\dot{m}}{\rho A_s U_t}$$

Pressure-rise coefficient: Pco

$$\Pi = \frac{p_{exit} - p_{inlet}}{\rho U_t^2} = \frac{PES - P2SW}{\rho U_t^2}$$

Power coefficient: Pwrco

$$P = \frac{T\left(\frac{\pi N}{30}\right)}{\rho U_t^3 A_s}$$

Efficiency: Eco

$$\eta = \frac{\phi \Pi}{P}$$

D.2. EQUATIONS USED BY HP VEE PROGRAM

Below are the equations and definitions used by the HP Vee program in Moyle's Lab 1 [Ref. 4] to calculate the values above. The order below follows the order in the lab's equation program "CallRedLabCC".

C in_hg = 13.62438

C ibf_inw = 5.176

Gam = 1.4

Cm = $\frac{(Gam-1)}{2}$

Ce = $\frac{(Gam-1)}{Gam}$

Cr = $\frac{1}{(Gam-1)}$

Ar = $\frac{1.5^2}{1.5^2-0.9^2}$

P_std = 30 * Cin_hg * Cibf_inw

Ro_std = 0.002367

T_std = 458.67 + 60

R_std = $\frac{P\_std * Ro\_std}{T\_std}$

Ut_std = $\frac{805}{30}$ * 2π * 1.5

As_std = π * $\left(1.5^2-0.9^2\right)$

Dps_tare = $\frac{(P@21+P@22)}{2}$*10000

Dps_tnk = Pot * 10000

Ps_datum = Pbar * Cinw_hg – Dps_tnk + Dps_tare

T_ro = TRO * 1000 + 458.67

T_dew = 1.8 * (9.29627 * Twet – 37.64990) + 32

T_dewc = $\frac{(T\_dew - 32)}{1.8}$

Ps_ro = Ps_datum + P2SW * 10000

Pvap_ro = Cinw_hg * (0.522 + 0.0159 * (T_dew – 60))

Ro_wqdry = 1 – 0.378 * $\frac{Pvap\_ro}{Ps\_ro - Pvap\_ro}$

R_w = $\frac{R\_std}{Ro\_wqdry}$

Tt_noz = T_ro

Dpts_noz = (Pot-Pos) * 10000

Ps_noz = Ps_datum + Pos * 10000

Pt_noz = Ps_datum + Pot * 10000

Rot_noz = $\frac{Pt\_noz}{R\_w * Tt\_noz}$ *Clbf_inw

M_nozc = $\left\{ \frac{\left[\left(\frac{Dpts\_noz}{Ps\_noz} + 1 \right)^{Ce} - 1 \right]}{Cm} \right\}^{0.5}$

Ts_noz = $\frac{Tt\_noz}{\left(1 + Cm * M\_nozc^2\right)^{Cr}}$

Ros_noz = $\frac{Rot\_noz}{\left(1 + Cm * M\_nozc^2\right)^{Cr}}$

Mnozi = $\frac{\sqrt{\frac{Dpts\_noz * Clbf\_inw}{0.5 * Ros\_noz}}}{\sqrt{Gam * R\_w * Ts\_noz}}$

Tt_2 = T_ro

Ps_2 = Ps_datum + $\frac{(P2SW + P2SW + P2SW) * 10000}{3}$

M_20 = 0.25

Mstep = $\frac{M\_20}{100}$

M_2 = M_20-Mstep * (I-1) 1<I<100

Ts_2 = $\frac{Tt\_2}{1\_Cm * M\_2^2}$

Pt_2 = Ps_2 * $\left(1 + Cm * M\_2^2\right)^{\frac{1}{Ce}}$

Rot_2 = $\frac{Pt\_2}{R\_w * Tt\_2} * Clbf\_inw$

Ros_2a = $\frac{Rot\_2}{\left(1 + Cm * M\_2^2\right)^{Cr}}$

Ros_2b = $\frac{M\_nozc * \sqrt{Ts\_noz}}{M\_2 * \sqrt{Ts\_2}} * Ros\_noz * Ar$

M_20 = M_2 + Mstep

Mstep = $\frac{Mstep}{100}$

Cycles = Cycles +1

Q_2 = 0.5 * Ps_2 * Gam * M_2^2

Ros_2 = $\frac{(Ros\_2b + Ros\_2a)}{2}$

Fbld = Fbld

Ut = $\frac{Fbld}{30}$ * 2π * 1.5

Torq = Torq * 100000

Shaftpwr = $\frac{Torq * Ut}{1.5}$

Dps_rise = (PES – P2SW) * 10000

Dtemp = T_ro – 458.67 -32

Alph = $\frac{\left(1 + 0.0000063 * Dtemp + 0.0000016 * Dtemp^2\right)}{1.0014308}$

As = As_std* $Alph^2$

Qtip = $\frac{0.5 * Ros\_2 * Ut^2}{Clbf\_inw}$

Qax = Dpts_noz * $\left(\frac{Ps\_noz}{Ps\_2}\right) * Ar^2$

V_2 = M_2 * $\sqrt{Gam * R\_w * Ts\_2}$

Mflow = Ros_2 * V_2 * As

Pr_e = $\frac{Ps\_datum + PES * 10000}{Pt\_2}$

Pr_i = $\frac{Ps\_datum + P2SW * 10000}{Pt\_2}$

Pr_ = $\frac{\mathrm{Pr}\_e}{\mathrm{Pr}\_i}$

Pwrs = $\frac{Shaftpwr}{550}$

Pwrtc = 0

Delta = $\frac{Pt\_2}{\left(\frac{P\_std}{Clbf\_inw}\right)}$

Theta = $\frac{Tt\_2}{T\_std}$

Omega = $\frac{R\_w}{R\_std}$

Ut_c = $\frac{Ut * Alph}{\sqrt{Omega * Theta}}$

Mflow_c = $\frac{Mflow * \sqrt{Omega * Theta}}{Delta * Alph^2}$

Pwrs_c = $\frac{Pwrs * \sqrt{Omega * Theta}}{Delta * Alph^2} * \left(\frac{Ut\_std}{Ut}\right)^3$

Fco = $\frac{Mflow\_c}{Ro\_std * As\_std * Ut\_std}$

Pco = $\frac{(\mathrm{Pr}\_ - 1) * P\_std}{0.5 * Ro\_std * Ut\_std^2}$

Pwrco = $\frac{Pwrs\_c}{0.5 * Ro\_std * Ut\_std^3 * As\_std} * 550$

Eco = $\frac{Mflow}{Shaftpwr} * \frac{R\_w}{Ce} * Tt\_2 * \left(\mathrm{Pr}\_^{Ce} - 1\right)$

Wco = $\frac{Pwrco}{Fco}$

Pco_e = Eco * Wco

APPENDIX E. VELOCITY DIAGRAMS

E.1. VELOCITY DIAGRAMS BUILD #1

1. Point Location # 3

Figures E1a-d show the velocity diagrams for point location # 3 for all throttle settings.

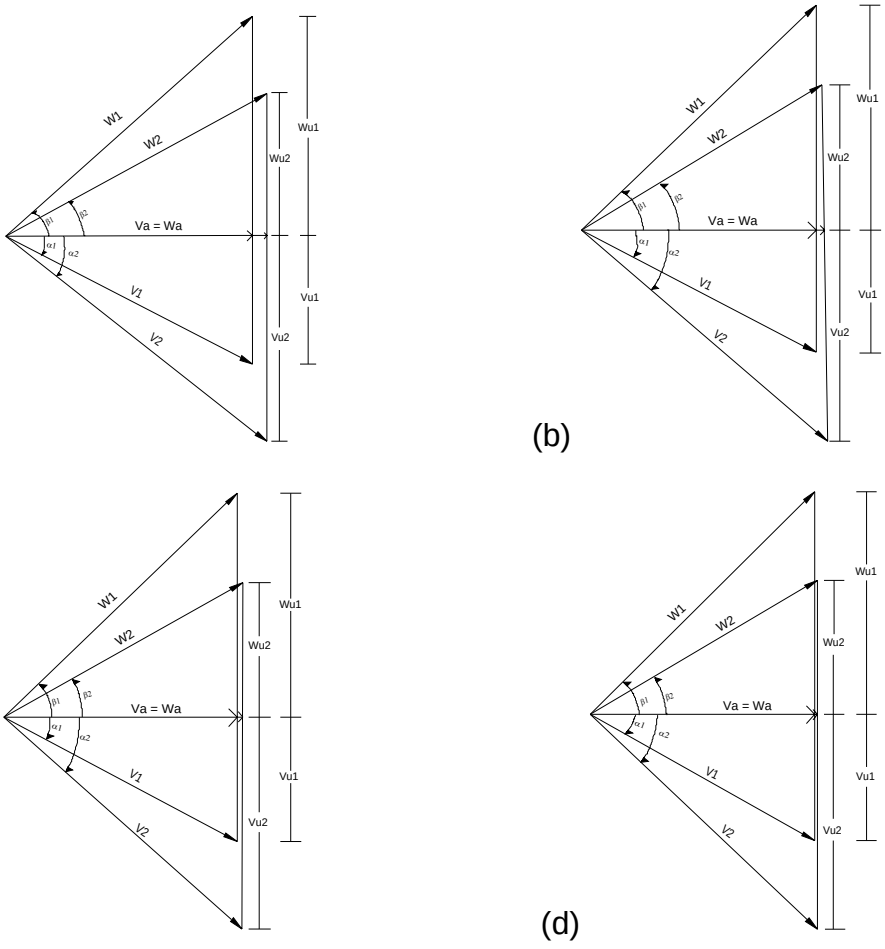

Figure E1. Point location #3 – (a) Open throttle (b) Throttle 5+4 (c) NOP (d) Near stall

2. Point Location # 5

Figures E2a-d show the velocity diagrams for point location # 5 for all throttle settings.

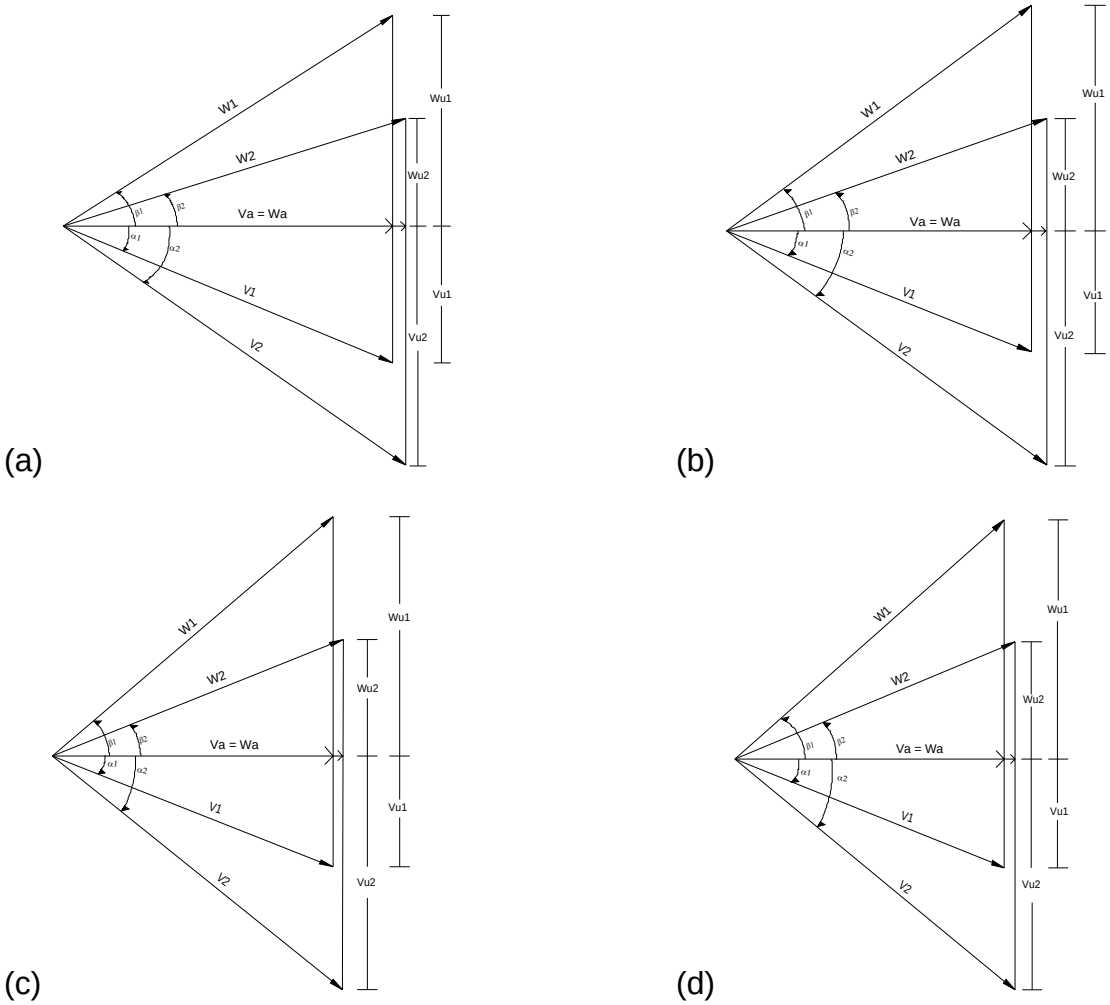

Figure E2. Point location #5– (a) Open throttle (b) Throttle 5+4 (c) NOP (d) Near stall

3. Point Location # 6

Figures E3a-c show the velocity diagrams for point location # 6 for all throttle settings except open throttle (throttle 5).

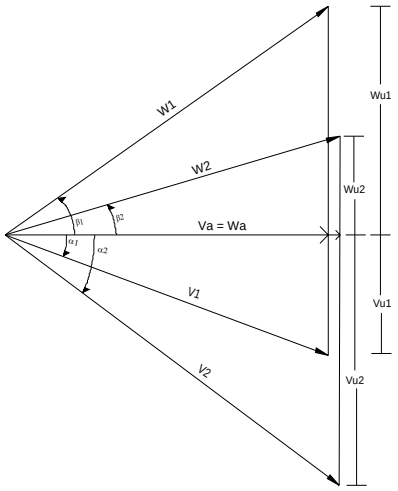

(a)

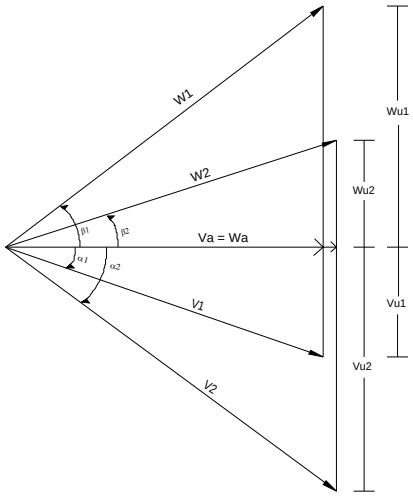

(b)

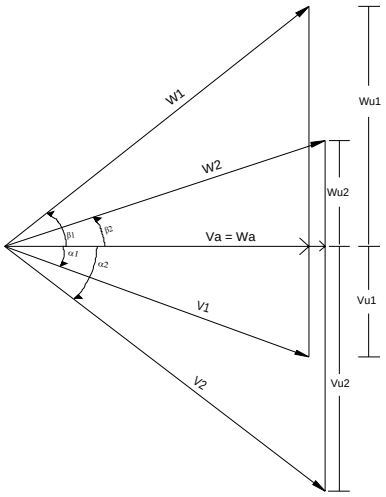

(c)

Figure E3. Point location #6– (a) Throttle 5+4 (b) NOP (c) Near stall

4. Tables for Velocity Diagrams

Tables E1-E4 have all of the values for the velocity diagrams for build #1.

Table E1. Values for all velocity diagrams for throttle setting 5 build #1

Location	α_2	α_1	β_2	β_1	Vu_2/U_2	Vu_1/U_1	Wu_2/U_2	Wu_1/U_1
2	-38.11	-28.08	35.28	47.13	0.526	0.331	0.474	0.669
3	-36.88	-26.35	27.46	40.38	0.591	0.368	0.409	0.632
4	-36.10	-24.29	21.78	36.47	0.646	0.379	0.354	0.621
5	-34.91	-22.50	17.42	32.51	0.690	0.394	0.310	0.606
6								
7								

Location	$Va_2/U_2 = Wa_2/U_2$	$Va_1/U_1 = Wa_1/U_1$	V_2/U_2	V_1/U_1	W_2/U_2	W_1/U_1
2	0.670	0.621	0.852	0.704	0.821	0.913
3	0.787	0.743	0.984	0.829	0.887	0.975
4	0.886	0.840	1.096	0.922	0.954	1.045
5	0.988	0.951	1.205	1.029	1.035	1.128
6						
7						

Table E2. Values for all velocity diagrams for throttle setting 5+4 build #1

Location	α_2	α_1	β_2	β_1	Vu_2/U_2	Vu_1/U_1	Wu_2/U_2	Wu_1/U_1
2	-41.96	-30.69	38.11	49.41	0.534	0.337	0.466	0.663
3	-40.67	-27.56	31.24	43.87	0.607	0.352	0.393	0.648
4	-37.79	-22.46	24.67	40.88	0.628	0.323	0.372	0.677
5	-37.06	-22.3	19.9	37.31	0.676	0.35	0.324	0.65
6	-36.04	-19.89	16.01	34.50	0.717	0.345	0.283	0.655
7	-33.49	-14.18	13.75	35.3	0.729	0.263	0.270	0.737

Location	$Va_2/U_2 = Wa_2/U_2$	$Va_1/U_1 = Wa_1/U_1$	V_2/U_2	V_1/U_1	W_2/U_2	W_1/U_1
2	0.594	0.568	0.799	0.660	0.755	0.873
3	0.707	0.674	0.932	0.76	0.809	0.935
4	0.810	0.782	1.025	0.846	0.891	1.034
5	0.895	0.853	1.122	0.922	0.952	1.072
6	0.986	0.953	1.219	1.014	1.026	1.156
7	1.103	1.041	1.322	1.074	1.136	1.275

Table E3. Values for all velocity diagrams for throttle setting 5+4+3 build #1

Location	α_2	α_1	β_2	β_1	Vu_2/U_2	Vu_1/U_1	Wu_2/U_2	Wu_1/U_1
2	-43.63	-33.18	39.65	49.86	0.535	0.355	0.465	0.645
3	-42.12	-28.5	30.22	44.25	0.608	0.358	0.392	0.642
4	-38.46	-22.52	26.33	42.77	0.616	0.309	0.384	0.690
5	-38.20	-21.18	21.36	39.72	0.668	0.318	0.332	0.682
6	-36.70	-19.25	17.96	37.42	0.697	0.313	0.303	0.687
7	-35.23	-15.94	15.14	36.88	0.723	0.276	0.277	0.724

Location	$Va_2/U_2 = Wa_2/U_2$	$Va_1/U_1 = Wa_1/U_1$	V_2/U_2	V_1/U_1	W_2/U_2	W_1/U_1
2	0.561	0.544	0.775	0.650	0.729	0.844
3	0.673	0.659	0.907	0.750	0.779	0.920
4	0.776	0.746	0.991	0.807	0.866	1.016
5	0.849	0.821	1.080	0.880	0.912	1.067
6	0.935	0.898	1.166	0.951	0.983	1.131
7	1.024	0.965	1.254	1.004	1.061	1.206

Table E4. Values for all velocity diagrams for throttle 5+4+3+2+1 build #1

Location	α_2	α_1	β_2	β_1	Vu_2/U_2	Vu_1/U_1	Wu_2/U_2	Wu_1/U_1
2	-45.31	-33.99	39.37	49.67	0.552	0.364	0.448	0.636
3	-42.82	-28.83	30.11	44.25	0.615	0.361	0.385	0.639
4	-39.55	-23.91	26.35	42.88	0.625	0.323	0.375	0.677
5	-38.28	-21.06	21.86	40.45	0.663	0.311	0.337	0.689
6	-37.39	-20.01	18.23	38.24	0.699	0.316	0.301	0.684
7	-36.09	-17.42	15.67	37.44	0.722	0.291	0.278	0.709

Location	$Va_2/U_2 = Wa_2/U_2$	$Va_1/U_1 = Wa_1/U_1$	V_2/U_2	V_1/U_1	W_2/U_2	W_1/U_1
2	0.546	0.540	0.776	0.651	0.706	0.834
3	0.664	0.656	0.905	0.749	0.768	0.916
4	0.757	0.729	0.982	0.797	0.845	0.995
5	0.840	0.808	1.070	0.866	0.905	1.062
6	0.914	0.868	1.151	0.924	0.962	1.105
7	0.991	0.926	1.226	0.971	1.029	1.166

E.2. VELOCITY DIAGRAMS BUILD #2

1. Point Location # 3

Figures E4a-d show the velocity diagrams for point location # 3 for all throttle settings.

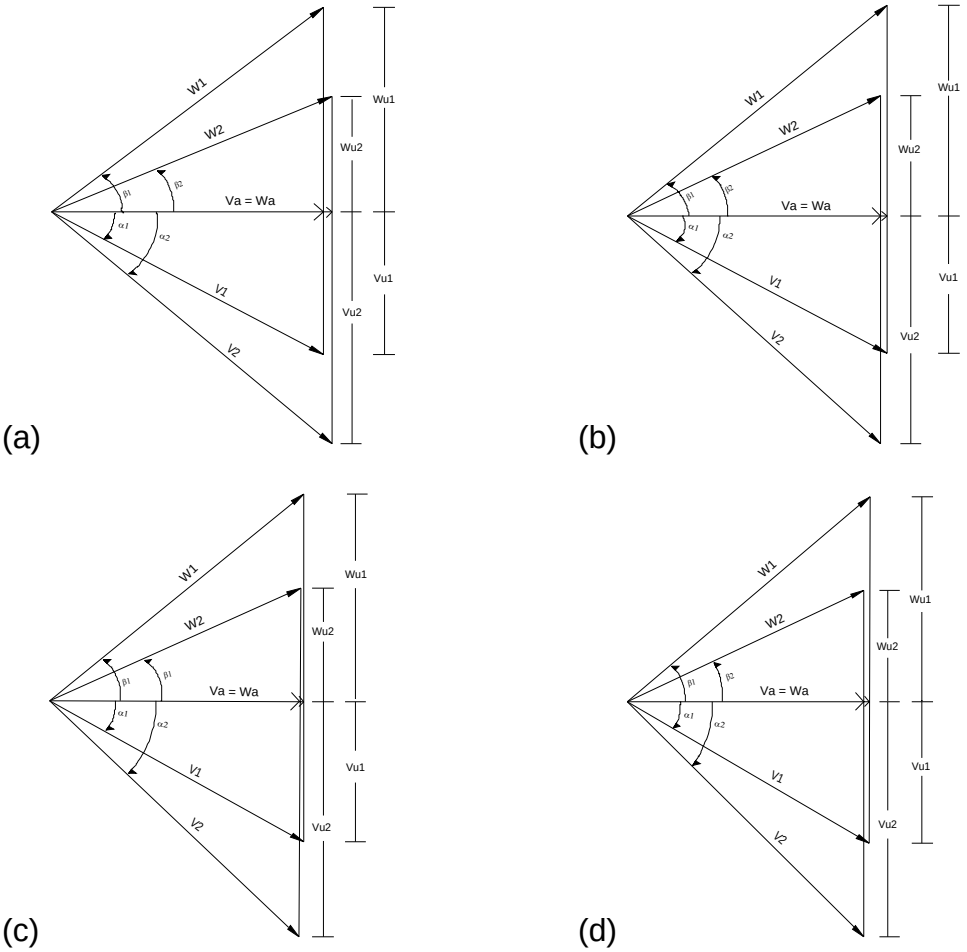

Figure E4. Point location #3 – (a) Open throttle (b) Throttle 5+4 (c) NOP (d) Near stall

2. Point Location # 5

Figures E5a-d show the velocity diagrams for point location # 5 for all throttle settings.

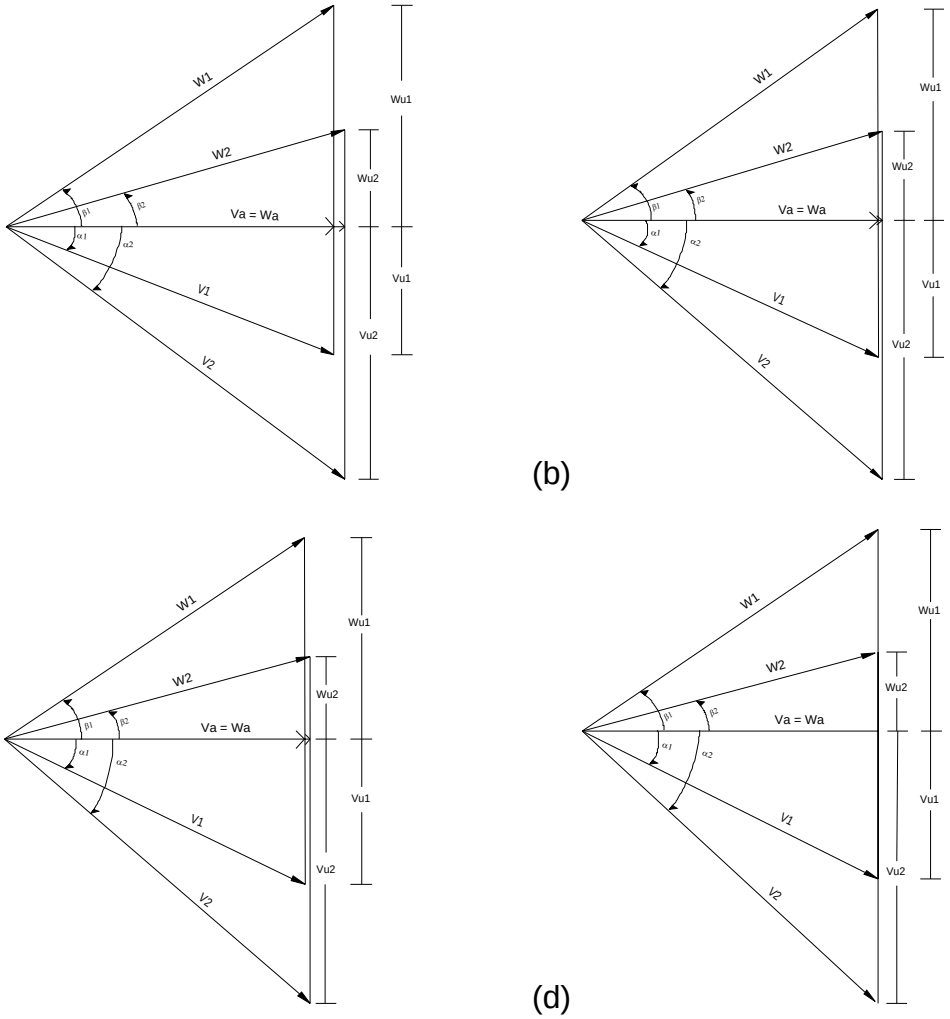

Figure E5. Point location #5 – (a) Open throttle (b) Throttle 5+4 (c) NOP (d) Near stall

3. Point Location # 6

Figures E6a-d show the velocity diagrams for point location # 6 for all throttle settings.

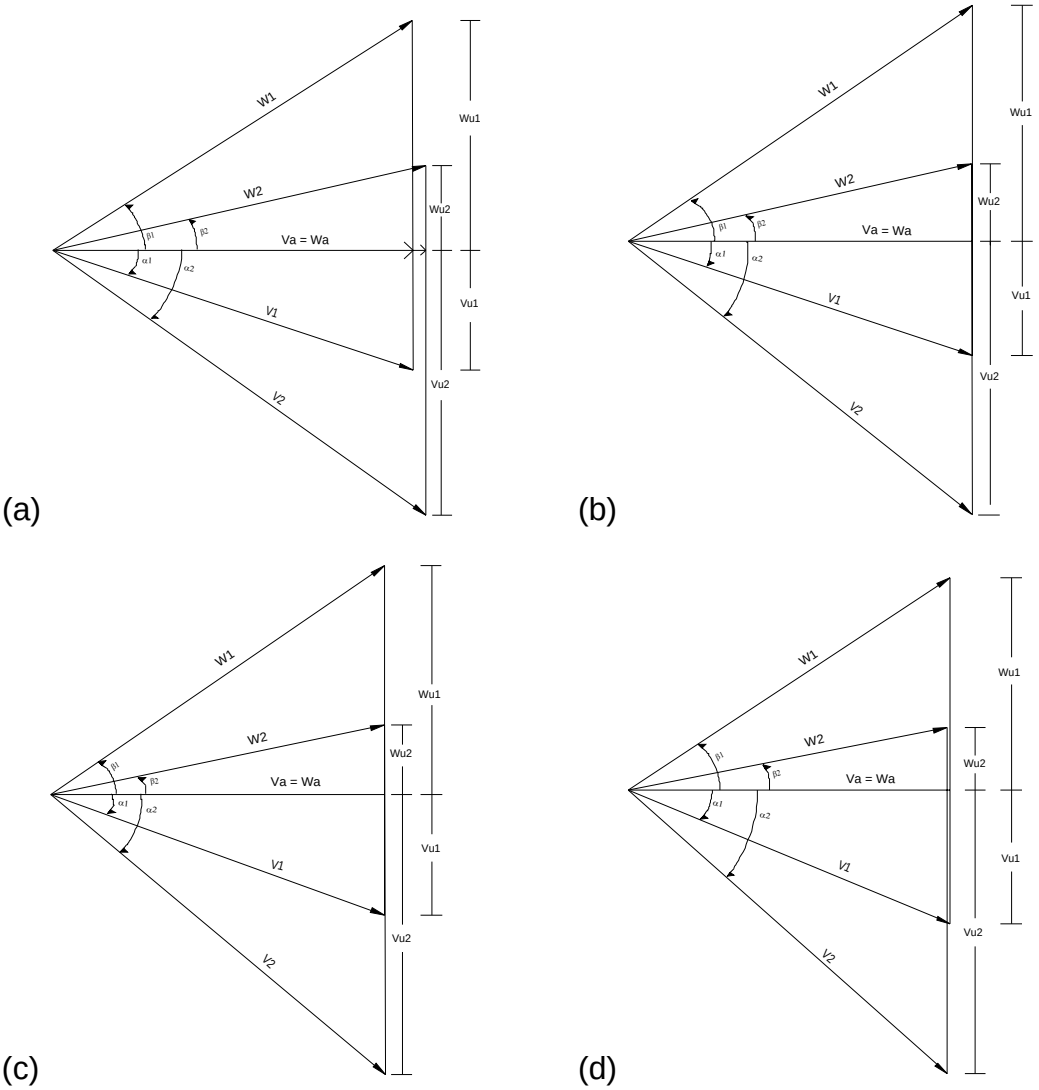

Figure E6. Point location #6 – (a) Open throttle (b) Throttle 5+4 (c) NOP (d) Near stall

4. Tables for Velocity Diagrams

Tables E5-E8 have all of the values for the velocity diagrams for Build # 2.

Table E5. Values for all velocity diagrams for throttle setting 5 build #2

Location	α_2	α_1	β_2	β_1	Vu_2/U_2	Vu_1/U_1	Wu_2/U_2	Wu_1/U_1
2	-43.64	-34.59	30.42	43.84	0.619	0.418	0.381	0.582
3	-40.12	-28.11	22.8	37.57	0.667	0.410	0.333	0.590
4	-40.79	-27.85	16.38	32.33	0.746	0.455	0.254	0.545
5	-36.08	-20.85	15.52	33.32	0.724	0.367	0.276	0.633
6	-34.38	-17.74	12.26	31.53	0.759	0.343	0.241	0.657
7	-32.67	-16.45	9.67	29.26	0.790	0.345	0.210	0.655

Location	$Va_2/U_2 = Wa_2/U_2$	$Va_1/U_1 = Wa_1/U_1$	V_2/U_2	V_1/U_1	W_2/U_2	W_1/U_1
2	0.649	0.606	0.897	0.736	0.753	0.840
3	0.792	0.767	1.035	0.870	0.859	0.968
4	0.864	0.861	1.141	0.974	0.901	1.019
5	0.994	0.963	1.230	1.031	1.032	1.152
6	1.109	1.071	1.344	1.125	1.135	1.256
7	1.232	1.169	1.464	1.219	1.25	1.340

Table E6. Values for all velocity diagrams for throttle setting 5+4 build #2

Location	α_2	α_1	β_2	β_1	Vu_2/U_2	Vu_1/U_1	Wu_2/U_2	Wu_1/U_1
2	-47.77	-36.30	34.13	46.10	0.619	0.414	0.381	0.586
3	-42.14	-27.99	25.48	39.28	0.655	0.394	0.345	0.606
4	-42.14	-27.29	19.81	35.81	0.715	0.417	0.285	0.583
5	-39.93	-24.09	15.99	34.63	0.745	0.393	0.255	0.607
6	-38.34	-18.26	12.65	34.30	0.779	0.326	0.221	0.674
7	-34.42	-16.31	12.55	32.79	0.755	0.312	0.245	0.688

Location	$Va_2/U_2 = Wa_2/U_2$	$Va_1/U_1 = Wa_1/U_1$	V_2/U_2	V_1/U_1	W_2/U_2	W_1/U_1
2	0.562	0.564	0.836	0.700	0.679	0.813
3	0.724	0.741	0.976	0.839	0.802	0.957
4	0.791	0.808	1.066	0.909	0.841	0.996
5	0.890	0.879	1.161	0.963	0.926	1.068
6	0.985	0.988	1.256	1.040	1.009	1.196
7	1.101	1.068	1.335	1.113	1.128	1.270

Table E7. Values for all velocity diagrams for throttle setting 5+4+3 build #2

Location	α_2	α_1	β_2	β_1	Vu_2/U_2	Vu_1/U_1	Wu_2/U_2	Wu_1/U_1
2	-48.43	-34.87	32.60	47.54	0.638	0.389	0.362	0.611
3	-43.25	-29.07	24.45	39.26	0.674	0.405	0.326	0.595
4	-42.15	-27.39	19.23	36.6	0.722	0.411	0.278	0.589
5	-40.89	-25.81	15.23	34.00	0.761	0.418	0.239	0.582
6	-40.11	-20.02	11.75	34.54	0.802	0.346	0.198	0.654
7	-36.14	-18.01	12.17	33.40	0.772	0.330	0.228	0.670

Location	$Va_2/U_2 = Wa_2/U_2$	$Va_1/U_1 = Wa_1/U_1$	V_2/U_2	V_1/U_1	W_2/U_2	W_1/U_1
2	0.566	0.559	0.853	0.681	0.672	0.828
3	0.717	0.728	0.984	0.833	0.788	0.940
4	0.797	0.793	1.075	0.893	0.844	0.988
5	0.878	0.863	1.162	0.959	0.910	1.041
6	0.952	0.950	1.245	1.011	0.972	1.153
7	1.057	1.016	1.309	1.068	1.081	1.217

Table E8. Values for all velocity diagrams for throttle 5+4+3+2+1 build #2

Location	α_2	α_1	β_2	β_1	Vu_2/U_2	Vu_1/U_1	Wu_2/U_2	Wu_1/U_1
2	-52.83	-38.07	33.22	45.87	0.668	0.432	0.332	0.568
3	-44.50	-30.07	24.92	39.81	0.679	0.410	0.321	0.590
4	-42.16	-26.99	19.84	36.58	0.715	0.407	0.285	0.593
5	-42.59	-26.48	14.85	34.09	0.776	0.424	0.224	0.576
6	-41.67	-22.55	11.06	33.43	0.820	0.386	0.180	0.614
7	-37.88	-19.33	11.68	33.1	0.790	0.350	0.210	0.650

Location	$Va_2/U_2 = Wa_2/U_2$	$Va_1/U_1 = Wa_1/U_1$	V_2/U_2	V_1/U_1	W_2/U_2	W_1/U_1
2	0.507	0.551	0.839	0.700	0.606	0.791
3	0.691	0.708	0.969	0.818	0.762	0.922
4	0.790	0.799	1.066	0.897	0.840	0.995
5	0.845	0.851	1.147	0.951	0.874	1.028
6	0.921	0.930	1.233	1.007	0.938	1.114
7	1.016	0.997	1.287	1.057	1.037	1.190

LIST OF REFERENCES

1. Gbadebo, S. A., Hynes, T. P., Cumpsty, N. A., 2004, “Influence of Surface Roughness on Three-Dimensional Seperation in Axial-compressors,” ASME Paper GT2004-53619, pp. 1-11.

2. Suder, K. L., Chima, R. V., Strazisar, A. J., and Roberts, W.B., 1994, “Effect of Adding Roughness and Thickness to a Transonic Axial-compressor Rotor,” ASME Paper 94-GT-339, pp. 1-20.

3. Bammert, K., and Woelk, G. U., 1980, “Influence of the Blading Surface Roughness on the Aerodynamic Behavior and Characteristic of an Axial-compressor,” Journal of Engineering for Power, 102(3), pp. 579-583.

4. Moyle, I.N., “Multistage Compressor – Advanced Aerodynamic Flow Field Experiments,“ Naval Postgraduate School, Monterey, California, Turbopropulsion Lab. TN/90-01, June 1990.

5. Moyle, I.N., “An Experimental and Analytic Study of Tip Clearance Effects In Axial Flow Compressors,” Doctoral Dissertation, University of Tasmania, Australia, December 1991; also Contractor Report NPS AA-92-001CR, Naval Postgraduate School, Monterey California, December 1991.

THIS PAGE INTENTIONALLY LEFT BLANK

INITIAL DISTRIBUTION LIST

1. Defense Technical Information Center
   Ft. Belvoir, Virginia

2. Dudley Knox Library
   Naval Postgraduate School
   Monterey, California

3. Department Chairman, Code ME
   Department of Mechanical and Astronautics Engineering
   Monterey, California

4. Dr. Garth V. Hobson, Code ME/HG
   Department of Mechanical and Astronautics Engineering
   Monterey, California

5. Dr. Raymond P. Shreeve, Code ME/SF
   Department of Mechanical and Astronautics Engineering
   Monterey, California

6. Naval Air Warfare Center
   AIR-4.4.T (Attn: Mr. R. Ravindranath)
   Propulsion and Power Engineering, Building 106
   Patuxent, Maryland

7. Naval Air Warfare Center
   AIR-4.4.T (Attn: Mr. M. Klein)
   Propulsion and Power Engineering, Building 106
   Patuxent, Maryland